Consistent Eulerian and Lagrangian variational formulations of non-linear kinematic hardening for solid media undergoing large strains and shocks

Thomas Heuzé, Nicolas Favrie

▶ **To cite this version:**

Thomas Heuzé, Nicolas Favrie. Consistent Eulerian and Lagrangian variational formulations of non-linear kinematic hardening for solid media undergoing large strains and shocks. Computer Methods in Applied Mechanics and Engineering, 2024, 433, pp.117480. ⟨10.1016/j.cma.2024.117480⟩. ⟨hal-05324919⟩

HAL Id: hal-05324919

https://hal.science/hal-05324919v1

Submitted on 21 Oct 2025

HAL is a multi-disciplinary open access archive for the deposit and dissemination of scientific research documents, whether they are published or not. The documents may come from teaching and research institutions in France or abroad, or from public or private research centers.

L'archive ouverte pluridisciplinaire **HAL**, est destinée au dépôt et à la diffusion de documents scientifiques de niveau recherche, publiés ou non, émanant des établissements d'enseignement et de recherche français ou étrangers, des laboratoires publics ou privés.

HAL Authorization

Consistent Eulerian and Lagrangian variational formulations of non-linear kinematic hardening for solid media undergoing large strains and shocks

Thomas Heuzé[a], Nicolas Favrie[b]

aResearch Institute in Civil and Mechanical Engineering (GeM), UMR 6183 CNRS École Centrale de Nantes, 1 rue de la Noë, F-44321 Nantes, France
bAix-Marseille Université, CNRS, IUSTI UMR 7343, 13543, Marseille, France

In this paper, two Eulerian and Lagrangian variational formulations of non-linear kinematic hardening are derived in the context of finite thermoplasticity. These are based on the thermo-mechanical variational framework introduced by Heuzé and Stainier (2022), and follow the concept of pseudo-stresses introduced by Mosler and Bruhns (2009). These formulations are derived from a thermodynamical framework and are based on the multiplicative split of the deformation gradient in the context of hyperelasticity. Both Lagrangian and Eulerian formulations are derived in a consistent manner via some transport associated with the mapping, and use quantities consistent with those updated by the set of conservation or balance laws written in these two cases. These Eulerian and Lagrangian formulations aims at investigating the importance of non-linear kinematic hardening for bodies submitted to cyclic impacts in dynamics, where Bauschinger and/or ratchetting effects are expected to occur. Continuous variational formulations of the local constitutive problems as well as discrete variational constitutive updates are derived in the Eulerian and Lagrangian settings. The discrete updates are coupled with the second order accurate flux difference splitting finite volume method, which permits to solve the sets of conservation laws. A set of test cases allow to show on the one hand the good behavior of variational constitutive updates, and on the other hand the good consistency of Lagrangian and Eulerian numerical simulations.

1. Introduction

In the elastic–plastic constitutive response of metallic materials when submitted to non-monotonic loadings, it is important to include a non-linear kinematic hardening on the one hand to describe the Bauschinger effect, associated with the decrease in the yield strength of the material in compression as a result of a prior deformation in tension, and on the other hand ratchetting effects associated with an increase of plastic strain at each load cycle, see [1]. One of the most famous model is that of Armstrong–Frederick [2,3], well-established in small strains, and which can be associated simple rheological interpretation. Many works have already discussed its extension to finite strain plasticity, from which two families of modeling have been established. A first one defines an evolution equation for the back-stresses, hence considered as an internal variable (so-called Chaboche-type approach), see model A of [4] and model I of [5]. A second approach consists in defining a strain-like internal variable by making a decomposition

* Corresponding author.
E-mail address: thomas.heuze@ec-nantes.fr (T. Heuzé).

of the plastic part of the deformation gradient into some energy storage and dissipative parts, hence defining a so-called center configuration between the initial and the intermediate ones. This idea was presented in [6] based on a simple rheological element, or also in [7]. It was then reused for numerical integration purpose in [4] (model C) or [8,9]. Of course, the linearization of both types of modeling allow to recover the small strain one [2].

For the numerical integration of these models, an important step was provided by Mosler [5] who recast these two families of modeling (called models I and II) into a variational framework. The variational framework is indeed very convenient to build thermodynamically consistent and numerically efficient constitutive updates. It also allows to reuse well-developed optimization algorithms, provides a symmetric Hessian matrix if a Newton method is used, and gives an error indicator based on the convexity/concavity of the optimal point of the functional useful to design adaptive methods [10–12]. Especially, using the concept of pseudo-stresses already introduced in [13–15], and well-adapted for yield function positively homogeneous of degree one, the solution process was shown to be performed on a very reduced number of unknowns, and appears as accurate as others [8]. Next, it was extended to coupled thermomechanics in [16–18] using a two-field thermal description, slightly modified from that initially introduced by Yang et *al.* [19].

In this paper, we are interested in investigating the use of non-linear kinematic hardening for bodies submitted to impacts in dynamics. This type of hardening is usually disregarded in numerical modelings dedicated to the simulation of impacts on solids [20–29]. Indeed if a strong pulse is applied on a body, or if it is impacted by a striker flying at a given velocity, the loading is usually monotonic and considering a sole isotropic hardening is usually sufficient. However, dynamic Bauschinger effect has already been studied experimentally, either by two successive test loadings first in tension then in compression of a specimen on a dedicated Hopkinson device [30], or via a single test using adapted torsion split Hopkinson bars [31]. Among other things, the latter allows to show that a reverse plastic loading can be triggered via the reflexion of waves at a free boundary. Another situation where kinematic hardening may be of importance is when a body is submitted to prescribed rough pulses in a cyclic manner, as it was studied numerically in the context of small strains in [32]. For instance, Laser Shock Peening can be used to mitigate back stresses in rolled stainless sheets [33]. In these cases, Bauschinger and/or ratchetting effects can occur, such that the use of non-linear kinematic hardening becomes important.

In fast solid dynamics, the solutions may consist of both continuous and discontinuous waves, which may propagate irreversible phenomena. The correct capturing of these waves is of crucial importance to properly understand the mechanical phenomena occurring within the medium. Especially, shock waves result from the equation of state accounted for, relating the hydrostatic pressure to the internal energy (see e.g. that of Mie-Grüneisen [34,35]) hence establishing some thermo-mechanical coupling on the volumetric part of the constitutive response. In addition, for these applications involving moderate levels of pressure, i.e. before the hydrodynamic assumption completely applies, the shear strength of the medium is still of great importance in its constitutive response, especially when it involves irreversible and thermo-mechanically coupled phenomena, such as thermal softening resulting from large inelastic strains and associated temperature rise. Recently, a variational formulation of thermo-mechanical constitutive update coupled to a set of conservation laws written in a total Lagrangian framework has been introduced in [36]. It allows to account for different types of thermo-mechanical coupling at the constitutive level, like thermal softening and an equation of state, while the solution in the discrete setting of these conservations laws will ensure that the right shock speeds will be computed. Especially, this variational constitutive update is compatible with any numerical scheme dedicated to the approximation of the solution of hyperbolic systems, like finite volumes [24–26,29,37], finite elements [38], Discontinuous Galerkin methods [39,40], particle methods [41], eventually coupled with a discontinuous approximation [28,42–44]. Its particularity lies in that it is driven by updated values of some strain measure and of the internal energy density, hence getting rid of the two-field thermal formulation employed in [16–19], while the concept of pseudo-stresses introduced by Mosler and co-workers [13–15] is adopted. Hence, such a thermo-mechanical variational framework is particularly well-suited to welcome the variational description of the non-linear kinematic hardening already advocated by Mosler in [5].

The solution of hyperbolic problems is rendered more difficult as the solid medium undergoes large strains and displacements. On the one hand, Lagrangian approaches permit to naturally follow material particles and the boundaries of a body, which is convenient for the integration of history-dependent constitutive response and for applying boundary conditions. However, Lagrangian approaches are subject to mesh entanglement, which require remeshing as well as diffusive and costly projection steps of internal variables. On the other hand, Eulerian approaches allow to compute incomparable levels of deformation of a body, while it requires interface tracking techniques and convection steps to follow the boundaries and transport internal variables which are less convenient for solid mechanics. However, depending on the particular study of interest, these two approaches can appear complementary. Then, there is a strong interest in formulating the equations of finite strain plasticity, and especially here with a non-linear kinematic hardening, in a consistent manner in both Lagrangian and Eulerian configurations through some transport associated with the mapping, but also using quantities consistent with those updated by the set of conservation or balance laws written in these two cases. Such consistent formulations of constitutive and conservation (or balance) laws also allows to derive adapted numerical integration algorithms of the constitutive model (or constitutive update), i.e. using either Lagrangian or Eulerian quantities. More precisely, the above so-called Chaboche approach that yields an evolution equation on the back stresses needs to be supplemented with some arbitrary objective time derivative to complete the writing of the evolution equation of the back stresses, whose choice is let to the user and is somewhat arbitrary since many different stress rate have been proposed [45], and each of these yields actual different models since different stress levels will be computed for the same loading path. For hypoelastic response for instance, the use of an objective stress rate renders the mathematical analysis of discontinuous solutions questionable as noticed in [46]. Defining consistent formulations of constitutive and conservation (or balance) between Eulerian and Lagrangian approaches

can actually be shown to choose one such objective time derivative, but this one is now already embedded in the modeling, whose choice is not let to the arbitrariness of the user.

In this work, consistent Eulerian and Lagrangian variational formulations of the non-linear kinematic hardening in finite strains are presented, using a parameterization of evolution equations with some pseudo-stresses, analog to that performed by Mosler [5] (its model I) in the intermediate configuration. Analog equations of finite plasticity with non-linear kinematic hardening are written in both initial and current configurations, but with different quantities. The Eulerian and Lagrangian quantities are chosen in these formulations so that to be consistent with Lagrangian conservation laws and Eulerian balance laws respectively. The two sets, each consisting of constitutive and conservation (or balance) laws, yield consistent Eulerian and Lagrangian writings of the hyperbolic thermo-mechanical initial boundary value problem. As could be expected, such approach leads to use a convected or Lie objective time derivative, but its main interest lies in that no explicit additional objective time derivative needs to be added within the evolution equation of the back stresses. The mechanical part of the continuous variational principles derived in these two settings look similar to that of [5], but defined with purely Eulerian or Lagrangian quantities respectively. Associated discrete variational principles then departs truly from that of Mosler [5] because of the chosen set of variables, and the time discretization of plastic flow rules. These variational formulations are embedded within the thermo-mechanical variational framework introduced in [36], in order to be couplable with any numerical scheme dedicated to the solution of hyperbolic problems. This variational approach relies on the definition of a functional augmented by the residual of the rate of the Legendre transform of Helmholtz's free energy density enforced to vanish through a Lagrange multiplier. The latter is identified to unit in the continuous case, and to a ratio between previous and updated values of the temperature in the discrete one, which enters the set of discrete stationarity equations and weight the computation of discrete stresses. Next, the second order accurate flux difference splitting finite volume method initially introduced by Leveque [47,48], and adapted for non-quadrilateral meshes [49] is used, which permits to solve the sets of conservation laws. Especially, it is also adapted to compute non-conservative terms arising in the Eulerian formulation. Finally, a set of numerical tests are conducted to show the good behavior of the proposed approach. First, test cases conducted at one material point allow to show the convergence of the discrete variational constitutive updates. Second, a set of numerical simulations involving cyclic loadings allow to show some effects particular of the non-linear kinematic hardening. Comparisons are performed between Eulerian and Lagrangian simulations, and show a good agreement. For the sake of simplicity, only Dirichlet boundary conditions are considered in these examples to focus on the study of non-linear kinematic hardening. Others would require the implementation of interface tracking techniques [26,50–54], which are not the purpose of the present work.

The paper is structured as follows. The Eulerian and Lagrangian modelings of the thermo-mechanical initial boundary value problem are presented in Sections 2 and 3 respectively. Then, the continuous and discrete variational formulations of the Eulerian and Lagrangian thermo-mechanical local constitutive problems are derived in Sections 4 and 5 respectively. Section 6 gives a brief summary of the flux difference splitting finite volume, and Section 7 shows a set of numerical examples.

2. Eulerian modeling of the thermo-mechanical initial boundary value problem

2.1. Eulerian form of Helmholtz's free energy

After the work of Lee [55], the kinematics for finite elastoplasticity follows a multiplicative decomposition of the deformation gradient $\mathbf{F}$ into an elastic part $\mathbf{F}^e$ and a plastic part $\mathbf{F}^p$:

$$\mathbf{F} = \mathbf{F}^e \cdot \mathbf{F}^p, \quad \det \mathbf{F}^e > 0, \quad \det \mathbf{F}^p > 0. \tag{1}$$

Eq. (1) also reads in indicial notation as

$$F_{i\alpha} = F^e_{iI} F^p_{I\alpha}, \tag{2}$$

where, for convenient purpose in the sequel of this paper, small case latin indices, big case latin indices and greek indices will refer to the current, intermediate and initial configurations respectively. Next, from the elastic part of the deformation gradient, the elastic right Cauchy–Green strain tensor

$$\mathbf{C}^e = (\mathbf{F}^e)^T \cdot \mathbf{F}^e \tag{3}$$

is generally used to compute stresses, in order to satisfy material frame indifference. Then, Helmholtz's free energy per unit mass w in the Eulerian setting is defined by summing the following several contributions

$$w((\mathbf{C}^e)^{-1}, T, \mathbf{Z}) = w^e((\mathbf{C}^e)^{-1}, T) + w^p(\mathbf{Z}, T) + w^{th}(T). \tag{4}$$

The specific elastically stored energy (recoverable) $w^e((\mathbf{C}^e)^{-1}, T)$ is chosen to be a function of the inverse of the elastic right Cauchy–Green strain tensor $(\mathbf{C}^e)^{-1} = (\mathbf{F}^e)^{-1} \cdot (\mathbf{F}^e)^{-T}$, and of the temperature T. The elastic energy $w^e((\mathbf{C}^e)^{-1}, T)$ should be a convex function of $(\mathbf{C}^e)^{-1}$, positive, and vanishes for $(\mathbf{C}^e)^{-1} = \mathbf{1}$, where $\mathbf{1}$ is the second order identity tensor. Moreover, in order to account for decoupled material response of volumetric and isochoric parts, the isochoric elastic deformation gradient $\bar{\mathbf{F}}^e$, the isochoric right Cauchy–Green strain tensor $\bar{\mathbf{C}}^e$ and its inverse $(\bar{\mathbf{C}}^e)^{-1}$ are introduced such that

$$\bar{\mathbf{F}}^e = (J^e)^{-1/3} \mathbf{F}^e, \quad J^e = \det \mathbf{F}^e, \quad \det \bar{\mathbf{F}}^e = 1 \tag{5}$$

$$\bar{\mathbf{C}}^e = (\bar{\mathbf{F}}^e)^T \cdot \bar{\mathbf{F}}^e, \quad (\bar{\mathbf{C}}^e)^{-1} = (\bar{\mathbf{F}}^e)^{-1} \cdot (\bar{\mathbf{F}}^e)^{-T}. \tag{6}$$

The specific elastically stored energy is then decomposed additively into volumetric and isochoric parts

$$w^e((\mathbf{C}^e)^{-1},T) = w^H(J^e,T) + \bar{w}^e((\bar{\mathbf{C}}^e)^{-1},T), \tag{7}$$

where the volumetric part $w^H(J^e,T)$ depends on the elastic jacobian determinant J^e and on the temperature T, while the isochoric component $\bar{w}^e((\bar{\mathbf{C}}^e)^{-1},T)$ is a function of both the inverse of the isochoric elastic Cauchy–Green strain tensor $(\bar{\mathbf{C}}^e)^{-1}$ and the temperature T.

The specific plastically stored energy (not recoverable) $w^p(\mathbf{Z},T)$ is a function of a set of internal variables $\mathbf{Z}$ and of the temperature T. In the sequel, the set of internal variables will only consist of a strain-like variable related to the kinematic hardening. For the sake of simplicity of the presentation, no isotropic hardening will be treated in the derivation of the modelings in this paper, since its treatment is rather classical and can be found in [13,14,56] in the Lagrangian case or in [24,29,57] in the Eulerian one. More precisely, the strain-like variable related to the kinematic hardening will be assumed to be the *Lagrangian* and symmetric second order tensor $\boldsymbol{\alpha}$ such that the specific plastically stored energy

$$w^p = w^p(\boldsymbol{\alpha},T) \tag{8}$$

is a convex function of $\boldsymbol{\alpha}$, positive, and vanishes for $\boldsymbol{\alpha} = \mathbf{0}$. This Lagrangian tensor *is defined in the initial configuration*, and its particular definition will be precised later, in Section 2.4. Finally, the partition (4) also introduces the specific thermally stored energy $w^{th}(T)$ due to heat capacity.

2.2. Preliminary kinematic compatibility relationships

We consider a continuum body whose current setting is denoted V, of boundary ∂V of outward unit normal $\mathbf{n}$. The motion of the domain V is described by the Eulerian velocity field $\mathbf{v}(\mathbf{x},t)$, $\mathbf{x}$ being the set of current coordinates. The kinematic compatibility between the deformation gradient $\mathbf{F}$ and the Eulerian velocity field $\mathbf{v}(\mathbf{x},t)$ reads:

$$\frac{d\mathbf{F}}{dt} = \mathbf{L}\cdot\mathbf{F}, \tag{9}$$

where $\mathbf{L} = \frac{\partial \mathbf{v}}{\partial \mathbf{x}}$ denotes the Eulerian velocity gradient, and $\frac{d}{dt}$ stands for the material time derivative. Taking the time derivative of the identity $\mathbf{F}\cdot\mathbf{F}^{-1} = \mathbf{1}$, where $\mathbf{1}$ is the second order identity tensor, and considering Eq. (9), one gets the following relationship

$$\frac{d\mathbf{F}^{-1}}{dt} + \mathbf{F}^{-1}\cdot\mathbf{L} = \mathbf{0}. \tag{10}$$

Some analog derivation process can be carried out with the elastic deformation gradient $\mathbf{F}^e$, i.e. taking the time derivative of the identity $\mathbf{F}^e\cdot(\mathbf{F}^e)^{-1} = \mathbf{1}$, and combination with Eqs. (1) and (9) yields

$$\frac{d(\mathbf{F}^e)^{-1}}{dt} = (\mathbf{F}^e)^{-1}\cdot(\mathbf{l}^p - \mathbf{L}), \tag{11}$$

where the plastic part of the Eulerian velocity gradient $\mathbf{l}^p$ is defined as the push-forward into the current setting of its counterpart $\mathbf{L}^p$ defined in the intermediate configuration

$$\mathbf{l}^p = \mathbf{F}^e\cdot\mathbf{L}^p\cdot(\mathbf{F}^e)^{-1}, \tag{12}$$

with

$$\mathbf{L}^p = \frac{d\mathbf{F}^p}{dt}\cdot(\mathbf{F}^p)^{-1}. \tag{13}$$

From Eq. (11), the time derivative of the inverse of the elastic right Cauchy–Green strain tensor $(\mathbf{C}^e)^{-1}$ is obtained as

$$\frac{d(\mathbf{C}^e)^{-1}}{dt} = 2(\mathbf{F}^e)^{-1}\cdot(\mathbf{l}^p - \mathbf{d})\cdot(\mathbf{F}^e)^{-T}, \tag{14}$$

with the Eulerian strain rate tensor defined as

$$\mathbf{d} = \frac{1}{2}(\mathbf{L} + \mathbf{L}^T). \tag{15}$$

2.3. Eulerian writing of the Clausius-Duhem inequality

In the absence of heat conduction, the total dissipation reduces to the internal dissipation expressed via the Clausius–Duhem inequality that reads in the Eulerian setting as

$$\mathscr{D}_{\text{int}} = \boldsymbol{\tau} : \mathbf{d} - \rho_0\left(\frac{dw}{dt} + \eta\frac{dT}{dt}\right) \geq 0, \tag{16}$$

where $\boldsymbol{\tau} = J\boldsymbol{\sigma}$ refers to the Kirchhoff stresses, deduced from the Cauchy stresses by multiplying by the jacobian determinant J, $\mathbf{d}$ is the Eulerian strain rate defined by Eq. (15), w denotes Helmholtz's specific free energy, T is the temperature, ρ_0 is the initial mass density and η denotes the specific entropy.

From Eqs. (4) and (8), the time derivative of Helmholtz's specific free energy is expanded as

$$\frac{dw}{dt} = \frac{\partial w}{\partial(\mathbf{C}^e)^{-1}} : \frac{d(\mathbf{C}^e)^{-1}}{dt} + \frac{\partial w}{\partial \boldsymbol{\alpha}} : \frac{d\boldsymbol{\alpha}}{dt} + \frac{\partial w}{\partial T}\frac{dT}{dt}. \tag{17}$$

Introducing Eq. (14) into Eq. (17), itself combined with Inequality (16) makes the internal dissipation expressed as

$$\begin{aligned}\mathscr{D}_{\text{int}} = &\left[\boldsymbol{\tau} + 2\rho_0(\mathbf{F}^e)^{-T}\cdot\frac{\partial w}{\partial(\mathbf{C}^e)^{-1}}\cdot(\mathbf{F}^e)^{-1}\right] : \mathbf{d}\\ &- 2\rho_0\left[(\mathbf{F}^e)^{-T}\cdot\frac{\partial w}{\partial(\mathbf{C}^e)^{-1}}\cdot(\mathbf{F}^e)^{-1}\right] : \mathbf{l}^p - \rho_0\frac{\partial w}{\partial\boldsymbol{\alpha}} : \frac{d\boldsymbol{\alpha}}{dt} - \rho_0\frac{dT}{dt}\left(\frac{\partial w}{\partial T}+\eta\right) \geq 0\end{aligned} \tag{18}$$

Application of the standard Coleman and Noll procedure [58–60] yields the state laws

$$\boldsymbol{\tau} = -2\rho_0(\mathbf{F}^e)^{-T}\cdot\frac{\partial w}{\partial(\mathbf{C}^e)^{-1}}\cdot(\mathbf{F}^e)^{-1} \tag{19}$$

$$\eta = -\frac{\partial w}{\partial T}. \tag{20}$$

By analogy, one defines the Lagrangian stress-like variable

$$\mathbf{Q} = \rho_0\frac{\partial w}{\partial\boldsymbol{\alpha}}, \tag{21}$$

associated with the Lagrangian strain-like variable $\boldsymbol{\alpha}$, such that the internal dissipation finally reads

$$\mathscr{D}_{\text{int}} = \boldsymbol{\tau} : \mathbf{l}^p - \mathbf{Q} : \frac{d\boldsymbol{\alpha}}{dt} \geq 0. \tag{22}$$

At this stage, the internal dissipation (22) consists of one term involving Eulerian quantities, and one term involving Lagrangian quantities, whose Eulerian analogs should be proposed.

2.4. Eulerian back stresses and evolution laws

One defines the Eulerian back stresses

$$\mathbf{q} = \mathbf{F}\cdot\mathbf{Q}\cdot\mathbf{F}^T \tag{23}$$

as the push forward of the Lagrangian stress-like variable $\mathbf{Q}$ (21), consistently with that performed on stresses, such that the effective stresses read

$$\boldsymbol{\xi} = \boldsymbol{\tau} - \mathbf{q} = \mathbf{F}\cdot(\mathbf{S}-\mathbf{Q})\cdot\mathbf{F}^T, \tag{24}$$

where $\mathbf{S} = \mathbf{F}^{-1}\cdot\boldsymbol{\tau}\cdot\mathbf{F}^{-T}$ is the second Piola–Kirchhoff stress tensor. In order to describe the dissipative phenomena associated with plasticity, and following the class of Generalized Standard Materials [61], one introduces the Eulerian plastic flow potential ϕ which we assume to be a convex function of the following set of arguments $(\boldsymbol{\tau},\mathbf{q})$, positive, and vanishes at zero. A non-linear kinematic hardening of Armstrong–Frederick-type [2,3] is chosen here, such that the plastic flow potential ϕ reads

$$\phi = f + \frac{b}{2c}\mathbf{q} : \mathbf{q}. \tag{25}$$

The yield function $f(\boldsymbol{\tau},\mathbf{q}) \leq 0$ defines the elastic convex, and is chosen here of the form

$$f(\boldsymbol{\tau},\mathbf{q}) = \tau_{\text{eq}}(\boldsymbol{\tau}-\mathbf{q}) - \sigma_y \leq 0, \tag{26}$$

where σ_y denotes the tensile yield stress, and $\tau_{\text{eq}}(\boldsymbol{\tau}-\mathbf{q})$ some equivalent stress which is assumed to be a positively homogeneous function of degree one of $\boldsymbol{\tau}-\mathbf{q}$. Applying the normality to ϕ (25), one gets the evolution equations

$$\mathbf{l}^p = \dot{\lambda}\frac{\partial\phi}{\partial\boldsymbol{\tau}} = \dot{\lambda}\frac{\partial f}{\partial\boldsymbol{\tau}} \tag{27}$$

$$\overset{\triangledown}{\mathbf{V}} = -\dot{\lambda}\frac{\partial\phi}{\partial\mathbf{q}} = \dot{\lambda}\left(\frac{\partial f}{\partial\boldsymbol{\tau}} - \frac{b}{c}\mathbf{q}\right) \tag{28}$$

where $\dot{\lambda}$ denotes the plastic multiplier, satisfying the complementarity conditions

$$\dot{\lambda} \geq 0,\ f \leq 0,\ \dot{\lambda}f = 0. \tag{29}$$

The flux-type variable $\overset{\triangledown}{\mathbf{V}}$, conjugate to the Eulerian back stresses $\mathbf{q}$, has been introduced in Eq. (28). Moreover, since the Kirchhoff stresses $\boldsymbol{\tau}$ are symmetric, hence the Eulerian plastic spin tensor vanishes $\mathbf{w}^p = \mathbf{0}$ according to Eq. (27), so that the plastic part of the Eulerian velocity gradient equals its symmetric part

$$\mathbf{l}^p \equiv \mathbf{d}^p, \tag{30}$$

namely the Eulerian plastic strain rate.

With evolution laws (27)–(28) at hand, the internal dissipation (22) can be written of the form

$$\mathscr{D}_{\text{int}} = \dot{\lambda}\left(\boldsymbol{\tau} : \frac{\partial\phi}{\partial\boldsymbol{\tau}} + \mathbf{q} : \frac{\partial\phi}{\partial\mathbf{q}}\right) \geq 0, \tag{31}$$

whose non-negativeness can be shown provided the Eulerian plastic flow potential ϕ satisfies its aforementioned properties. Provided the definition of the Eulerian back stresses (23) and the evolution Eq. (28), the second term of the internal dissipation (22), written with Lagrangian quantities, can be written with Eulerian ones as

$$\begin{aligned} -\mathbf{Q} : \frac{d\boldsymbol{\alpha}}{dt} &= -\left(\mathbf{F}\cdot\mathbf{Q}\cdot\mathbf{F}^T\right) : \left(\mathbf{F}^{-T}\cdot\frac{d\boldsymbol{\alpha}}{dt}\cdot\mathbf{F}^{-1}\right) \\ &= -\mathbf{q} : \overset{\triangledown}{\mathbf{V}} = \dot{\lambda}\mathbf{q} : \frac{\partial\phi}{\partial\mathbf{q}}, \end{aligned} \tag{32}$$

where the flux-type variable $\overset{\triangledown}{\mathbf{V}}$ is identified as

$$\overset{\triangledown}{\mathbf{V}} = \left(\mathbf{F}^{-T}\cdot\frac{d\boldsymbol{\alpha}}{dt}\cdot\mathbf{F}^{-1}\right), \tag{33}$$

which is a push-forward of the time derivative of the Lagrangian variable $\boldsymbol{\alpha}$, and hence stands for a convected or Lie time derivative of the variable $\mathbf{V}$. This is clearly a consequence of the choice made for the Eulerian back stresses (23). Accordingly, the variable $\mathbf{V}$ enters the arguments of the plastic part of Helmholtz's specific free energy

$$w^p(\boldsymbol{\alpha}, T) = \tilde{w}^p(\mathbf{V}, T), \tag{34}$$

with the associated state law

$$\tilde{\mathbf{q}} = \rho_0 \frac{\partial \tilde{w}^p}{\partial \mathbf{V}}. \tag{35}$$

Time differentiation of Eq. (34) gives

$$\begin{aligned} &\frac{\partial w^p}{\partial\boldsymbol{\alpha}} : \frac{d\boldsymbol{\alpha}}{dt} = \frac{\mathbf{Q}}{\rho_0} : \frac{d\boldsymbol{\alpha}}{dt} \\ =&\frac{\partial \tilde{w}^p}{\partial\mathbf{V}} : \frac{d\mathbf{V}}{dt}, \end{aligned} \tag{36}$$

which also equals $\frac{\mathbf{q}}{\rho_0} : \overset{\triangledown}{\mathbf{V}}$ by identification with Eq. (32), provided Eq. (35).

Hence, from the definition of Eulerian back stresses (23), the internal dissipation can be rewritten as

$$\mathscr{D}_{\text{int}} = \boldsymbol{\tau} : \mathbf{l}^p - \mathbf{q} : \overset{\triangledown}{\mathbf{V}} \geq 0, \tag{37}$$

with $\overset{\triangledown}{\mathbf{V}}$ defined by Eq. (33). If the plastic part of Helmholtz's specific free energy is defined as

$$w^p(\boldsymbol{\alpha}, T) = \frac{c}{2\rho_0}\boldsymbol{\alpha} : \boldsymbol{\alpha}, \tag{38}$$

using Eq. (21), on gets

$$\mathbf{q} = c\mathbf{F}\cdot\boldsymbol{\alpha}\cdot\mathbf{F}^T, \tag{39}$$

then the evolution Eq. (28) takes the form

$$\overset{\triangledown}{\mathbf{V}} = -\dot{\lambda}\frac{\partial\phi}{\partial\mathbf{q}} = \dot{\lambda}\left(\frac{\partial f}{\partial\boldsymbol{\tau}} - b\mathbf{F}\cdot\boldsymbol{\alpha}\cdot\mathbf{F}^T\right), \tag{40}$$

which looks like the well-known Armstrong–Frederick form, though not exactly. The framework of computation of Eq. (40) will be precised in Section 4.1. Introducing Eqs. (27) and (28) into the internal dissipation (31), accounting for the yield function which is positively homogeneous of degree one, yielding [14]

$$\tau_{\text{eq}} = (\boldsymbol{\tau} - \mathbf{q}) : \frac{\partial f}{\partial\boldsymbol{\tau}}, \tag{41}$$

and considering the yield criterion (26) assumed to be reached, the internal dissipation finally reads

$$\mathscr{D}_{\text{int}} = \dot{\lambda}\left(\sigma_y + \frac{b}{c}\mathbf{q} : \mathbf{q}\right) \geq 0. \tag{42}$$

Remark 1. The Eulerian back stresses defined by Eq. (23) had led the Eulerian variable $\mathbf{V}$ to be related to the Lagrangian one $\boldsymbol{\alpha}$ through Eq. (33), that is through a convective time rate. Taking the material time derivative of the Eulerian back stresses (23), and combination with Eqs. (9), (28) and (33) gives the equation governing the time evolution of these back stresses

$$\frac{d\mathbf{q}}{dt} - \mathbf{L}\cdot\mathbf{q} - \mathbf{q}\cdot\mathbf{L}^T = -\dot{\lambda}\mathbf{F}\cdot\left[\frac{\partial^2 w}{\partial\boldsymbol{\alpha}^2} : \left(\mathbf{F}^T\cdot\frac{\partial\phi}{\partial\mathbf{q}}\cdot\mathbf{F}\right)\right]\cdot\mathbf{F}^T, \tag{43}$$

in which a Lie objective time derivative applied on $\mathbf{q}$ can be recognized on the left-hand-side.

2.5. Eulerian balance equations

2.5.1. Basic conservation laws

In the Eulerian setting, the following set of conservation laws should be satisfied

$$\frac{\partial \rho}{\partial t} + \mathrm{div}\,(\rho \mathbf{v}) = 0 \tag{44}$$

$$\frac{\partial (\rho \mathbf{v})}{\partial t} + \mathrm{div}\,(\rho \mathbf{v} \otimes \mathbf{v} - \boldsymbol{\sigma}) = \mathbf{0} \tag{45}$$

$$\frac{\partial (\rho \mathscr{E})}{\partial t} + \mathrm{div}\,(\rho \mathscr{E} \mathbf{v} - \mathbf{v} \cdot \boldsymbol{\sigma}) = 0 \tag{46}$$

where Eqs. (44), (45) and (46) refer to the mass conservation, the conservation of linear momentum (in the absence of body forces here), and the conservation of the total energy (in the absence of heat conduction and heat source) respectively. The Cauchy stress tensor $\boldsymbol{\sigma}$ appearing in Eqs. (45) and (46) is symmetric due to the angular momentum balance, and $\mathscr{E}$ denotes the Eulerian total energy per unit mass defined as

$$\mathscr{E} = e + \frac{|\mathbf{v}|^2}{2}, \tag{47}$$

summing the Eulerian specific internal energy e and the specific kinetic energy. The divergence operator appearing in Eqs. (44), (45) and (46) is computed with respect to the set of current coordinates $\mathbf{x}$. The above conservation laws should be supplemented with some kinematic compatibility relationships in order to make evolve in time some strain measures related to both the global kinematics and its elastic part.

2.5.2. Transport equation for the kinematics

From Eq. (10), the following equation can be written

$$\frac{d\mathbf{F}^{-T}}{dt} + \mathbf{L}^T \cdot \mathbf{F}^{-T} = \mathbf{0}, \tag{48}$$

where $\mathbf{F}^{-T}$ gathers columnwise the cobasis vectors $\mathbf{e}^{(\alpha)}$, $1 \leq \alpha \leq 3$, such that $\mathbf{F}^{-T} = (\mathbf{e}^{(1)}, \mathbf{e}^{(2)}, \mathbf{e}^{(3)})$. The cobasis vectors $\mathbf{e}^{(\alpha)}$ are defined as

$$(\mathbf{e}^{(\alpha)})_i = \frac{\partial X_\alpha}{\partial x_i}, \tag{49}$$

where X_α, $1 \leq \alpha \leq 3$, denote the initial coordinates. Eq. (48) should be added the compatibility equation

$$\mathrm{curl}\ \mathbf{F}^{-T} = 0, \tag{50}$$

where the curl operator is defined in the case of cartesian coordinates via the third order alternating operator π_{ijk} as

$$(\mathrm{curl}\ \mathbf{F}^{-T})_{i\alpha} = \pi_{ijk} \frac{\partial (\mathbf{F}^{-T})_{k\alpha}}{\partial x_j}. \tag{51}$$

Usually, Eq. (48) cannot be solved directly with classical conservative numerical schemes [48] since it is not written in conservative form. In addition, the convective term appearing when expressing the material time derivative

$$\frac{d(\mathbf{F}^{-T})_{i\alpha}}{dt} = \frac{\partial (\mathbf{F}^{-T})_{i\alpha}}{\partial t} + \frac{\partial (\mathbf{F}^{-T})_{i\alpha}}{\partial x_j} v_j \tag{52}$$

cannot be correctly integrated over a space–time domain as it is classically done with conservative schemes, especially when discontinuities occur as shown in [46]. In the latter case, both $\mathbf{v}$ and $\mathbf{F}^{-T}$ may have some discontinuous components, such that the presence of the gradient of $\mathbf{F}^{-T}$ in this term prevents the integral to be correctly computed. Rather, on the one hand the components of the convective term such that $i = j$ are factorized in a conservative form with these of the last term of Eq. (48). On the other hand, the remaining components of the convective term (such that $i \neq j$) are integrated by part, and reassembled with the former components, in such a way that one gets the following transport equation for $\mathbf{F}^{-T}$

$$\frac{\partial (\mathbf{F}^{-T})_{i\alpha}}{\partial t} + \frac{\partial ((\mathbf{F}^{-T})_{i\alpha} v_j)}{\partial x_j} + \sum_{j,j\neq i} \left(\frac{\partial v_j}{\partial x_i} (\mathbf{F}^{-T})_{j\alpha} - (\mathbf{F}^{-T})_{i\alpha} \frac{\partial v_j}{\partial x_j} \right) = 0. \tag{53}$$

The remaining nonconservative terms of Eq. (53) now only involve $\mathbf{F}^{-T}$ and not its gradient, such that a proper numerical scheme compatible with a consistent treatment of discontinuous solutions can be derived as already shown in [46,50]. An adaptation of this scheme in the framework of the flux difference splitting finite volume method [47,48] is described in Section 6.3.

2.5.3. Transport equation for the elastic part of the kinematics

From Eq. (11), an analog equation to Eq. (48) can be written for $(\mathbf{F}^e)^{-T}$ as

$$\frac{d(\mathbf{F}^e)^{-T}}{dt} + \mathbf{L}^T \cdot (\mathbf{F}^e)^{-T} = (\mathbf{l}^p)^T \cdot (\mathbf{F}^e)^{-T}, \tag{54}$$

where $(\mathbf{F}^e)^{-T}$ gathers columnwise the vectors of the elastic cobasis $\tilde{\mathbf{e}}^{(\alpha)}$, $1 \leq \alpha \leq 3$, such that $(\mathbf{F}^e)^{-T} = (\tilde{\mathbf{e}}^{(1)}, \tilde{\mathbf{e}}^{(2)}, \tilde{\mathbf{e}}^{(3)})$. Eq. (54) has a source term involving the plastic flow defined by Eq. (27). Following an analog reasoning as the one done above for $\mathbf{F}^{-T}$, the transport equation for the elastic part of the kinematics reads

$$\frac{\partial (\mathbf{F}^{e^{-T}})_{iI}}{\partial t} + \frac{\partial ((\mathbf{F}^{e^{-T}})_{iI} v_j)}{\partial x_j} + \sum_{j,j\neq i} \left(\frac{\partial v_j}{\partial x_i} (\mathbf{F}^{e^{-T}})_{jI} - (\mathbf{F}^{e^{-T}})_{iI} \frac{\partial v_j}{\partial x_j} \right) = l^{p^T}_{ij} (\mathbf{F}^{e^{-T}})_{jI}. \tag{55}$$

2.5.4. Transport equations for plastic variables

The strain-like Lagrangian variable $\boldsymbol{\alpha}$ related to the kinematic hardening is also the purpose of the transport Eq. (33). First, observe that $\boldsymbol{\alpha}$ is symmetric. It results from the symmetry of Kirchhoff stresses $\boldsymbol{\tau}$, which involve that of back stresses $\mathbf{q}$. The latter implies these of $\overset{\nabla}{\mathbf{V}}$ and $\boldsymbol{\alpha}$ via Eqs. (28) and (33) respectively. Second, its material time derivative also includes a transport via the velocity field, analog to Eq. (52), which is also integrated by parts to avoid derivatives on the sole variable $\boldsymbol{\alpha}$, for the same reasons already mentioned in Sections 2.5.2 and 2.5.3. Hence, the transport equation on $\boldsymbol{\alpha}$ reads

$$\frac{\partial \boldsymbol{\alpha}}{\partial t} + \text{div}\ (\boldsymbol{\alpha} \otimes \mathbf{v}) - \boldsymbol{\alpha}(\text{div}\ \mathbf{v}) = -\dot{\lambda} \mathbf{F}^T \cdot \frac{\partial \phi}{\partial \mathbf{q}} \cdot \mathbf{F}. \tag{56}$$

Besides, the cumulated plastic strain ε_{eq} should also be transported, and is solution of

$$\frac{\partial \varepsilon_{eq}}{\partial t} + \text{div}\ (\varepsilon_{eq} \mathbf{v}) - \varepsilon_{eq}(\text{div}\ \mathbf{v}) = \dot{\lambda}. \tag{57}$$

2.5.5. First order system of balance laws

Gathering Eqs. (44), (45), (46), (53), (55), (56) and (57) allows to form the system of balance laws

$$\frac{\partial \mathscr{U}}{\partial t} + \text{div}\, \mathscr{F}(\mathscr{W}) + \mathscr{B} \cdot \boldsymbol{\nabla} \mathscr{W} = \mathscr{S}(\mathscr{U}, \mathscr{W}), \tag{58}$$

where $\mathscr{U}$, $\mathscr{F}$, $\mathscr{W}$, and $\mathscr{S}$ denote the vector of balanced quantities, the flux vector, the vector of auxiliary quantities, and $\mathscr{S}$ the source term respectively. Vectors $\mathscr{U}$, $\mathscr{F}$ and $\mathscr{S}$ are defined as

$$\mathscr{U} = \begin{Bmatrix} \rho \\ \rho \mathbf{v} \\ \rho \mathscr{E} \\ \{\mathbf{e}^{(\alpha)}\}_{1\leq\alpha\leq3} \\ \{\tilde{\mathbf{e}}^{(\alpha)}\}_{1\leq\alpha\leq3} \\ \boldsymbol{\alpha} \\ \varepsilon_{eq} \end{Bmatrix} \quad ; \quad \mathscr{F} = \begin{Bmatrix} \rho \mathbf{v} \\ \rho \mathbf{v} \otimes \mathbf{v} - \boldsymbol{\sigma} \\ \rho \mathscr{E} \mathbf{v} - \mathbf{v} \cdot \boldsymbol{\sigma} \\ \{\mathbf{e}^{(\alpha)} \otimes \mathbf{v}\}_{1\leq\alpha\leq3} \\ \{\tilde{\mathbf{e}}^{(\alpha)} \otimes \mathbf{v}\}_{1\leq\alpha\leq3} \\ \boldsymbol{\alpha} \otimes \mathbf{v} \\ \varepsilon_{eq} \mathbf{v} \end{Bmatrix} \quad ; \quad \mathscr{S} = \begin{Bmatrix} 0 \\ \mathbf{0} \\ 0 \\ \{\mathbf{0}\}_{1\leq\alpha\leq3} \\ \{(\mathbf{l}^p)^T \cdot \tilde{\mathbf{e}}^{(\alpha)}\}_{1\leq\alpha\leq3} \\ -\dot{\lambda} \mathbf{F}^T \cdot \frac{\partial \phi}{\partial \mathbf{q}} \cdot \mathbf{F} \\ \dot{\lambda} \end{Bmatrix}, \tag{59}$$

whereas the nonconservative term $\mathscr{B} \cdot \boldsymbol{\nabla} \mathscr{W}$ and the auxiliary vector $\mathscr{W}$ are defined as

$$\mathscr{B} \cdot \boldsymbol{\nabla} \mathscr{W} = \begin{Bmatrix} 0 \\ \mathbf{0} \\ 0 \\ \sum_{j,j\neq i} \left(\frac{\partial v_j}{\partial x_i} (\mathbf{F}^{-T})_{j\alpha} - (\mathbf{F}^{-T})_{i\alpha} \frac{\partial v_j}{\partial x_j} \right) \\ \sum_{j,j\neq i} \left(\frac{\partial v_j}{\partial x_i} (\mathbf{F}^{e^{-T}})_{jI} - (\mathbf{F}^{e^{-T}})_{iI} \frac{\partial v_j}{\partial x_j} \right) \\ -\alpha_{\alpha\beta} \frac{\partial v_j}{\partial x_j} \\ -\varepsilon_{eq} \frac{\partial v_j}{\partial x_j} \end{Bmatrix} \quad ; \quad \mathscr{W} = \begin{Bmatrix} \rho \\ \mathbf{v} \\ \boldsymbol{\sigma} \end{Bmatrix}. \tag{60}$$

System (58) has also well-defined shock jump relationships, which were derived in the hyperelastic case in [46,50], and are not repeated here. The closure of the above system is performed by a set of constitutive equations. The latter consists of its reversible contribution, expressed through the definition of Helmholtz's specific free energy (4), especially yielding the state laws (19), (20), (35). It also consists of its dissipative part, expressed through the yield function (26) and the plastic flow potential (25), yielding the plastic flow rule (27), the kinematic hardening evolution law (28) and complementarity conditions (29). Finally, System (58) must also be supplemented with appropriate initial and boundary conditions.

3. Lagrangian modeling of the thermo-mechanical initial boundary value problem

3.1. Lagrangian form of Helmholtz's specific free energy

In the Lagrangian setting, Helmholtz's specific free energy per unit mass W is also defined by summing its elastic, plastic and thermal contributions

$$W(\mathbf{C}^e, T, \boldsymbol{\alpha}) = W^e(\mathbf{C}^e, T) + W^p(\boldsymbol{\alpha}, T) + W^{th}(T), \tag{61}$$

where the specific elastically stored energy (recoverable) $W^e(\mathbf{C}^e, T)$ is now chosen to be a function of the elastic right Cauchy–Green strain tensor $\mathbf{C}^e$ (3), and of the temperature T. It should also be a convex function of $\mathbf{C}^e$, positive, and vanishes for $\mathbf{C}^e = \mathbf{1}$. In the same line with its Eulerian counterpart (4), it can be split into volumetric and isochoric parts, such that

$$W^e(\mathbf{C}^e, T) = W^H(J^e, T) + \bar{W}^e(\bar{\mathbf{C}}^e, T), \tag{62}$$

where the volumetric part $W^H(J^e, T)$ depends on the elastic jacobian determinant J^e and on the temperature T, while the isochoric component $\bar{W}^e(\bar{\mathbf{C}}^e, T)$ is a function of both the isochoric elastic Cauchy–Green strain tensor $\bar{\mathbf{C}}^e$ and the temperature T.

The specific plastically stored energy (not recoverable) W^p is also a convex function of the Lagrangian strain-like second order tensor $\boldsymbol{\alpha}$, related to the kinematic hardening, and of the temperature T. Finally, $W^{th}(T)$ is the specific thermally stored energy due to heat capacity, and is classically chosen after [62] as

$$W^{th}(T) = C_0 \left((T - T_0) - T \ln \frac{T}{T_0} \right), \tag{63}$$

where C_0 denotes some heat capacity per unit mass, and T_0 refer to some reference temperature.

3.2. Lagrangian writing of the Clausius–Duhem inequality

One defines the Lagrangian plastic velocity gradient

$$\mathcal{L}^p = \mathbf{F}^{-1} \cdot \mathbf{l}^p \cdot \mathbf{F} \tag{64}$$

as the pull-back of the plastic part of the Eulerian velocity gradient $\mathbf{l}^p$ (see Eq. (12)) to the initial configuration. Introducing Eq. (64) into the Eulerian expression of the internal dissipation (22) gives its Lagrangian form

$$\mathscr{D}_{\text{int}} = \mathfrak{M} : \mathcal{L}^p - \mathbf{Q} : \frac{d\boldsymbol{\alpha}}{dt} \geq 0, \tag{65}$$

where the *Lagrangian* Mandel-like stress tensor $\mathfrak{M}$, analog of the true Mandel stress tensor $\boldsymbol{\Sigma}$ defined in the intermediate configuration, is defined so that to be conjugate to $\mathcal{L}^p$ in the initial configuration

$$\mathfrak{M} = \mathbf{F}^T \cdot \boldsymbol{\tau} \cdot \mathbf{F}^{-T}. \tag{66}$$

It is also related to Piola–Kirchhoff stress tensors as

$$\mathfrak{M} = \mathbf{F}^T \cdot \mathbf{P} = \mathbf{C} \cdot \mathbf{S}, \tag{67}$$

where $\mathbf{P}$ and $\mathbf{S}$ are the first and second Piola–Kirchhoff stress tensors respectively. Since the elastic right Cauchy–Green strain tensor $\mathbf{C}^e$ (3) has been chosen to be an argument of the specific elastically stored energy (62), and following some analog Coleman-Noll procedure [58–60] in the Lagrangian case [5, Eq. (3)] as the one followed in Section 2.3, one first gets the following elastic law

$$\mathfrak{M} = (\mathbf{F}^p)^T \cdot \boldsymbol{\Sigma} \cdot (\mathbf{F}^p)^{-T}, \quad \boldsymbol{\Sigma} = 2\rho_0 \mathbf{C}^e \cdot \frac{\partial W}{\partial \mathbf{C}^e}, \tag{68}$$

where the Lagrangian Mandel-like stress tensor $\mathfrak{M}$ is the pull-back of the Mandel stress tensor $\boldsymbol{\Sigma}$ to the initial configuration. This procedure also gives the Lagrangian analog of the thermal state law (20). Observe that, according to Eq. (66), the Lagrangian Mandel-like stress tensor $\mathfrak{M}$ is not symmetric. Even for elastically isotropic constitutive response, for which the Mandel stress tensor $\boldsymbol{\Sigma}$ is symmetric, Eq. (68) shows that the Lagrangian Mandel-like stress tensor $\mathfrak{M}$ will not be symmetric as plastic strains develop, since $\mathbf{F}^p$ is not a rotation.

3.3. Lagrangian back stresses and evolution laws

One defines the Lagrangian back stresses $\mathfrak{Q}$ as

$$\mathfrak{Q} = \mathbf{C} \cdot \mathbf{Q}, \tag{69}$$

where $\mathbf{C}$ is the right Cauchy–Green strain tensor, such that the Mises effective stress be the same in both Eulerian and Lagrangian writings

$$\text{tr}[\text{dev}(\boldsymbol{\tau} - \mathbf{q}) \cdot \text{dev}(\boldsymbol{\tau} - \mathbf{q})] = \text{tr}[\text{dev}(\mathfrak{M} - \mathfrak{Q}) \cdot \text{dev}(\mathfrak{M} - \mathfrak{Q})], \tag{70}$$

where tr[·] denotes the trace operator. Next, following the class of Generalized Standard Materials [61], one introduces the Lagrangian plastic flow potential $\boldsymbol{\Phi}$ which we assume to be a convex function of the following set of arguments $(\mathfrak{M}, \mathfrak{Q})$, positive, and vanishes at zero. It also follows an Armstrong–Frederick-type [2,3] form, such that it reads

$$\boldsymbol{\Phi} = F + \frac{b}{2c}\mathfrak{Q} : \mathfrak{Q}. \tag{71}$$

The Lagrangian yield function $F(\mathfrak{M}, \mathfrak{Q}) \leq 0$ defines the elastic convex with Lagrangian quantities, and is chosen here of the form

$$F(\mathfrak{M}, \mathfrak{Q}) = \mathfrak{M}_{\text{eq}}(\mathfrak{M}, \mathfrak{Q}) - \sigma_y \leq 0, \tag{72}$$

where σ_y denotes the same tensile yield stress than in Eq. (26) thanks to the equality of square norms (70), and $\mathfrak{M}_{\text{eq}}(\boldsymbol{\tau} - \mathbf{q})$ some equivalent stress which is assumed to be a positively homogeneous function of degree one of $\mathfrak{M} - \mathfrak{Q}$. Applying the normality to $\boldsymbol{\Phi}$ (71), one gets the evolution equations

$$\mathcal{L}^p = \dot{\Lambda}\frac{\partial \boldsymbol{\Phi}}{\partial \mathfrak{M}} = \dot{\Lambda}\frac{\partial F}{\partial \mathfrak{M}} \tag{73}$$

$$\frac{d\boldsymbol{\chi}}{dt} = -\dot{\Lambda}\frac{\partial \boldsymbol{\Phi}}{\partial \mathfrak{Q}} = \dot{\Lambda}\left(\frac{\partial F}{\partial \mathfrak{M}} - \frac{b}{c}\mathfrak{Q}\right) \tag{74}$$

where $\dot{\Lambda}$ denotes the Lagrangian plastic multiplier, satisfying the complementarity conditions

$$\dot{\Lambda} \geq 0,\ F \leq 0,\ \dot{\Lambda}F = 0. \tag{75}$$

The flux-type variable $\frac{d\boldsymbol{\chi}}{dt}$, conjugate to the Lagrangian back stresses $\mathfrak{Q}$, has been introduced in Eqs. (74). Since the Lagrangian Mandel-like stress tensor $\mathfrak{M}$ is not symmetric, the Lagrangian plastic velocity gradient $\mathcal{L}^p$ also does not. With evolution laws (73)–(74) at hand, the internal dissipation (65) can be written of the form

$$\mathscr{D}_{\text{int}} = \dot{\Lambda}\left(\mathfrak{M} : \frac{\partial \boldsymbol{\Phi}}{\partial \mathfrak{M}} + \mathfrak{Q} : \frac{\partial \boldsymbol{\Phi}}{\partial \mathfrak{Q}}\right) \geq 0, \tag{76}$$

whose non-negativeness can be shown provided the Lagrangian plastic flow potential $\boldsymbol{\Phi}$ satisfies its aforementioned properties. Similarly to Eq. (34), the Lagrangian variable $\boldsymbol{\chi}$, whose rate is conjugate to the Lagrangian back stresses $\mathfrak{Q}$ (69) in the evolution Eq. (74), can enter the set of arguments of the plastic part of the Lagrangian Helmholtz specific free energy

$$W^p(\boldsymbol{\alpha}, T) = \tilde{W}^p(\boldsymbol{\chi}, T). \tag{77}$$

From the Lagrangian back stresses (69) and their associated evolution Eqs. (74), the second term of the internal dissipation (65) is rewritten as

$$\begin{aligned} -\rho_0 \frac{\partial W^p}{\partial \boldsymbol{\alpha}} : \frac{d\boldsymbol{\alpha}}{dt} &= -\rho_0 \frac{\partial \tilde{W}^p}{\partial \boldsymbol{\chi}} : \frac{\partial \boldsymbol{\chi}}{\partial \boldsymbol{\alpha}} : \frac{\partial \boldsymbol{\alpha}}{\partial \boldsymbol{\chi}} : \frac{d\boldsymbol{\chi}}{dt} \\ &= -\mathfrak{Q} : \frac{d\boldsymbol{\chi}}{dt} = \dot{\Lambda}\mathfrak{Q} : \frac{\partial \boldsymbol{\Phi}}{\partial \mathfrak{Q}} \end{aligned} \tag{78}$$

provided the following state law is defined

$$\mathfrak{Q} = \rho_0 \frac{\partial \tilde{W}^p}{\partial \boldsymbol{\chi}}. \tag{79}$$

Defining the plastic part of the Lagrangian Helmholtz specific free energy similarly as (38) gives

$$\tilde{W}^p(\boldsymbol{\chi}, T) = \frac{c}{2\rho_0}\boldsymbol{\chi} : \boldsymbol{\chi}, \tag{80}$$

yielding the relation

$$\mathfrak{Q} = c\boldsymbol{\chi}. \tag{81}$$

Notice that one also gets by identification

$$\boldsymbol{\chi} = \mathbf{C} \cdot \boldsymbol{\alpha}, \tag{82}$$

valid only with the expression (80) of the plastically stored specific energy. The evolution Eq. (74) then also takes the well-known Armstrong–Frederick form

$$\frac{d\boldsymbol{\chi}}{dt} = \dot{\Lambda}\left(\frac{\partial F}{\partial \mathfrak{M}} - b\boldsymbol{\chi}\right), \tag{83}$$

which is the Lagrangian analog of Eq. (40). The yield function F (72) being positively homogeneous of degree one, one gets [14]

$$\mathfrak{M}_{\text{eq}} = (\mathfrak{M} - \mathfrak{Q}) : \frac{\partial F}{\partial \mathfrak{M}}. \tag{84}$$

Introducing the evolution Eqs. (73) and (74) into the internal dissipation (76), and considering the yield criterion (72) as an equality, the internal dissipation finally reads

$$\mathscr{D}_{\text{int}} = \dot{\Lambda}\left(\sigma_y + \frac{b}{c}\mathfrak{Q} : \mathfrak{Q}\right) \geq 0. \tag{85}$$

Remark 2. Thanks to the square norm equality (70), the Eulerian (42) and Lagrangian (85) expressions of the internal dissipation can be deduced from each other. Accordingly, the Eulerian and Lagrangian plastic multiplier are equal, namely $\dot{\lambda} = \dot{\Lambda}$.

3.4. Relationship with the modeling of non-linear kinematic hardening based on the center-configuration

The Eulerian and Lagrangian modelings derived here can be related to the non-linear kinematic hardening based on the so-called center configuration introduced in [6,7]. Especially, the internal dissipation is written in such modeling as

$$\mathscr{D}_{\text{int}} = \boldsymbol{\Sigma} : \mathbf{L}^p - \mathbf{Q}^k : \mathbf{L}^k \geq 0, \tag{86}$$

where $\mathbf{Q}^k$ and $\mathbf{L}^k$ are quantities defined in the intermediate configuration, and following the notations of Mosler [5] as

$$\mathbf{Q}^k = 2\mathbf{C}^k \cdot \frac{\partial \psi^p}{\partial \mathbf{C}^k} \tag{87}$$

$$\mathbf{L}^k = (\mathbf{F}^k)^{-1} \cdot \frac{d\mathbf{F}^k}{dt}, \tag{88}$$

where $\mathbf{C}^k = (\mathbf{F}^k)^T \cdot \mathbf{F}^k$, $\mathbf{F}^k$ denotes the mapping from the intermediate configuration to the so-called center configuration, and ψ^p is the plastically stored energy. Equating the internal dissipation (86) with these defined in the initial (65) of current (22) settings (and accounting for (32)) yields

$$\begin{aligned}\mathbf{Q}^k : \mathbf{L}^k &= \left[(\mathbf{F}^p)^{-1} \cdot \mathbf{Q}^k \cdot (\mathbf{F}^p)^{-T}\right] : \left[(\mathbf{F}^p)^T \cdot \mathbf{L}^k \cdot \mathbf{F}^p\right] = \left[\mathbf{F}^e \cdot \mathbf{Q}^k \cdot (\mathbf{F}^e)^T\right] : \left[(\mathbf{F}^e)^{-T} \cdot \mathbf{L}^k \cdot (\mathbf{F}^e)^{-1}\right] \\ &= \mathbf{Q} : \frac{d\boldsymbol{\alpha}}{dt} = \mathbf{q} : \overset{\triangledown}{\mathbf{V}},\end{aligned}$$

such that these modelings are equivalent if

$$\mathbf{Q} = (\mathbf{F}^p)^{-1} \cdot \mathbf{Q}^k \cdot (\mathbf{F}^p)^{-T} \tag{89}$$

$$\frac{d\boldsymbol{\alpha}}{dt} = (\mathbf{F}^p)^T \cdot \mathbf{L}^k \cdot \mathbf{F}^p \tag{90}$$

$$\mathbf{q} = \mathbf{F}^e \cdot \mathbf{Q}^k \cdot (\mathbf{F}^e)^T \tag{91}$$

$$\overset{\triangledown}{\mathbf{V}} = (\mathbf{F}^e)^{-T} \cdot \mathbf{L}^k \cdot (\mathbf{F}^e)^{-1} \tag{92}$$

where Eqs. (90) and (92) can be deduced from each other using Eqs. (33) and (1), and the variables Ω and χ can be deduced from Eqs. (89) and (90) using Eqs. (69) and (82).

3.5. Lagrangian conservation laws

Let us consider now the initial configuration V_0 of the continuum body V, of boundary ∂V_0 and outward unit normal $\mathbf{N}$. Its motion is described by the mapping $\boldsymbol{\phi}(\mathbf{X}, t)$, where $\mathbf{X} \in V_0$ denotes the position of a material point in the initial configuration. The following set of conservation laws should be satisfied

$$\frac{\partial J}{\partial t} - \text{DIV}\,(\mathbf{H}^T \cdot \mathbf{v}) = 0 \tag{93}$$

$$\frac{\partial \mathbf{F}}{\partial t} - \text{DIV}\,(\mathbf{v} \otimes \mathbf{1}) = 0 \tag{94}$$

$$\frac{\partial (\rho_0 \mathbf{v})}{\partial t} - \text{DIV}\,\mathbf{P} = \mathbf{0} \tag{95}$$

$$\frac{\partial (\rho_0 \mathcal{E})}{\partial t} - \text{DIV}\,(\mathbf{P}^T \cdot \mathbf{v}) = 0 \tag{96}$$

where the material divergence operator DIV is computed with respect to the set of initial coordinates $\mathbf{X}$. Eq. (93) follows from the conservation of the volume map [63], and is a conservation law written on the jacobian determinant J, $\mathbf{H} = J\mathbf{F}^{-T}$ denoting the cofactor of the deformation gradient $\mathbf{F}$. Eq. (94) is the conservation of the deformation gradient, and follows from the geometrical compatibility between the deformation gradient and the velocity field

$$\frac{\partial \mathbf{F}}{\partial t} = \frac{\partial \mathbf{v}}{\partial \mathbf{X}}, \tag{97}$$

from which Eq. (9) also follows. Notice also that the two above geometrical equations can be supplemented with the conservation of the area map written on the cofactor $\mathbf{H}$, as shown in [63], but is not considered here. Eq. (95) is the conservation of linear momentum (written in the absence of body forces here), $\rho_0(\mathbf{X}) = \rho(\mathbf{X}, t = 0)$ is the reference mass density, and $\mathbf{P}$ denotes the first Piola–Kirchhoff stress tensor. Finally, Eq. (96) is the conservation of the total energy (in the absence of heat conduction and heat source), and $\mathcal{E}$ denotes the Lagrangian total energy per unit mass defined as

$$\mathcal{E} = E + \frac{|\mathbf{v}|^2}{2}, \tag{98}$$

summing the Lagrangian specific internal energy E and the specific kinetic energy.

3.6. First order system of conservation laws

Gathering Eqs. (93), (94), (95), and (96), allows to form the system of conservation laws

$$\frac{\partial \mathcal{U}}{\partial t} + \mathrm{DIV}\, \mathcal{F}(\mathcal{W}) = 0, \tag{99}$$

where $\mathcal{U}$, $\mathcal{F}$, and $\mathcal{W}$ denote the vector of conserved quantities, the flux vector, and the vector of auxiliary quantities respectively. These quantities are defined as

$$\mathcal{U} = \begin{Bmatrix} J \\ \mathbf{F} \\ \rho_0 \mathbf{v} \\ \rho_0 \mathcal{E} \end{Bmatrix} \quad ; \quad \mathcal{F} = \begin{Bmatrix} -\mathbf{H}\cdot\mathbf{v} \\ -\mathbf{v}\otimes\mathbf{1} \\ -\mathbf{P} \\ -\mathbf{P}^T\cdot\mathbf{v} \end{Bmatrix} \quad ; \quad \mathcal{W} = \begin{Bmatrix} J \\ \mathbf{P} \\ \mathbf{v} \\ T \end{Bmatrix} \tag{100}$$

where the temperature T is introduced in the auxiliary vector $\mathcal{W}$. Notice that no source term appears in System (99) in the Lagrangian case, leading to a system of conservations laws. Conversely, the Eulerian system (58) includes a source term containing the plastic flow. System (99) reduces to the well-known Rankine–Hugoniot jump conditions across any discontinuity of fields

$$S[\mathcal{U}] = [\mathcal{F}]\cdot\mathbf{N}, \tag{101}$$

where $\mathbf{N}$ is the material normal of the discontinuity surface moving at speed S, and $[\bullet]$ denotes the jump of the quantity $(\bullet)$ across the discontinuity, such that $[\bullet] = (\bullet)^+ - (\bullet)^-$.

The closure of the above system of conservation laws (99) is performed by a set of constitutive equations. The latter consists of its reversible contribution, expressed through the definition of the Lagrangian Helmholtz's specific free energy (61), especially yielding the state laws (20), (68), (79). It also consists of its dissipative part, expressed through the yield function (72) and the plastic flow potential (71), yielding the plastic flow rule (73), the kinematic hardening evolution law (74) and complementarity conditions (75). Finally, System (99) must also be supplemented with appropriate initial and boundary conditions.

4. Variational formulation of the Eulerian thermo-mechanical local constitutive problem

4.1. Godunov splitting solution scheme, and pre-processing for the source step

In the Eulerian setting, the first order system of Eqs. (58) includes a source term, with particular contributions related to the transport equations of the elastic part of the kinematics (55), and plastic variables (56), (57). From the computational viewpoint, a convenient solution process follows from the Godunov splitting [64], which amounts to first solve the homogeneous part of system (58), then solve a set of ordinary differential equations including the source term, i.e. without convection terms, taking the solution of the first step as an initial condition. Over a discrete time increment $[t_n, t_{n+1}]$, the solution process is thus of the form

$$\mathbf{U}^{n+1} = \mathbf{S}^{(\Delta t)}\mathbf{C}^{(\Delta t)}\mathbf{U}^n, \tag{102}$$

where $\mathbf{U}$ denotes discrete quantities associated with the vector $\mathscr{U}$ (see Eq. (59)), but defined via the numerical scheme described in Section 6. The discrete operators $\mathbf{C}^{(\Delta t)}$ and $\mathbf{S}^{(\Delta t)}$ depend on the time step size Δt, are related to the convection and source steps respectively, and chained so that to update the solution at time t_{n+1}.

Since the source term is active only for these cells where plasticity is progressing, the solution at the end of the first step will be called *a trial elastic one*: each grid cell is provided with the trial elastic state $\{(\mathbf{F}^e)^{-T}, \boldsymbol{\alpha}, \varepsilon_{eq}\}_{\mathrm{trial}}$. However, $\mathbf{V}$ appears a better input variable than $\boldsymbol{\alpha}$ to build a constitutive update, according to the Eulerian constitutive modeling described in Section 2. Observe that from Eqs. (32) and (36), one gets the equality

$$\tilde{\mathbf{q}} : \frac{d\mathbf{V}}{dt} = \mathbf{q} : \overset{\triangledown}{\mathbf{V}}. \tag{103}$$

During the source step, the computation of the source term is performed at fixed strain and rotation rates, i.e. $\mathbf{L} = \mathbf{0}, \dot{\mathbf{F}} = \mathbf{0}$. Hence, the identity $\frac{d\mathbf{V}}{dt} = \overset{\triangledown}{\mathbf{V}}\Big|_{\mathbf{L}=\mathbf{0}}$ holds during the stage of computation of the source term. As a consequence of Eq. (103), $\tilde{\mathbf{q}} = \mathbf{q}$ also holds during the source step. If the plastic specific energy $\tilde{w}^p(\mathbf{V}, T)$ in Eq. (34) is defined with a quadratic expression of $\mathbf{V}$, analog to that of $w^p(\boldsymbol{\alpha}, T)$ given in Eq. (38), then provided Eq. (39), one can identify a one-to-one mapping between the variables $\mathbf{V}$ and $\boldsymbol{\alpha}$ at fixed value of the deformation gradient $\mathbf{F}_{n+1}$:

$$\mathbf{V} = \mathbf{F}_{n+1}\cdot\boldsymbol{\alpha}\cdot\mathbf{F}_{n+1}^T. \tag{104}$$

Consequently, after the convection step, the trial kinematic variable is updated with the true kinematics:

$$\mathbf{V}_{\mathrm{trial}} = \mathbf{F}_{n+1}\cdot\boldsymbol{\alpha}_{\mathrm{trial}}\cdot\mathbf{F}_{\mathrm{n+1}}^T, \tag{105}$$

before doing a constitutive update. Observe also that if Eq. (104) is introduced in Eq. (40), one recognizes a well-known Armstrong–Frederick law

$$\frac{d\mathbf{V}}{dt} = \overset{\triangledown}{\mathbf{V}}\Big|_{\mathbf{L}=\mathbf{0}} = \dot{\lambda}\left(\frac{\partial f}{\partial \boldsymbol{\tau}} - b\mathbf{V}\right)\Big|_{\mathbf{L}=\mathbf{0}}, \tag{106}$$

but here only valid during the source step, i.e. at fixed strain and rotation rates.

4.2. Continuous variational formulation

Following [36], one introduces the following Eulerian functional

$$\mathscr{L}(\dot{\mathscr{X}},\beta;\mathscr{X}) = D + \beta\frac{d}{dt}(T\eta + w((\mathbf{C}^e)^{-1},T,\mathbf{V}) - e), \tag{107}$$

which is built from the functional introduced in [19]

$$D = \frac{de}{dt} - T\frac{d\eta}{dt} + \frac{\mathscr{D}_{\text{int}}}{\rho_0} = \dot{w}_\tau + \frac{\mathscr{D}_{\text{int}}}{\rho_0}, \tag{108}$$

which sums the reversible power per unit mass received by the system $\dot{w}_\tau$ and the internal dissipation per unit mass $\mathscr{D}_{\text{int}}/\rho_0$, and from the residual of the rate of the Legendre transform of the Eulerian Helmholtz specific free energy $w((\mathbf{C}^e)^{-1},T,\mathbf{V})$, enforced to vanish through the Lagrange multiplier β. Notice that the specific internal dissipation $\mathscr{D}_{\text{int}}/\rho_0$ appearing in Eq. (108) takes the place in rate-independent plasticity of some dissipation pseudo-potential φ including rate effects in viscoplasticity, see [14,36,56,65]. In the Eulerian functional (107), it is assumed that the time rates of the specific internal energy de/dt (47), of the cobasis vectors $d\mathbf{F}^{-T}/dt$ and of the (trial) elastic cobasis vectors $d(\mathbf{F}^e)^{-T}/dt$ are known from the solution of the homogeneous part of the set of Eulerian balance laws (58), and that the state vector $\mathscr{X} = \{e,(\mathbf{C}^e)^{-1},\eta,\mathbf{V},T\}$ is also assumed to be known and fixed here.

Following the work of Mosler and co-workers [5,13–15], the flow rule and the evolution equations are parameterized on the one hand with the Eulerian plastic multiplier $\dot{\lambda}$, and on the other hand with some pseudo-stresses, which are *a priori* different from their physical counterparts, and serve for the parameterization of the flow direction. In the present Eulerian setting, the flow direction appearing in Eqs. (27) and (28) is computed with the pseudo-Kirchhoff stresses $\tilde{\boldsymbol{\tau}}$ such that

$$\frac{\partial f}{\partial \boldsymbol{\tau}} = \left.\frac{\partial f}{\partial \boldsymbol{\tau}}\right|_{\tilde{\boldsymbol{\tau}}}. \tag{109}$$

The same flow direction is obtained with these pseudo-stresses provided the equivalent stress measure $\tau_{\text{eq}}(\boldsymbol{\tau},\mathbf{q})$ defining the shape of the yield function is a positively homogeneous function of degree one, namely

$$\tau_{\text{eq}}(c\mathbf{A}) = c\tau_{\text{eq}}(\mathbf{A}), \quad \forall \mathbf{A},\ \forall c\in\mathbb{R}^+, \tag{110}$$

although they are different from their physical counterpart, i.e. $\tilde{\boldsymbol{\tau}} \neq (\boldsymbol{\tau}-\mathbf{q})$.

Let us start expressing the Eulerian functional (107) with this parameterization. Especially, the combination of Eqs. (14), (17), (19), and accounting for the evolution laws (27) and (28), gives the expression of the time derivative of the Eulerian Helmholtz specific free energy

$$\begin{aligned}\frac{dw}{dt} &= \frac{\boldsymbol{\tau}:\mathbf{d}}{\rho_0} + \frac{1}{\rho_0}\left[(-\boldsymbol{\tau}+\mathbf{q}):\left.\frac{\partial f}{\partial\boldsymbol{\tau}}\right|_{\tilde{\boldsymbol{\tau}}} - \frac{b}{c}\mathbf{q}:\mathbf{q}\right]\dot{\lambda} + \frac{\partial w}{\partial T}\frac{dT}{dt}\\ &= \frac{\boldsymbol{\tau}:\mathbf{d}}{\rho_0} + \frac{\partial w}{\partial\dot{\lambda}}\dot{\lambda} + \frac{\partial w}{\partial T}\frac{dT}{dt}\end{aligned} \tag{111}$$

Introducing Eq. (111) into the Eulerian functional (107), and accounting for the Eulerian expression of the internal dissipation (42), one gets

$$\begin{aligned}\mathscr{L} = \beta\frac{\boldsymbol{\tau}:\mathbf{d}}{\rho_0} &+ \frac{de}{dt}(1-\beta) + (-T+\beta T)\frac{d\eta}{dt} + \beta\left(\eta + \frac{\partial w}{\partial T}\right)\frac{dT}{dt}\\ &+ \frac{\dot{\lambda}}{\rho_0}\left[\sigma_y + (1-\beta)\frac{b}{c}\mathbf{q}:\mathbf{q} + \beta(-\boldsymbol{\tau}+\mathbf{q}):\left.\frac{\partial f}{\partial\boldsymbol{\tau}}\right|_{\tilde{\boldsymbol{\tau}}}\right].\end{aligned} \tag{112}$$

Fixing $\mathbf{d}=\mathbf{0}$ to be consistent with Section 4.1, the stationarity conditions of the Eulerian functional (112) are computed with respect to the specific entropy rate $d\eta/dt \equiv \dot{\eta}$, the temperature rate $dT/dt \equiv \dot{T}$, the Eulerian plastic multiplier $\dot{\lambda}$, the Eulerian Kirchhoff pseudo-stresses $\tilde{\boldsymbol{\tau}}$, and the Lagrange multiplier β

$$\frac{\partial\mathscr{L}}{\partial\dot{\eta}} = -T+\beta T = 0 \tag{113}$$

$$\frac{\partial\mathscr{L}}{\partial\dot{T}} = \beta\left(\eta + \frac{\partial w}{\partial T}\right) = 0 \tag{114}$$

$$\frac{\partial\mathscr{L}}{\partial\dot{\lambda}} = \frac{1}{\rho_0}\left[\sigma_y + (1-\beta)\frac{b}{c}\mathbf{q}:\mathbf{q} + \beta(-\boldsymbol{\tau}+\mathbf{q}):\left.\frac{\partial f}{\partial\boldsymbol{\tau}}\right|_{\tilde{\boldsymbol{\tau}}}\right] = 0 \tag{115}$$

$$\frac{\partial\mathscr{L}}{\partial\tilde{\boldsymbol{\tau}}} = \frac{\dot{\lambda}\beta}{\rho_0}(-\boldsymbol{\tau}+\mathbf{q}):\left.\frac{\partial^2 f}{\partial\boldsymbol{\tau}\partial\boldsymbol{\tau}}\right|_{\tilde{\boldsymbol{\tau}}} = 0 \tag{116}$$

$$\frac{\partial\mathscr{L}}{\partial\beta} = \frac{d}{dt}(T\eta + w((\mathbf{C}^e)^{-1},T,\mathbf{V}) - e) = 0 \tag{117}$$

The optimization problem defined with the Eulerian functional (107) thus reads

$$\mathscr{W} = \underset{\dot{\eta},\dot{T},\beta}{\text{stat}}\ \underset{\dot{\lambda},\tilde{\boldsymbol{\tau}}}{\text{inf}}\ \mathscr{L}|_{\mathbf{d}=0} \tag{118}$$

The stationarity with respect to $\dot{\eta}$ (113) gives the expected result of the Lagrange multiplier which is equal to unity, i.e. $\beta = 1$. Substitution of this Lagrange multiplier into Eqs. (114), (115) and (116), namely the stationarities with respect to the temperature rate, the Eulerian plastic multiplier and the Kirchhoff pseudo-stresses, and accounting for the identity (41), one gets

$$\eta = -\frac{\partial w}{\partial T} \tag{119}$$

$$\frac{1}{\rho_0}\left[\sigma_y + (-\boldsymbol{\tau} + \mathbf{q}) : \left.\frac{\partial f}{\partial \boldsymbol{\tau}}\right|_{\tilde{\boldsymbol{\tau}}}\right] = -\frac{f}{\rho_0} = 0 \tag{120}$$

$$\frac{\dot{\lambda}}{\rho_0}(-\boldsymbol{\tau} + \mathbf{q}) : \left.\frac{\partial^2 f}{\partial \boldsymbol{\tau}\partial \boldsymbol{\tau}}\right|_{\tilde{\boldsymbol{\tau}}} = 0 \tag{121}$$

which are the definition of the specific entropy (119), the opposite of the Eulerian expression of the yield function (up to the inverse of the initial mass density) (120) which vanishes during the plastic flow, and the enforcement of the correct flow direction (121) compatible with the stresses.

Once the optimization (118) has been performed, the stresses are obtained by computing the partial derivative of the optimized Eulerian functional $\mathscr{W}$ with respect to the Eulerian strain rate tensor $\mathbf{d}$:

$$\frac{\partial \mathscr{W}}{\partial \mathbf{d}} = \frac{\boldsymbol{\tau}}{\rho_0}. \tag{122}$$

Observe that Eq. (122) results from a chain derivative of the specific free energy w involving $(\mathbf{C}^e)^{-1}$, and is equivalent to Eq. (19).

4.3. A first order accurate discrete variational constitutive update

From the continuous variational principle written in the Eulerian setting, an incremental variational constitutive update is now derived. Consider a discrete time increment $[t_n, t_{n+1}]$, the solution of the first step of the splitting gives the trial state vector $\mathscr{X}_{\text{trial}} = \left\{\{\eta, T, (\mathbf{C}^e)^{-1}, \mathbf{V}\}_{\text{trial}}, \{e, \mathbf{F}^{-T}\}_{n+1}\right\}$, where the data $\{e, \mathbf{F}^{-T}\}_{n+1}$ are final ones since they will remain fixed during the second step of the splitting scheme, and $\eta_{\text{trial}} = \eta_n$ because the first step is adiabatic by construction. An incremental functional $\mathscr{I}(\mathscr{X}_{n+1}, \beta_{n+1}; \mathscr{X}_{\text{trial}})$ is sought in such a way that it approximates the integral of the Eulerian functional $\mathscr{L}$ (107) over the time increment Δt:

$$\begin{aligned} &\int_{t_n}^{t_{n+1}} \mathscr{L}(\dot{\mathscr{X}}(\tau), \beta(\tau); \mathscr{X}(\tau)) d\tau \approx \mathscr{I}(\mathscr{X}_{n+1}, \beta_{n+1}; \mathscr{X}_{\text{trial}}) \\ &\mathscr{I}(\mathscr{X}_{n+1}, \beta_{n+1}; \mathscr{X}_{\text{trial}}) = \Delta e - T_n \Delta \eta + \frac{1}{\rho_0}\int_{t_n}^{t_{n+1}} \mathscr{D}_{\text{int}}(\tau) d\tau + \beta_{n+1}\Delta(T\eta + w((\mathbf{C}^e)^{-1}, T, \mathbf{V}) - e) \end{aligned} \tag{123}$$

where the operator $\Delta(\cdot) = (\cdot)_{n+1} - (\cdot)_n$ denotes the finite difference between the values of the quantity $(\cdot)$ evaluated at times t_{n+1} and t_n, and the integral of the internal dissipation over the time increment is approximated with a backward-Euler scheme as suggested in [5]:

$$\int_{t_n}^{t_{n+1}} \mathscr{D}_{\text{int}}(\tau) d\tau \approx \Delta\lambda\sigma_y + \Delta\lambda \frac{b}{c}\mathbf{q}_{n+1} : \mathbf{q}_{n+1} \tag{124}$$

leading to a first order accurate integration scheme. Moreover, since the temperature appearing in the second term of Eq. (123) is evaluated at time t_n, the numerical scheme here derived thus appears to be semi-implicit. The incremental Eulerian functional (123) is thus rewritten as

$$\mathscr{I} = \Delta e(1 - \beta_{n+1}) + (-T_n + \beta_{n+1}T_{n+1})\eta_{n+1} + (1 - \beta_{n+1})T_n\eta_n + \frac{\Delta\lambda}{\rho_0}\left(\sigma_y + \frac{b}{c}\mathbf{q}_{n+1} : \mathbf{q}_{n+1}\right) + \beta_{n+1}\Delta w, \tag{125}$$

where $\mathbf{q}_{n+1}$ is defined by its associated state law (35), consistently with remarks of Section 4.1, and w_{n+1} is a function of its arguments (see Eq. (4)) expressed at time t_{n+1}. Other quantities appearing in Eq. (125) are independent ones.

The incremental variational update takes thus the following form

$$\mathscr{J}_{n+1} = \underset{(\eta, T, \beta)_{n+1}}{\text{stat}} \quad \inf_{\Delta\lambda, \tilde{\boldsymbol{\tau}}_{n+1}} \mathscr{I}(\mathscr{X}_{n+1}, \beta_{n+1}; \mathscr{X}_{\text{trial}}) \tag{126}$$

where the incremental functional (125) is optimized with respect to the updated specific entropy η_{n+1} and temperature T_{n+1}, the increment of Eulerian plastic multiplier $\Delta\lambda$, the updated Kirchhoff pseudo-stresses $\tilde{\boldsymbol{\tau}}_{n+1}$ and Lagrange multiplier β_{n+1}. The stationarity conditions in the Eulerian discrete case read as

$$\frac{\partial \mathscr{I}}{\partial \eta_{n+1}} = -T_n + \beta_{n+1}T_{n+1} = 0 \tag{127}$$

$$\frac{\partial \mathscr{I}}{\partial T_{n+1}} = \beta_{n+1}\left(\eta_{n+1} + \left.\frac{\partial w}{\partial T}\right|_{n+1}\right) = 0 \tag{128}$$

$$\frac{\partial \mathscr{I}}{\partial \Delta\lambda} = \frac{1}{\rho_0}\left(\sigma_y + \frac{b}{c}\mathbf{q}_{n+1} : \mathbf{q}_{n+1}\right) + \frac{2b\Delta\lambda}{\rho_0}\mathbf{q}_{n+1} : \left.\frac{\partial \mathbf{V}}{\partial \Delta\lambda}\right|_{n+1} + \beta_{n+1}\frac{\partial w}{\partial \Delta\lambda} = 0 \tag{129}$$

$$\frac{\partial \mathscr{I}}{\partial \tilde{\boldsymbol{\tau}}_{n+1}} = \frac{2\Delta\lambda b}{\rho_0}\mathbf{q}_{n+1} : \left.\frac{\partial \mathbf{V}}{\partial \tilde{\boldsymbol{\tau}}}\right|_{n+1} + \beta_{n+1}\frac{\partial w}{\partial \tilde{\boldsymbol{\tau}}_{n+1}} = 0 \tag{130}$$

$$\frac{\partial \mathscr{I}}{\partial \beta_{n+1}} = \Delta(T\eta + w - e) = 0 \tag{131}$$

The stationarity with respect to the updated specific entropy η_{n+1} (127) gives the updated value of the Lagrange multiplier

$$\beta_{n+1} = \frac{T_n}{T_{n+1}}, \tag{132}$$

which is not equal to unity anymore, but is close to it, especially since the absolute temperatures are considered here. Accordingly, Eq. (128) gives the discrete updated expression of the specific entropy:

$$\eta_{n+1} = -\left.\frac{\partial W}{\partial T}\right|_{n+1}. \tag{133}$$

Next, from Eq. (11), setting $\dot{\mathbf{F}} = 0$, and hence setting the Eulerian velocity gradient $\mathbf{L}$ to zero after Eq. (9), and introducing the Eulerian plastic flow rule (27) accounting for Eq. (30), one gets

$$\frac{d(\mathbf{F}^e)^{-1}}{dt} = \dot{\lambda}(\mathbf{F}^e)^{-1} \cdot \frac{\partial f}{\partial \boldsymbol{\tau}}, \tag{134}$$

which is approximated by

$$(\mathbf{F}^e)^{-1}_{n+1} = (\mathbf{F}^e)^{-1}_{\text{trial}} \cdot \exp\left(\Delta\lambda \left.\frac{\partial f}{\partial \boldsymbol{\tau}}\right|_{\tilde{\boldsymbol{\tau}}_{n+1}}\right), \tag{135}$$

where the parameterization through the Eulerian pseudo-Kirchhoff stresses $\tilde{\boldsymbol{\tau}}_{n+1}$ has been used. From Eq. (135), the updated inverse of the elastic right Cauchy–Green strain tensor reads as

$$(\mathbf{C}^e)^{-1}_{n+1} = (\mathbf{F}^e)^{-1}_{\text{trial}} \cdot \exp\left(2\Delta\lambda \left.\frac{\partial f}{\partial \boldsymbol{\tau}}\right|_{\tilde{\boldsymbol{\tau}}_{n+1}}\right) \cdot (\mathbf{F}^e)^{-T}_{\text{trial}} \tag{136}$$

since the pseudo-Kirchhoff stresses $\tilde{\boldsymbol{\tau}}$ and their physical counterparts $\boldsymbol{\tau}$ are symmetric. Besides, a time discretization of the evolution law (106) is performed with a backward Euler time scheme, hence still following [5], from which discrete expressions of $\mathbf{V}_{n+1}$ and its derivatives follow

$$\mathbf{V}_{n+1} = \frac{\mathbf{V}_{\text{trial}} + \Delta\lambda \left.\frac{\partial f}{\partial \boldsymbol{\tau}}\right|_{\tilde{\boldsymbol{\tau}}_{n+1}}}{1 + b\Delta\lambda} \tag{137}$$

$$\frac{\partial \mathbf{V}_{n+1}}{\partial \Delta\lambda} = \frac{1}{1 + b\Delta\lambda}\left(\left.\frac{\partial f}{\partial \boldsymbol{\tau}}\right|_{\tilde{\boldsymbol{\tau}}_{n+1}} - b\mathbf{V}_{n+1}\right) \tag{138}$$

$$\left.\frac{\partial \mathbf{V}}{\partial \tilde{\boldsymbol{\tau}}}\right|_{n+1} = \frac{\Delta\lambda}{1 + b\Delta\lambda} \left.\frac{\partial^2 f}{\partial \boldsymbol{\tau}\partial \boldsymbol{\tau}}\right|_{\tilde{\boldsymbol{\tau}}_{n+1}} \tag{139}$$

where $\mathbf{V}_{\text{trial}}$ is evaluated after the convection step. From Eqs. (136), and Eqs. (137)–(139), the partial derivative of Helmholtz's specific free energy w with respect to the increment of Eulerian plastic multiplier $\Delta\lambda$ is computed as

$$\left.\frac{\partial w}{\partial \Delta\lambda}\right|_{n+1} = \left.\frac{\partial w^e}{\partial \Delta\lambda}\right|_{n+1} + \left.\frac{\partial w^p}{\partial \Delta\lambda}\right|_{n+1} \tag{140}$$

$$\left.\frac{\partial w^e}{\partial \Delta\lambda}\right|_{n+1} = \left[2(\mathbf{F}^e)^{-T}_{\text{trial}} \cdot \left.\frac{\partial w^e}{\partial (\mathbf{C}^e)^{-1}}\right|_{n+1} \cdot (\mathbf{F}^e)^{-1}_{\text{trial}}\right] : D\exp\left(2\Delta\lambda \left.\frac{\partial f}{\partial \boldsymbol{\tau}}\right|_{\tilde{\boldsymbol{\tau}}_{n+1}}\right) : \left.\frac{\partial f}{\partial \boldsymbol{\tau}}\right|_{\tilde{\boldsymbol{\tau}}_{n+1}} \tag{141}$$

$$\left.\frac{\partial w^p}{\partial \Delta\lambda}\right|_{n+1} = \frac{\mathbf{q}_{n+1}}{\rho_0(1 + b\Delta\lambda)} : \left(\left.\frac{\partial f}{\partial \boldsymbol{\tau}}\right|_{\tilde{\boldsymbol{\tau}}_{n+1}} - b\mathbf{V}_{n+1}\right) \tag{142}$$

where $D\exp(\mathbf{A})$ stands for the derivative of the exponential mapping of the matrix $\mathbf{A}$, computed with standard procedures [66]. Similarly, the partial derivative of specific free energy w with respect to the updated Eulerian Kirchhoff pseudo-stresses $\tilde{\boldsymbol{\tau}}_{n+1}$ reads

$$\left.\frac{\partial w}{\partial \tilde{\boldsymbol{\tau}}}\right|_{n+1} = \left.\frac{\partial w^e}{\partial \tilde{\boldsymbol{\tau}}}\right|_{n+1} + \left.\frac{\partial w^p}{\partial \tilde{\boldsymbol{\tau}}}\right|_{n+1} \tag{143}$$

$$\left.\frac{\partial w^e}{\partial \tilde{\boldsymbol{\tau}}}\right|_{n+1} = \Delta\lambda\left[2(\mathbf{F}^e)^{-T}_{\text{trial}} \cdot \left.\frac{\partial w^e}{\partial (\mathbf{C}^e)^{-1}}\right|_{n+1} \cdot (\mathbf{F}^e)^{-1}_{\text{trial}}\right] : D\exp\left(2\Delta\lambda \left.\frac{\partial f}{\partial \boldsymbol{\tau}}\right|_{\tilde{\boldsymbol{\tau}}_{n+1}}\right) : \left.\frac{\partial^2 f}{\partial \boldsymbol{\tau}\partial \boldsymbol{\tau}}\right|_{\tilde{\boldsymbol{\tau}}_{n+1}} \tag{144}$$

$$\left.\frac{\partial w^p}{\partial \tilde{\boldsymbol{\tau}}}\right|_{n+1} = \frac{\Delta\lambda}{\rho_0(1 + b\Delta\lambda)}\mathbf{q}_{n+1} : \left.\frac{\partial^2 f}{\partial \boldsymbol{\tau}\partial \boldsymbol{\tau}}\right|_{\tilde{\boldsymbol{\tau}}_{n+1}} \tag{145}$$

Introducing Eqs. (140), (141) and (142) into the discrete stationarity Eq. (129), and Eqs. (143), (144) and (145) into the discrete stationarity Eq. (130), one can check their consistency

$$\lim_{\Delta t \to 0} \frac{\partial \mathscr{I}}{\partial \Delta\lambda} = \frac{1}{\rho_0}\left[(-\boldsymbol{\tau} + \mathbf{q})_{n+1} : \left.\frac{\partial f}{\partial \boldsymbol{\tau}}\right|_{\tilde{\boldsymbol{\tau}}_{n+1}} + \sigma_y\right] = -\frac{f_{n+1}}{\rho_0} = 0 \tag{146}$$

$$\lim_{\Delta t \to 0} \frac{\partial \mathscr{I}}{\partial \tilde{\boldsymbol{\tau}}_{n+1}} = \frac{\Delta\lambda}{\rho_0}\left[(-\boldsymbol{\tau} + \mathbf{q})_{n+1} : \left.\frac{\partial^2 f}{\partial \boldsymbol{\tau}\partial \boldsymbol{\tau}}\right|_{\tilde{\boldsymbol{\tau}}_{n+1}}\right] = 0 \tag{147}$$

with their continuous counterparts (120) and (121).

In the case of a splitting of the elastic energy w^e into isochoric and volumetric contributions (7), the partial derivative $\frac{\partial w^e}{\partial (\mathbf{C}^e)^{-1}}$ is computed as

$$\frac{\partial w^e}{\partial (\mathbf{C}^e)^{-1}} = \frac{\partial \bar{w}^e}{\partial (\mathbf{C}^e)^{-1}} - \frac{J^e}{2}\frac{\partial w^H}{\partial J^e}\mathbf{C}^e, \tag{148}$$

where $P = \rho_0 \frac{\partial w^H}{\partial J^e}$ is the hydrostatic pressure.

Gathering Eqs. (129), (130) and (131), a balanced system of equations is defined written on the unknown vector

$$\bar{\mathscr{X}}_{n+1} = \{T, \Delta\lambda, \tilde{\boldsymbol{\tau}}\}_{n+1}. \tag{149}$$

Once $\bar{\mathscr{X}}_{n+1}$ is known, the state vector $\mathscr{X}_{n+1}$ can be updated. If a Newton method is used, the following linear system of equations should be solved at each iteration k of the iterative process

$$\mathbf{K}^{(k)} \delta\bar{\mathscr{X}}^{(k)} = -\mathbf{R}^{(k)}, \tag{150}$$

with $\delta\bar{\mathscr{X}}^{(k)} = \bar{\mathscr{X}}^{(k+1)} - \bar{\mathscr{X}}^{(k)}$, and with the Hessian matrix and the residual vector expressed as

$$\mathbf{K}^{(k)} = \begin{bmatrix} \frac{\partial^2 \mathscr{I}}{\partial T^2} & \frac{\partial^2 \mathscr{I}}{\partial T \partial \Delta\lambda} & \frac{\partial^2 \mathscr{I}}{\partial T \partial \tilde{\boldsymbol{\tau}}} \\ \frac{\partial^2 \mathscr{I}}{\partial \Delta\lambda \partial T} & \frac{\partial^2 \mathscr{I}}{\partial \Delta\lambda^2} & \frac{\partial^2 \mathscr{I}}{\partial \Delta\lambda \partial \tilde{\boldsymbol{\tau}}} \\ \frac{\partial^2 \mathscr{I}}{\partial \tilde{\boldsymbol{\tau}} \partial T} & \frac{\partial^2 \mathscr{I}}{\partial \tilde{\boldsymbol{\tau}} \partial \Delta\lambda} & \frac{\partial^2 \mathscr{I}}{\partial \tilde{\boldsymbol{\tau}} \partial \tilde{\boldsymbol{\tau}}} \end{bmatrix}, \quad \mathbf{R}^{(k)} = \begin{pmatrix} \frac{\partial \mathscr{I}}{\partial T} \\ \frac{\partial \mathscr{I}}{\partial \Delta\lambda} \\ \frac{\partial \mathscr{I}}{\partial \tilde{\boldsymbol{\tau}}} \end{pmatrix}^{(k)}. \tag{151}$$

Notice also that by construction the Hessian matrix is symmetric. Its entries associated with unknowns $\{\Delta\lambda, \tilde{\boldsymbol{\tau}}\}$ can be computed analogously to these already detailed in [14,15]. Other iterative strategies can also be used, such as partitioned schemes [67,68] which are not detailed here. Finally, it is convenient to parameterize the pseudo-stresses $\tilde{\boldsymbol{\tau}}$ in the solution process with spherical coordinates to enforce $\|\tilde{\boldsymbol{\tau}}\| = 1$, as shown in [15], which allows to eliminate any singularity of the Hessian matrix.

In order to account for the yield threshold, a prediction–correction algorithm is followed, whose thermoelastic prediction is performed by solving Eq. (131) solely to get the trial temperature T_{trial}, from which, in addition to the trial inverse of the elastic right Cauchy–Green strain tensor $(\mathbf{C}^e_{\text{trial}})^{-1} = (\mathbf{F}^{\mathbf{e}})^{-1}_{\text{trial}} \cdot (\mathbf{F}^{\mathbf{e}})^{-T}_{\text{trial}}$, the trial elastic stresses can be computed as

$$\boldsymbol{\tau}_{\text{trial}} = -2\rho_0 (\mathbf{F}^{\mathbf{e}})^{-T}_{\text{trial}} \cdot \left. \frac{\partial w^e}{\partial (\mathbf{C}^e)^{-1}} \right|_{\text{trial}} \cdot (\mathbf{F}^{\mathbf{e}})^{-1}_{\text{trial}}. \tag{152}$$

Next, the slope of the incremental potential with respective to the increment of plastic multiplier $\frac{\partial \mathscr{I}}{\partial \Delta\lambda}$ (129) is evaluated for $\Delta\lambda = 0^+$. Since $\mathscr{I}$ is convex with respect to $\Delta\lambda$, if the slope $\frac{\partial \mathscr{I}}{\partial \Delta\lambda} < 0$ is negative, the optimal $\Delta\lambda$ is positive. Actually, it amounts to check that $f^{\text{trial}}_{n+1} > 0$. Then, the Newton method (150) can be applied.

Once the optimization (126) has been performed, the updated Kirchhoff stresses are computed as

$$\left. \frac{\partial \mathscr{J}}{\partial \mathbf{d}} \right|_{n+1} = \frac{T_n}{T_{n+1}} \left. \frac{\partial w}{\partial \mathbf{d}} \right|_{n+1} = \frac{\boldsymbol{\tau}_{n+1}}{\rho_0}. \tag{153}$$

Finally, the entropy is updated with Eq. (128).

4.4. Parameterization of pseudo-stresses

The Kirchhoff pseudo-stresses $\tilde{\boldsymbol{\tau}}$ are parameterized with spherical coordinates, amongst others to enforce $\|\tilde{\boldsymbol{\tau}}\| = 1$ as shown in [15]. Some simplifications can be conducted though. First, since the plastic flow rule (27) is traceless for a pressure-independent yield function, the pseudo-stresses then satisfy

$$\text{tr}[\tilde{\boldsymbol{\tau}}] = 0. \tag{154}$$

Following the parameterization introduced in [15], they read

$$\tilde{\boldsymbol{\tau}} = \sum_{k=1}^{3} \tilde{\tau}_k(\psi) \mathbf{B}_k \tag{155}$$

$$\tilde{\tau}_k(\psi) = \sqrt{\frac{2}{3}} \sin\left[\frac{2}{3}\pi k - \psi\right], \quad k = 1, 2, 3 \tag{156}$$

where $\mathbf{B}_k$ is an element of the eigenbasis of $\tilde{\boldsymbol{\tau}}$, and ψ an unknown angle which allows to span flow directions. Second, it is convenient to parameterize the eigenbasis $\mathbf{B}_k$ from its trial counterpart $\mathbf{B}^{\text{trial}}_k$, computed during the thermoelastic prediction.

However, the discrete update formula (136) shows that $(\mathbf{C}^e)^{-1}$ will not be coaxial to $(\mathbf{C}^e)^{-1}_{\text{trial}}$, simply because the Kirchhoff pseudo-stresses $\tilde{\boldsymbol{\tau}}$ lies in the current setting, and cannot share the eigenbasis of $(\mathbf{C}^e)^{-1}_{\text{trial}}$. This is clearly a consequence of that the plastic flow rule (27) is written in the current setting, and not in the intermediate one, which was guided by the construction of consistent modelings in both Eulerian and Lagrangian settings in the presence of a non-linear kinematic hardening. As a direct consequence of this choice, trial and true eigenbasis of the Kirchhoff pseudo-stresses will not be coaxial even in case of elastic isotropy, conversely

to results obtained with purely isotropic hardening, see e.g. [36]. The Kirchhoff pseudo-stresses are then parameterized as

$$\tilde{\boldsymbol{\tau}}(\psi,\varphi,\theta,\chi) = \mathbf{R}^T(\varphi,\theta,\chi)\cdot\left[\sum_{k=1}^{3}\tilde{\tau}_k(\psi)\mathbf{B}_k^{\text{trial}}\right]\cdot\mathbf{R}(\varphi,\theta,\chi), \tag{157}$$

with four unknown angles $(\psi,\varphi,\theta,\chi)$ to describe the plastic flow direction in 3D, hence increasing the computational complexity, though still profit from the symmetry of $\tilde{\boldsymbol{\tau}}$. For two-dimensional analyses under consideration in Sections 6 and 7, only the two angles (ψ,θ) are sufficient to parameterize the flow direction

$$\tilde{\boldsymbol{\tau}}^{2D}(\psi,\theta) = \mathbf{R}^T(\theta)\cdot\left[\sum_{k=1}^{3}\tilde{\tau}_k(\psi)\mathbf{B}_k^{\text{trial}}\right]\cdot\mathbf{R}(\theta), \tag{158}$$

where $\mathbf{R}(\theta)$ is a rotation about the out-of-plane direction, so that only one additional unknown is added in the solution process with respect to the purely isotropic hardening, see [36]. The unknown vector consists of four scalar unknowns $\mathscr{X}_{n+1} = \{T,\Delta\lambda,\psi,\theta\}_{n+1}$. Denoting the vector $\mathbf{X} = \{\psi,\theta\}$ parameterizing the flow direction, Eq. (130) is replaced by

$$\left.\frac{\partial\mathscr{I}}{\partial\mathbf{X}}\right|_{n+1} = \left.\frac{\partial\mathscr{I}}{\partial\tilde{\boldsymbol{\tau}}^{2D}}\right|_{n+1} : \left.\frac{\partial\tilde{\boldsymbol{\tau}}^{2D}}{\partial\mathbf{X}}\right|_{n+1} = 0. \tag{159}$$

5. Variational formulation of the Lagrangian thermo-mechanical local constitutive problem

5.1. Continuous variational formulation

Similarly to the Eulerian setting detailed in Section 4, a Lagrangian variational formulation of the thermo-mechanical local constitutive problem can also be derived. In line with Eq. (107), one introduces the following Lagrangian functional:

$$\mathcal{L}(\dot{\mathfrak{X}},\beta;\mathfrak{X}) = D + \beta\frac{d}{dt}(T\eta + W(\mathbf{C}^e,T,\chi) - E), \tag{160}$$

which is built from the functional

$$D = \frac{dE}{dt} - T\frac{d\eta}{dt} + \frac{\mathscr{D}_{\text{int}}}{\rho_0} = \dot{W}_\tau + \frac{\mathscr{D}_{\text{int}}}{\rho_0}, \tag{161}$$

obtained by summing the reversible power per unit mass received by the system $\dot{W}_\tau$ and the specific internal dissipation $\mathscr{D}_{\text{int}}/\rho_0$, and from the residual of the rate of the Legendre transform of the Lagrangian Helmholtz specific free energy $W(\mathbf{C}^e,T,\chi)$, enforced to vanish through the Lagrange multiplier β. In the Lagrangian functional (160), it is assumed that the time rates of the specific internal energy dE/dt and of the deformation gradient $d\mathbf{F}/dt$ (and that of the jacobian determinant dJ/dt if Eq. (93) is considered) are known from the set of Lagrangian conservation laws (99), and that the state vector $\mathfrak{X} = \{E,\mathbf{C}^e,\eta,\chi,T\}$ is also assumed to be known and fixed.

An analog parameterization of the Lagrangian evolutions laws (73) and (74) is also performed using the Lagrangian plastic multiplier $\dot{\Lambda}$ and some pseudo-stresses.

Remark 3. Although a first choice seeming natural for these pseudo-stresses could be some Lagrangian Mandel pseudo-stresses $\tilde{\mathfrak{M}}$, it would require to handle a non-symmetric tensor, which in addition to be cumbersome would lead to a less efficient computational complexity since more unknown parameters would be required to parameterize it, see [15]. In order to circumvent the issue of non-symmetric tensor, one could then think to build pseudo-stresses from the second Piola–Kirchhoff stress tensor $\tilde{\mathbf{S}}$, whose deviatoric component reads [69]

$$\text{dev}(\tilde{\mathbf{S}}) = \tilde{\mathbf{S}} - \frac{(\tilde{\mathbf{S}}:\mathbf{C})\mathbf{C}^{-1}}{3}. \tag{162}$$

Unfortunately, this choice turns out to be even worse than the first one. Indeed, provided such pseudo-stresses, the flow direction is computed for the Mises yield function as

$$\left.\frac{\partial F}{\partial\mathfrak{M}}\right|_{\tilde{\mathbf{S}}} = \sqrt{\frac{3}{2}}\frac{\text{dev}(\tilde{\mathbf{S}})\cdot\mathbf{C}}{\|\xi\|} \quad \text{with } \|\xi\| = \sqrt{\text{tr}[\text{dev}(\tilde{\mathbf{S}})\cdot\mathbf{C}\cdot\text{dev}(\tilde{\mathbf{S}})\cdot\mathbf{C}]}. \tag{163}$$

On the one hand, a parameterization analog to Eqs. (154)–(156) is not compatible with $\tilde{\mathbf{S}}$, provided the expression of its deviatoric component (162). On the other hand, such parameterization also aims at enforcing a unit norm, but which would not ensure $\|\xi\| = 1$ here as in the Eulerian case.

The best choice of pseudo-stresses for the Lagrangian variational formulation is still the Kirchhoff pseudo-stresses $\tilde{\boldsymbol{\tau}}$, which is an Eulerian tensor, and whose parameterization is given by Eqs. (156) and (157). Some Lagrangian Mandel pseudo-stresses can be rebuilt from the Kirchhoff ones as

$$\tilde{\mathfrak{M}} = \mathbf{F}^T\cdot\tilde{\boldsymbol{\tau}}\cdot\mathbf{F}^{-T}. \tag{164}$$

First, Eq. (164) ensures $\mathrm{tr}[\tilde{\mathcal{M}}] = 0$ if Eq. (154) holds, which enforces a traceless flow direction. Second, a unit norm $\|\tilde{\mathcal{M}}\| = 1$ is also enforced if $\|\tilde{\boldsymbol{\tau}}\| = 1$ holds. The flow direction then reads:

$$\frac{\partial F}{\partial \mathcal{M}} = \left.\frac{\partial F}{\partial \mathcal{M}}\right|_{\tilde{\mathcal{M}}(\tilde{\boldsymbol{\tau}})} \equiv \left.\frac{\partial F}{\partial \mathcal{M}}\right|_{\tilde{\boldsymbol{\tau}}}, \tag{165}$$

which yields the same flow direction when computed with the Lagrangian Mandel pseudo-stresses $\tilde{\mathcal{M}} \neq (\mathcal{M} - \Omega)$, provided the equivalent stress measure $\mathcal{M}_{\mathrm{eq}}(\mathcal{M}, \Omega)$ defining the shape of the yield function is a positively homogeneous function of degree one, namely

$$\mathcal{M}_{\mathrm{eq}}(c\mathbf{A}) = c\mathcal{M}_{\mathrm{eq}}(\mathbf{A}), \quad \forall \mathbf{A},\ \forall c \in \mathbb{R}^+. \tag{166}$$

Hence, the Lagrangian functional (160) can first be expressed explicitly following this parameterization.

Let us start by expressing the time derivative of Helmholtz's specific free energy involved in Eq. (160), which reads

$$\frac{dW}{dt} = \frac{\partial W^e}{\partial \mathbf{C}^e} : \frac{d\mathbf{C}^e}{dt} + \frac{\partial W}{\partial T}\frac{dT}{dt} + \frac{\partial W}{\partial \boldsymbol{\chi}} : \frac{d\boldsymbol{\chi}}{dt}. \tag{167}$$

From Eqs. (1) and (3), the time derivative of the elastic right Cauchy–Green strain tensor is expressed as

$$\frac{d\mathbf{C}^e}{dt} = -(\mathbf{C}^e : \mathbf{L}^p + (\mathbf{C}^e : \mathbf{L}^p)^T) + (\mathbf{F}^p)^{-T} \cdot \frac{d\mathbf{C}}{dt} \cdot (\mathbf{F}^p)^{-1}, \tag{168}$$

where $\mathbf{L}^p$ denotes the plastic velocity gradient defined in the intermediate configuration by Eq. (13). From Eq. (168), the first term in the time derivative of Helmholtz'free energy in Eq. (167) reads

$$\frac{\partial W^e}{\partial \mathbf{C}^e} : \frac{d\mathbf{C}^e}{dt} = \frac{1}{\rho_0}\left[-\mathcal{M} : \mathcal{L}^p + \frac{\mathbf{S}}{2} : \frac{d\mathbf{C}}{dt}\right]. \tag{169}$$

Introducing Eq. (169) and the Lagrangian evolution laws (73) and (74) expressed with the Lagrangian pseudo-stresses $\tilde{\mathcal{M}}$ into the expression of the time derivative of Helmholtz's specific free energy (Eq. (167)), and accounting for the definition (79), one gets

$$\begin{aligned}\frac{dW}{dt} &= \frac{\mathbf{S}}{2\rho_0} : \frac{d\mathbf{C}}{dt} + \frac{1}{\rho_0}\left[(-\mathcal{M} + \Omega) : \left.\frac{\partial F}{\partial \mathcal{M}}\right|_{\tilde{\boldsymbol{\tau}}} - \frac{b}{c}\Omega : \Omega\right]\dot{\Lambda} + \frac{\partial W}{\partial T}\frac{dT}{dt} \\ &= \frac{\mathbf{S}}{2\rho_0} : \frac{d\mathbf{C}}{dt} + \frac{\partial W}{\partial \Lambda}\dot{\Lambda} + \frac{\partial W}{\partial T}\frac{dT}{dt}\end{aligned} \tag{170}$$

which is now expressed with the aforementioned parameterization. Introducing Eq. (170) into the Lagrangian functional (160), and accounting for the Lagrangian expression of the internal dissipation (85), it yields

$$\begin{aligned}\mathcal{L} = {} & \frac{\beta}{2\rho_0}\mathbf{S} : \frac{d\mathbf{C}}{dt} + \frac{dE}{dt}(1-\beta) + (-T + \beta T)\frac{d\eta}{dt} + \beta\left(\eta + \frac{\partial W}{\partial T}\right)\frac{dT}{dt} \\ & + \frac{\dot{\Lambda}}{\rho_0}\left[\sigma_y + (1-\beta)\frac{b}{c}\Omega : \Omega + \beta(-\mathcal{M} + \Omega) : \left.\frac{\partial F}{\partial \mathcal{M}}\right|_{\tilde{\boldsymbol{\tau}}}\right].\end{aligned} \tag{171}$$

Fixing first $d\mathbf{C}/dt = \mathbf{0}$ for consistency purpose with Section 4.1, the stationarity conditions of the Lagrangian functional (171) computed with respect to the specific entropy rate $d\eta/dt \equiv \dot{\eta}$, the temperature rate $dT/dt \equiv \dot{T}$, the Lagrangian plastic multiplier $\dot{\Lambda}$, the Kirchhoff pseudo-stresses $\tilde{\boldsymbol{\tau}}$, and the Lagrange multiplier β give respectively

$$\frac{\partial \mathcal{L}}{\partial \dot{\eta}} = -T + \beta T = 0 \tag{172}$$

$$\frac{\partial \mathcal{L}}{\partial \dot{T}} = \beta\left(\eta + \frac{\partial W}{\partial T}\right) = 0 \tag{173}$$

$$\frac{\partial \mathcal{L}}{\partial \dot{\Lambda}} = \frac{1}{\rho_0}\left[\sigma_y + (1-\beta)\frac{b}{c}\Omega : \Omega + \beta(-\mathcal{M} + \Omega) : \left.\frac{\partial F}{\partial \mathcal{M}}\right|_{\tilde{\mathcal{M}}}\right] = 0 \tag{174}$$

$$\frac{\partial \mathcal{L}}{\partial \tilde{\boldsymbol{\tau}}} = \frac{\dot{\Lambda}\beta}{\rho_0}(-\mathcal{M} + \Omega) : \left.\frac{\partial^2 F}{\partial \mathcal{M}\partial \mathcal{M}}\right|_{\tilde{\boldsymbol{\tau}}} : \frac{\partial \mathcal{M}}{\partial \tilde{\boldsymbol{\tau}}} = 0 \tag{175}$$

$$\frac{\partial \mathcal{L}}{\partial \beta} = \frac{d}{dt}(T\eta + W(\mathbf{C}^e, T, \boldsymbol{\chi}) - E) = 0 \tag{176}$$

The optimization problem defined with the Lagrangian functional (160) thus reads

$$\mathcal{W} = \underset{\dot{\eta},\dot{T},\beta}{\mathrm{stat}}\ \underset{\dot{\Lambda},\tilde{\boldsymbol{\tau}}}{\inf}\ \mathcal{L}|_{\dot{\mathbf{C}}=0} \tag{177}$$

The stationarity Eqs. (172), (173) and (176) are the analogs of Eulerian Eqs. (113), (114) and (117). Again, Eq. (172) gives the same result for the Lagrange multiplier, $\beta = 1$. Its substitution into Eqs. (173), (174) and (175) gives

$$\eta = -\frac{\partial W}{\partial T} \tag{178}$$

$$-\frac{F}{\rho_0} = 0 \tag{179}$$

$$\frac{\dot{\Lambda}}{\rho_0}(-\mathcal{M} + \Omega) : \left.\frac{\partial^2 F}{\partial \mathcal{M}\partial \mathcal{M}}\right|_{\tilde{\boldsymbol{\tau}}} : (\mathbf{F} \otimes \mathbf{F}^{-T}) = 0 \tag{180}$$

which are the definition of the specific entropy (178), the opposite of the yield function (up to the inverse of the initial mass density) which vanishes during the plastic flow (179), accounting for the formula $\mathcal{M}_{\text{eq}} = (\mathcal{M} - \mathfrak{Q}) : \left.\frac{\partial F}{\partial \mathcal{M}}\right|_{\tilde{\tau}}$ [13], and the enforcement of the correct flow direction (180) compatible with the stresses.

Once the optimization (177) performed, the stresses are obtained by computing the partial derivative of the optimized Lagrangian functional $\mathcal{W}$ with respect to the rate of the right Cauchy–Green strain tensor $\dot{\mathbf{C}}$:

$$\frac{\partial \mathcal{W}}{\partial \dot{\mathbf{C}}} = \frac{\mathbf{S}}{2\rho_0} = \frac{\mathbf{C}^{-1} \cdot \mathcal{M}}{2\rho_0}. \tag{181}$$

Remark 4. If the thermo-mechanical coupling is disregarded, the derivation of the above variational formulation is completely analog to that performed in [5] for its model I, provided his set of variables $\{\boldsymbol{\Sigma}, \mathbf{Q}, \mathbf{L}^p, \boldsymbol{\alpha}\}$[1] defined in the intermediate configuration are replaced by $\{\mathcal{M}, \mathfrak{Q}, \mathcal{L}^p, \chi\}$ which are Lagrangian ones and hence defined in the initial configuration. The main interest of that change of variables lies in that the variable χ associated with the non-linear kinematic hardening is now a Lagrangian one, which hence does not need the addition of any objective time derivative by the user. Actually as already mentioned in Section 2.4 and in Remark 1, the construction of this modeling and the choice of the variable χ (or $\boldsymbol{\alpha}$, see Eq. (82)) can also be related to the choice of a convected time derivative of Eulerian quantities, but in an *a posteriori* manner, and is thus transparent for the user. An equivalence with his model II [5], the so-called center-configuration, is also possible as shown in Section 3.4. Then, the set of material parameters σ_y, b and c are identical to these used for his model II.

5.2. A first order accurate discrete variational constitutive update

An incremental variational constitutive update can also be derived in the Lagrangian setting. Consider a discrete time increment $[t_n, t_{n+1}]$, the material state vector $\mathfrak{X}_n = \{E_n, \mathbf{C}^e_n, \eta_n, \chi_n, T_n\}$ known at time t_n, and data $\{E, \mathbf{F}, J\}_{n+1}$ known and updated at time t_{n+1} through the solution of the discrete conservation laws. Then, an incremental functional $\mathfrak{I}(\mathfrak{X}_{n+1}, \beta_{n+1}; \mathfrak{X}_n)$ is sought in such a way that it approximates the integral of the Lagrangian functional $\mathcal{L}$ (160) over the time increment Δt:

$$\begin{aligned} &\int_{t_n}^{t_{n+1}} \mathcal{L}(\dot{\mathfrak{X}}(\tau), \beta(\tau); \mathfrak{X}(\tau)) d\tau \approx \mathfrak{I}(\mathfrak{X}_{n+1}, \beta_{n+1}; \mathfrak{X}_n) \\ &\mathfrak{I}(\mathfrak{X}_{n+1}, \beta_{n+1}; \mathfrak{X}_n) = \Delta E - T_n \Delta\eta + \frac{\Delta\Lambda}{\rho_0}\left(\sigma_y + \frac{b}{c}\mathfrak{Q}_{n+1} : \mathfrak{Q}_{n+1}\right) + \beta_{n+1}\Delta(T\eta + W(\mathbf{C}^e, T, \chi) - E) \end{aligned} \tag{182}$$

where the integral of the internal dissipation over the time increment is still approximated with a backward-Euler scheme as suggested in [5]. The incremental variational update takes thus the following form

$$\mathfrak{J}_{n+1} = \underset{(\eta,T,\beta)_{n+1}}{\text{stat}} \quad \inf_{\Delta\Lambda, \tilde{\tau}_{n+1}} \mathfrak{I}(\mathfrak{X}_{n+1}, \beta_{n+1}; \mathfrak{X}_n) \tag{183}$$

The stationarity conditions in the Lagrangian discrete case read similar to these in the Eulerian case (127)–(131)

$$\frac{\partial \mathfrak{I}}{\partial \eta_{n+1}} = -T_n + \beta_{n+1} T_{n+1} = 0 \tag{184}$$

$$\frac{\partial \mathfrak{I}}{\partial T_{n+1}} = \beta_{n+1}\left(\eta_{n+1} + \left.\frac{\partial W}{\partial T}\right|_{n+1}\right) = 0 \tag{185}$$

$$\frac{\partial \mathfrak{I}}{\partial \Delta\Lambda} = \frac{1}{\rho_0}\left(\sigma_y + \frac{b}{c}\mathfrak{Q}_{n+1} : \mathfrak{Q}_{n+1}\right) + \frac{2b\Delta\Lambda}{\rho_0}\mathfrak{Q}_{n+1} : \left.\frac{\partial \chi}{\partial \Delta\Lambda}\right|_{n+1} + \beta_{n+1}\frac{\partial W}{\partial \Delta\Lambda} = 0 \tag{186}$$

$$\frac{\partial \mathfrak{I}}{\partial \tilde{\boldsymbol{\tau}}_{n+1}} = \left(\frac{2\Delta\Lambda b}{\rho_0}\mathfrak{Q}_{n+1} : \left.\frac{\partial \chi}{\partial \mathcal{M}}\right|_{n+1} + \beta_{n+1}\left.\frac{\partial W}{\partial \mathcal{M}}\right|_{n+1}\right) : (\mathbf{F}_{n+1} \otimes \mathbf{F}^{-T}_{n+1}) = 0 \tag{187}$$

$$\frac{\partial \mathfrak{I}}{\partial \beta_{n+1}} = \Delta(T\eta + W - E) = 0 \tag{188}$$

giving an analog expression for the Lagrange multiplier (184) as the Eulerian one (132). Eqs. (185), (186), (187) and (188) are the Lagrangian analogs of Eulerian ones (128), (129), (130) and (131). Besides, a time discretization of the evolution law (83) is performed with a backward Euler time scheme, giving discrete expressions of the variable χ and its derivatives

$$\chi_{n+1} = \frac{\chi_n + \Delta\Lambda \left.\frac{\partial F}{\partial \mathcal{M}}\right|_{\tilde{\tau}_{n+1}}}{1 + b\Delta\Lambda} \tag{189}$$

$$\left.\frac{\partial \chi}{\partial \Delta\Lambda}\right|_{n+1} = \frac{1}{1 + b\Delta\Lambda}\left(\left.\frac{\partial F}{\partial \mathcal{M}}\right|_{\tilde{\tau}_{n+1}} - b\chi_{n+1}\right) \tag{190}$$

$$\left.\frac{\partial \chi}{\partial \mathcal{M}}\right|_{n+1} = \frac{\Delta\Lambda}{1 + b\Delta\Lambda}\left.\frac{\partial^2 F}{\partial \mathcal{M}\partial \mathcal{M}}\right|_{\tilde{\tau}_{n+1}} \tag{191}$$

[1] The notations are here extracted from [5] and *do not* correspond to these defined in the present paper, except the Mandel stress tensor $\boldsymbol{\Sigma}$.

which are the Lagrangian analogs of Eqs. (137), (138) and (139). Next, the combination of the Lagrangian plastic flow rule (73) with Eqs. (1), (13) and (64), then discretized in time, gives the updated expression of the elastic part of the deformation gradient

$$\mathbf{F}^e_{n+1} = \mathbf{F}_{n+1} \cdot \exp\left(-\Delta\Lambda \left.\frac{\partial F}{\partial \mathfrak{M}}\right|_{\tilde{\boldsymbol{\tau}}_{n+1}}\right) \cdot (\mathbf{F}^p_n)^{-1}. \tag{192}$$

The partial derivative of the specific free energy W with respect to $\Delta\Lambda$ involved in the stationarity Eq. (186) reads

$$\left.\frac{\partial W}{\partial \Delta\Lambda}\right|_{n+1} = \left.\frac{\partial W^e}{\partial \Delta\Lambda}\right|_{n+1} + \left.\frac{\partial W^p}{\partial \Delta\Lambda}\right|_{n+1} \tag{193}$$

$$\left.\frac{\partial W^e}{\partial \Delta\Lambda}\right|_{n+1} = -\frac{1}{\rho_0}\left[(\mathbf{F}^p_{n+1})^T \cdot \boldsymbol{\Sigma}_{n+1} \cdot (\mathbf{F}^p_n)^{-T}\right] : D\exp\left(-\Delta\Lambda \left.\frac{\partial F}{\partial \mathfrak{M}}\right|_{\tilde{\boldsymbol{\tau}}_{n+1}}\right) : \left.\frac{\partial F}{\partial \mathfrak{M}}\right|_{\tilde{\boldsymbol{\tau}}_{n+1}} \tag{194}$$

$$\left.\frac{\partial W^p}{\partial \Delta\Lambda}\right|_{n+1} = \frac{\mathfrak{Q}_{n+1}}{\rho_0(1+b\Delta\Lambda)} : \left(\left.\frac{\partial F}{\partial \mathfrak{M}}\right|_{\tilde{\boldsymbol{\tau}}_{n+1}} - b\boldsymbol{\chi}_{n+1}\right) \tag{195}$$

with updated Mandel stresses defined as

$$\boldsymbol{\Sigma}_{n+1} = 2\rho_0 \mathbf{C}^e_{n+1} \cdot \left.\frac{\partial W^e}{\partial \mathbf{C}^e}\right|_{n+1}. \tag{196}$$

The updated plastic part of the deformation gradient $\mathbf{F}^p_{n+1}$ appearing in Eq. (194) is computed by combining Eqs. (1) and (192), such that

$$(\mathbf{F}^p_{n+1})^T \cdot \boldsymbol{\Sigma}_{n+1} \cdot (\mathbf{F}^p_n)^{-T} = 2\rho_0 \mathbf{C}_{n+1} \cdot \exp\left(-\Delta\Lambda \left.\frac{\partial F}{\partial \mathfrak{M}}\right|_{\tilde{\boldsymbol{\tau}}_{n+1}}\right) \cdot (\mathbf{F}^p_n)^{-1} \cdot \left.\frac{\partial W^e}{\partial \mathbf{C}^e}\right|_{n+1} \cdot (\mathbf{F}^p_n)^{-T}. \tag{197}$$

In the case of a splitting of the elastic energy W^e into isochoric and volumetric contributions (62), the partial derivative $\frac{\partial W^e}{\partial \mathbf{C}^e}$ is computed as

$$\frac{\partial W^e}{\partial \mathbf{C}^e} = \frac{\partial \bar{W}^e}{\partial \mathbf{C}^e} + \frac{\partial W^H}{\partial J^e}\frac{J^e}{2}(\mathbf{C}^e)^{-1}, \tag{198}$$

where $P = \rho_0 \frac{\partial W^H}{\partial J^e}$ is the hydrostatic pressure. The partial derivative of the specific free energy W with respect to the updated Lagrangian pseudo-stresses $\tilde{\mathfrak{M}}_{n+1}$ involved in the stationarity Eq. (187) reads

$$\left.\frac{\partial W}{\partial \mathfrak{M}}\right|_{n+1} = \left.\frac{\partial W^e}{\partial \mathfrak{M}}\right|_{n+1} + \left.\frac{\partial W^p}{\partial \mathfrak{M}}\right|_{n+1} \tag{199}$$

$$\left.\frac{\partial W^e}{\partial \mathfrak{M}}\right|_{n+1} = -\frac{\Delta\Lambda}{\rho_0}\left[(\mathbf{F}^p_{n+1})^T \cdot \boldsymbol{\Sigma}_{n+1} \cdot (\mathbf{F}^p_n)^{-T}\right] : D\exp\left(-\Delta\Lambda \left.\frac{\partial F}{\partial \mathfrak{M}}\right|_{\tilde{\mathfrak{M}}_{n+1}}\right) : \left.\frac{\partial^2 F}{\partial \mathfrak{M}\partial \mathfrak{M}}\right|_{\tilde{\boldsymbol{\tau}}_{n+1}} \tag{200}$$

$$\left.\frac{\partial W^p}{\partial \mathfrak{M}}\right|_{n+1} = \frac{\Delta\Lambda}{\rho_0(1+b\Delta\Lambda)}\mathfrak{Q}_{n+1} : \left.\frac{\partial^2 F}{\partial \mathfrak{M}\partial \mathfrak{M}}\right|_{\tilde{\boldsymbol{\tau}}_{n+1}} \tag{201}$$

Introducing Eqs. (189)–(191), (193)–(195), (199)–(201) and the expression of the Lagrange multiplier (132) into the stationarity Eqs. (186) and (187) gives their complete discrete expressions:

$$\begin{aligned}\frac{\partial \mathfrak{I}}{\partial \Delta\Lambda} &= \frac{1}{\rho_0}\left\{\left(\sigma_y + \frac{b}{c}\mathfrak{Q}_{n+1} : \mathfrak{Q}_{n+1}\right) + \frac{2b\Delta\Lambda}{(1+b\Delta\Lambda)}\mathfrak{Q}_{n+1} : \left(\left.\frac{\partial F}{\partial \mathfrak{M}}\right|_{\tilde{\boldsymbol{\tau}}_{n+1}} - b\boldsymbol{\chi}_{n+1}\right)\right.\\ &+\frac{T_n}{T_{n+1}}\left[-\left[(\mathbf{F}^p_{n+1})^T \cdot \boldsymbol{\Sigma}_{n+1} \cdot (\mathbf{F}^p_n)^{-T}\right] : D\exp\left(-\Delta\Lambda \left.\frac{\partial F}{\partial \mathfrak{M}}\right|_{\tilde{\boldsymbol{\tau}}_{n+1}}\right) : \left.\frac{\partial F}{\partial \mathfrak{M}}\right|_{\tilde{\boldsymbol{\tau}}_{n+1}}\right.\\ &\left.\left.+\frac{\mathfrak{Q}_{n+1}}{(1+b\Delta\Lambda)} : \left(\left.\frac{\partial F}{\partial \mathfrak{M}}\right|_{\tilde{\boldsymbol{\tau}}_{n+1}} - b\boldsymbol{\chi}_{n+1}\right)\right]\right\} = 0\end{aligned} \tag{202}$$

$$\begin{aligned}\frac{\partial \mathfrak{I}}{\partial \tilde{\boldsymbol{\tau}}_{n+1}} &= \frac{1}{\rho_0}\left\{\frac{2b\Delta\Lambda^2}{(1+b\Delta\Lambda)}\mathfrak{Q}_{n+1} : \left.\frac{\partial^2 F}{\partial \mathfrak{M}\partial \mathfrak{M}}\right|_{\tilde{\boldsymbol{\tau}}_{n+1}}\right.\\ &+\frac{T_n}{T_{n+1}}\left[-\Delta\Lambda\left[(\mathbf{F}^p_{n+1})^T \cdot \boldsymbol{\Sigma}_{n+1} \cdot (\mathbf{F}^p_n)^{-T}\right] : D\exp\left(-\Delta\Lambda \left.\frac{\partial F}{\partial \mathfrak{M}}\right|_{\tilde{\boldsymbol{\tau}}_{n+1}}\right) : \left.\frac{\partial^2 F}{\partial \mathfrak{M}\partial \mathfrak{M}}\right|_{\tilde{\boldsymbol{\tau}}_{n+1}}\right.\\ &\left.\left.+\frac{\Delta\Lambda}{(1+b\Delta\Lambda)}\mathfrak{Q}_{n+1} : \left.\frac{\partial^2 F}{\partial \mathfrak{M}\partial \mathfrak{M}}\right|_{\tilde{\boldsymbol{\tau}}_{n+1}}\right]\right\} : (\mathbf{F}_{n+1} \otimes \mathbf{F}^{-T}_{n+1}) = 0\end{aligned} \tag{203}$$

which are consistent with their respective continuous counterparts (174) and (175), accounting for Eq. (172):

$$\lim_{\Delta t\to 0}\frac{\partial \mathfrak{I}}{\partial \Delta\Lambda} = \frac{1}{\rho_0}\left[(-\mathfrak{M}+\mathfrak{Q})_{n+1} : \left.\frac{\partial F}{\partial \mathfrak{M}}\right|_{\tilde{\boldsymbol{\tau}}_{n+1}} + \sigma_y\right] = -\frac{F_{n+1}}{\rho_0} = 0 \tag{204}$$

$$\lim_{\Delta t\to 0}\frac{\partial \mathfrak{I}}{\partial \tilde{\boldsymbol{\tau}}_{n+1}} = \frac{\Delta\Lambda}{\rho_0}\left[(-\mathfrak{M}+\mathfrak{Q})_{n+1} : \left.\frac{\partial^2 F}{\partial \mathfrak{M}\partial \mathfrak{M}}\right|_{\tilde{\boldsymbol{\tau}}_{n+1}} : \left.\frac{\partial \mathfrak{M}}{\partial \tilde{\boldsymbol{\tau}}}\right|_{n+1}\right] = 0 \tag{205}$$

Gathering Eqs. (188), (202) and (203), one defines a balanced system of equations solved on the unknown vector

$$\tilde{\mathfrak{X}}_{n+1} = \{T, \Delta\Lambda, \mathbf{X}\}_{n+1}, \tag{206}$$

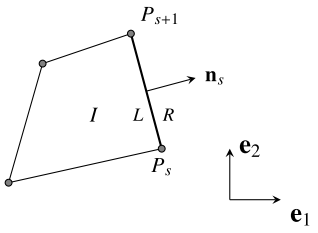

Fig. 1. Quadrangular finite volume.

whose the updated material state vector $\mathfrak{X}_{n+1}$ is a function, and $\tilde{\boldsymbol{\tau}}(\mathbf{X})$ is given by Eq. (158). A Newton method yields the following linear system of equations should be solved at each iteration k of the iterative process

$$\mathbf{K}^{(k)}\delta\bar{\mathfrak{X}}^{(k)} = -\mathbf{R}^{(k)}, \tag{207}$$

with $\delta\bar{\mathfrak{X}}^{(k)} = \bar{\mathfrak{X}}^{(k+1)} - \bar{\mathfrak{X}}^{(k)}$, with analog Hessian matrix and residual vector as Eq. (151). An analog prediction–correction scheme is followed during the solution process, whose thermoelastic prediction is first performed by solving the discrete Legendre transform (188), with the updated trial elastic deformation gradient $\mathbf{F}^e_{\text{trial}} = \mathbf{F}_{n+1} \cdot (\mathbf{F}^p_n)^{-1}$, and with no plastic flow $\Delta\Lambda = 0$. The trial elastic stresses thus read

$$\mathfrak{M}_{\text{trial}} = 2\rho_0(\mathbf{F}^p_n)^T \cdot \mathbf{C}^e_{\text{trial}} \cdot \left.\frac{\partial W^e}{\partial \mathbf{C}^e}\right|_{\text{trial}} \cdot (\mathbf{F}^p_n)^{-T}. \tag{208}$$

Once the discrete optimization (183) has been performed, and the unknown vector $\mathfrak{X}_{n+1}$ has been updated, the stresses can be computed by taking the partial derivative of the optimized Lagrangian functional $\mathcal{J}$ with respect to the updated right Cauchy–Green strain tensor $\mathbf{C}$:

$$\begin{aligned}\left.\frac{\partial \mathcal{J}}{\partial \mathbf{C}}\right|_{n+1} &= \frac{T_n}{T_{n+1}} \left.\frac{\partial W}{\partial \mathbf{C}}\right|_{n+1} \\ &= \frac{\mathbf{S}_{n+1}}{2\rho_0} = \frac{\mathbf{C}^{-1}_{n+1} \cdot \mathfrak{M}_{n+1}}{2\rho_0}\end{aligned} \tag{209}$$

Finally, the specific entropy η_{n+1} is updated with Eq. (185).

6. The flux difference splitting finite volume method

6.1. Decomposition of interface fluxes into waves and fluctuations

The finite volume method is based on the subdivision of the computational domain into elementary cells. In cell-centered versions of finite volume methods, an approximation $\mathbf{U}_I$ is defined in each cell I by integral averaging of the vector of the conserved quantities $\mathcal{U}$ (100) in the Lagrangian setting, or of the vector of balanced quantities $\mathscr{U}$ (59) in the Eulerian setting. If we consider the quadrangular grid cell I shown in Fig. 1, of area $|A_I|$, each edge s ($1 \le s \le 4$) of outward unit normal $\mathbf{n}_s$ and of length L_s joins the points P_s and P_{s+1}. The integration of a system of conservation laws, as the one in the Lagrangian setting (99), over the grid cell I in the Lagrangian setting yields the following system of ordinary differential equations:

$$\left(\frac{d\mathbf{U}}{dt}\right)_I = -\frac{1}{|A_I|}\sum_{s=1}^{N} L_s\mathbf{F}_s \tag{210}$$

where $\mathbf{F}_s$, $1 \le s \le N$, denote the numerical fluxes defined at cell interfaces. The order of accuracy, the physical content but also the computation cost of the finite volume method essentially result from the definition of these numerical fluxes. Commonly, the approach consists in defining a Riemann problem at each cell interface, whose approximate solution allows to compute these fluxes. For instance, when they are computed with the stationary solution ($x/t = 0$) of the Riemann problem, the well known Godunov's method [70] is obtained. The latter is also retrieved by the flux-difference splitting formulation, introduced by Leveque [47,48], which splits the interface numerical fluxes into fluctuations, hence accounting for waves contributions. These fluctuations are denoted by the operators $\mathcal{A}^{\pm}_k\Delta\mathbf{U}_k$, and the weighted sum of numerical fluxes expresses as a function of them as:

$$\sum_{s=1}^{N} L_s\mathbf{F}_s = \sum_{k=1}^{P} L_k\mathcal{A}^{+}_k\Delta\mathbf{U}_k + \sum_{l=1}^{Q} L_l\mathcal{A}^{-}_l\Delta\mathbf{U}_l \tag{211}$$

where $P + Q = N$, N being the number of edges of grid cell I. This summation is performed on negative fluctuations for the Q edges having an outward unit normal, and on positive fluctuations for the P edges having an inward unit normal (see Fig. 2). These fluctuations provide the contribution of first order numerical fluxes to grid cell I.

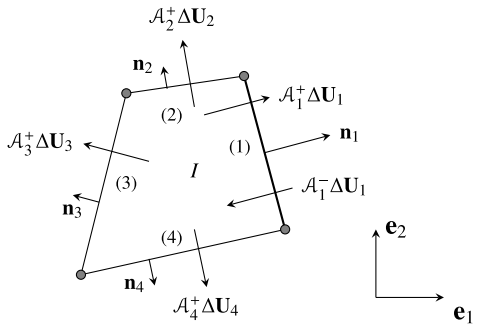

Fig. 2. Fluctuations defined at each cell interface.

Assuming that the edge k of unit normal $\mathbf{n}_k$ has left (L) and right (R) states known in adjacent grid cells (see Fig. 1), rightward (+) and leftward (−) fluctuations defined in the local frame of edge k read

$$\begin{aligned}\mathcal{A}_k^+\Delta\mathbf{U}_k &= (\mathcal{F}(\mathbf{U}_R) - \mathcal{F}(\mathbf{U}^*))\cdot\mathbf{n}_k\\ \mathcal{A}_k^-\Delta\mathbf{U}_k &= (\mathcal{F}(\mathbf{U}^*) - \mathcal{F}(\mathbf{U}_L))\cdot\mathbf{n}_k\end{aligned} \tag{212}$$

where $\mathbf{U}^*$ denotes the stationary solution (given for $x/t = 0$) of the Riemann problem, which can be computed after having projected the jump of the (averaged) conserved vector $\Delta\mathbf{U}_k = (\mathbf{U}_R - \mathbf{U}_L)_k$ across the edge k onto the considered characteristic basis $\mathbf{R}_k^{(p)} \equiv \mathbf{R}^{(p)}(\mathbf{n}_k)$

$$\Delta\mathbf{U}_k = \sum_{p=1}^{M_w}\mathfrak{W}_k^{(p)} = \sum_{p=1}^{M_w}\alpha_k^{(p)}\mathbf{R}_k^{(p)} = \mathbf{R}_k\boldsymbol{\alpha}_k, \tag{213}$$

where M_w is the number of waves, then determining the coefficients $\alpha_k^{(p)}$ the wave strengths $\mathfrak{W}_k^{(p)}$, $1 \le p \le M_w$ consist of.

6.2. HLLC approximate Riemann solver for the Eulerian system

The HLLC approximate Riemann solver [64] considers three discontinuous waves, one of which is a contact wave, separating four constant states named $(L, *\ L, *\ R, R)$. Considering an edge k of unit normal $\mathbf{n}_k$ has left (L) and right (R) states known in adjacent grid cells, Rankine–Hugoniot conditions across these waves of speed S_L, S_* and S_R read

$$\begin{aligned}\mathbf{F}_{*L} - \mathbf{F}_L &= S_L(\mathbf{U}_{*L} - \mathbf{U}_L)\\ \mathbf{F}_{*R} - \mathbf{F}_{*L} &= S_*(\mathbf{U}_{*R} - \mathbf{U}_{*L})\\ \mathbf{F}_{*R} - \mathbf{F}_R &= S_R(\mathbf{U}_{*R} - \mathbf{U}_R).\end{aligned} \tag{214}$$

Equating the normal stress σ_{NN} and velocity v_N components of states $(*\ L, *\ R)$ yields the expression of the wavespeed S_* also equal to the normal velocity v_N^*

$$S_* = \frac{(\rho v_N^2 - \sigma_{NN})_L - (\rho v_N^2 - \sigma_{NN})_R - S_L(\rho v_N)_L + S_R(\rho v_N)_R}{(\rho v_N)_L - (\rho v_N)_R - S_L\rho_R + S_R\rho_R} = v_N^*, \tag{215}$$

which can be assessed using the estimates of Davis [71] of the leftward and rightward pressure wavespeeds

$$\begin{aligned}S_L &= \max(v_{N_L} + c_L, v_{N_R} + c_R)\\ S_R &= \max(v_{N_L} - c_L, v_{N_R} - c_R).\end{aligned}$$

From these wavespeeds, the expressions of the conservative variables in the areas $*\ L, *\ R$ are determined as

$$\rho_{L,R}^* = \rho_{L,R}\frac{S_L - (v_N)_{L,R}}{S_{L,R} - S_*}$$

$$\sigma_{NN}^* = \frac{(v_{N_R} - S_R)\rho_R\sigma_{NN_L} - (v_{N_L} - S_L)\rho_L\sigma_{NN_R} + (v_{N_L} - S_L)\rho_L(v_{N_R} - S_R)\rho_R(v_{N_R} - v_{N_L})}{(v_{N_R} - S_R)\rho_R - (v_{N_L} - S_L)\rho_L}$$

$$\sigma_{NT}^* = \frac{(v_{N_R} - S_R)\rho_R\sigma_{NT_L} - (v_{N_L} - S_L)\rho_L\sigma_{NT_R} + (v_{N_L} - S_L)\rho_L(v_{N_R} - S_R)\rho_R(v_{T_R} - v_{T_L})}{(v_{N_R} - S_R)\rho_R - (v_{N_L} - S_L)\rho_L}$$

$$v_{T_{L,R}}^* = v_{T_{L,R}} + \frac{\sigma_{NT}^* - \sigma_{NT_{L,R}}}{(v_{N_{L,R}} - S_{L,R})\rho_{L,R}}$$

$$\mathscr{E}_{L,R}^* = \frac{\rho_{L,R}\mathscr{E}_{L,R}(v_{n_{L,R}} - S_{L,R}) - \sigma_{NN_{L,R}}v_{T_{L,R}} - \sigma_{NT_{L,R}}v_{T_{L,R}} + \sigma_{NN}^*S_* + \sigma_{NT}^*v_{T_{L,R}}}{\rho_{L,R}^*(S_* - S_{L,R})}$$

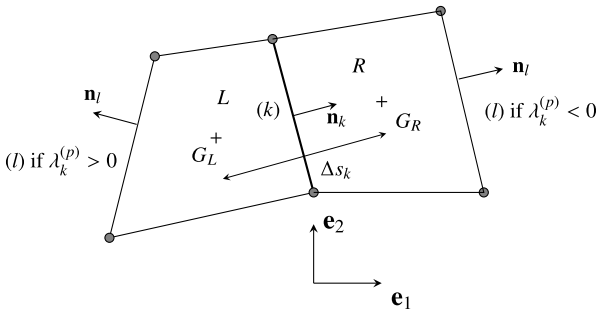

Fig. 3. Illustration of upwind edges of edge k for wave comparison purpose.

$$(F_{NN}^{-T})^*_{L,R} = \frac{(F_{NN}^{-T})_{L,R}(\upsilon_{N_{L,R}} - S_{L,R}) + (F_{TN}^{-T})_{L,R}(\upsilon_{T_{L,R}} - \upsilon^*_{T_{L,R}})}{S_* - S_{L,R}} \; ; \; (F_{NT}^{-T})^*_{L,R} = \frac{(F_{NT}^{-T})_{L,R}(\upsilon_{N_{L,R}} - S_{L,R}) + (F_{TT}^{-T})_{L,R}(\upsilon_{T_{L,R}} - \upsilon^*_{T_{L,R}})}{S_* - S_{L,R}}$$

$$(\alpha_{NN})^*_{L,R} = (\alpha_{NN})_{L,R} \; ; \quad (\alpha_{NT})^*_{L,R} = (\alpha_{NT})_{L,R} \; ; \quad (\varepsilon_{eq})^*_{L,R} = (\varepsilon_{eq})_{L,R}$$

where subscript N, T denote normal and tangential components. The components of $(\mathbf{F}^e)^{-T}$ follow analog formula than those derived above for $\mathbf{F}^{-T}$. Plastic variables $(\boldsymbol{\alpha}, \varepsilon_{eq})$ do not jump with pressure waves, only with the contact one. Once the states in the star regions known, the HLLC flux is then computed according to wavespeeds from Rankine–Hugoniot conditions (214) as

$$\mathbf{F}_{HLLC} = \begin{cases} \mathbf{F}_L & \text{if} \quad 0 \le S_L, \\ \mathbf{F}_{*L} & \text{if} \quad S_L \le 0 \le S_*, \\ \mathbf{F}_{*R} & \text{if} \quad S_* \le 0 \le S_R, \\ \mathbf{F}_R & \text{if} \quad S_R \le 0. \end{cases} \tag{216}$$

6.3. Treatment of non-conservative terms

In the Eulerian setting, System (58) also embodies the non-conservative terms $\mathscr{B} \cdot \boldsymbol{\nabla} \mathscr{W}$ (60), which in the two-dimensional case, can be developed as $\mathscr{B}_1 \frac{\partial \mathscr{W}}{\partial x_1} + \mathscr{B}_2 \frac{\partial \mathscr{W}}{\partial x_2}$. Following [48], normal fluctuations to an edge k can be computed as

$$\begin{aligned} \mathcal{A}_k^+ \Delta \mathbf{W}_k &= \sum_{i=1}^{2} n_i^{(k)} \mathbf{B}_i(\mathbf{U}_R) \cdot (\mathbf{W}_R - \mathbf{W}^*)_k \\ \mathcal{A}_k^- \Delta \mathbf{W}_k &= \sum_{i=1}^{2} n_i^{(k)} \mathbf{B}_i(\mathbf{U}_L) \cdot (\mathbf{W}^* - \mathbf{W}_L)_k \end{aligned} \tag{217}$$

where $\mathbf{W}^*$ denotes the stationary solution (given for $(x/t) = 0$), the matrices $\mathbf{B}_i$, $i = 1, 2$ are derived from $\mathscr{B}_i$, $i = 1, 2$, and are either evaluated with the left or with the right state to get the leftward or rightward normal fluctuations respectively. Fluctuations (217) are then added to conservative ones (212) since System (58) consists of both conservative and non-conservative terms.

6.4. High order fluxes

The class of total variation non-increasing methods [47,48] represents one way to improve the above first order scheme, and allows to meet both a high order of accuracy in areas where the solution is regular together with a high resolution of discontinuities without spurious numerical oscillations when they occur. This class of methods can be implemented by adding high order fluxes to first order ones, which are limited so that a non-increasing total variation of the numerical solution be satisfied at each time step. These second order numerical fluxes read

$$\tilde{\mathbf{F}}_k^{\mathrm{HO}} = \frac{1}{2} \sum_{p=1}^{M_w} |\lambda_k^{(p)}| \left(1 - \frac{\Delta t}{\Delta s_k} |\lambda_k^{(p)}|\right) \tilde{\mathfrak{W}}_k^{(p)}, \tag{218}$$

where Δs_k refers to the distance between barycenters of grid cells sharing edge k, as shown in Fig. 3, and $\tilde{\mathfrak{W}}_k^{(p)} = \tilde{\alpha}_k^{(p)} \mathbf{R}_k^{(p)}$ denotes the limited wave strength. Waves are limited based on an upwind ratio $\theta_k^{(p)}$ defined for the wave p at the edge k as:

$$\theta_k^{(p)} = \frac{\mathfrak{W}_l^{(p)}(\mathbf{n}_k) \cdot \mathfrak{W}_k^{(p)}}{\|\mathfrak{W}_k^{(p)}\|^2} \tag{219}$$

where l denotes the upwind edge, or more precisely either the opposed edge of grid cell L to edge k if $\lambda_k^{(p)} > 0$, or the opposed edge of grid cell R to edge k if $\lambda_k^{(p)} < 0$, see Fig. 3. The upwind ratio (219) can be understood as a certain measure of the local regularity of

the solution. For noncartesian quadrangles, upwind and downwind edges do not necessarily share the same normal. Following [49], the computation of the upwind ratio (219) is performed with wave strengths recomputed in the same local reference frame of edge k. The weighting coefficients $\alpha_l^{(p)}$ of the wave strengths $\mathfrak{W}_l^{(p)}$ express in the local frame of edge k as:

$$\boldsymbol{\alpha}_l(\mathbf{n}_k) = \mathbf{R}^{-1}(\mathbf{n}_k) \cdot \Delta\mathbf{U}_l \tag{220}$$

where $\Delta\mathbf{U}_l$ is the jump across edge l of the conserved vector. The wave strengths associated with edge l are then corrected when expressed in the frame of edge k as:

$$\mathbb{W}_l(\mathbf{n}_k) = \text{diag}\,(\boldsymbol{\alpha}_l(\mathbf{n}_k)) \cdot \mathbf{R}(\mathbf{n}_k) = \left[\text{diag}\,([\mathbf{K}(\mathbf{n}_k)]^{-1} \cdot \Delta\mathbf{U}_l)\right] \cdot \mathbf{R}(\mathbf{n}_k) \tag{221}$$

where $\mathbb{W}_l(\mathbf{n}_k)$ is the matrix whose columns are wave strength vectors $\mathfrak{W}^{(p)}$, $1 \leq p \leq M_w$.

The wave strength $\tilde{\mathfrak{W}}_k^{(p)}$ of wave p associated with edge k is limited using some classical limiting function $\tilde{\phi}(\theta_k^{(p)})$ applied to wave coefficients such as:

$$\tilde{\alpha}_k^{(p)} = \tilde{\phi}(\theta_k^{(p)})\alpha_k^{(p)}, \tag{222}$$

many of which permit to obtain different known finite volume schemes [72]. Here, the classical minmod limiter is used [73]:

$$\tilde{\phi}(\theta) = \max(0, \min(1, \theta)). \tag{223}$$

6.5. Explicit time integration

Gathering first order fluctuations and additional numerical fluxes, and considering an explicit Euler time integration, the state of grid cell i is updated at time t_{n+1} with the following formula:

$$\mathbf{U}_I^{n+1} = \mathbf{U}_I^n - \frac{\Delta t}{|A_I|}\left(\sum_{k=1}^{P} L_k \mathcal{A}_k^+ \Delta\mathbf{U}_k + \sum_{l=1}^{Q} L_l \mathcal{A}_l^- \Delta\mathbf{U}_l\right) - \frac{\Delta t}{|A_I|}\left(\sum_{k=1}^{P} L_k \tilde{\mathbf{F}}_k^{\text{out}} - \sum_{l=1}^{Q} L_l \tilde{\mathbf{F}}_l^{\text{in}}\right) \tag{224}$$

where $\tilde{\mathbf{F}}_l^{\text{in}}$ and $\tilde{\mathbf{F}}_k^{\text{out}}$ refer to inward and outward additional numerical fluxes, respectively associated with the Q and P edges having either an outward or inward normal relative to grid cell I. These additional numerical fluxes sum both second order and transverse ones

$$\tilde{\mathbf{F}}_l^{\text{in}} = \tilde{\mathbf{F}}_l^{\text{HO}} + \tilde{\mathbf{F}}_l^{\text{tran}}. \tag{225}$$

7. Numerical examples

7.1. Test cases performed at one material point

Elementary loading paths are first investigated at the scale of one material point. The two variational constitutive updates are driven by updated values of their respective specific internal energies and strain measures at time t_{n+1}, whose consistency should be enforced to provide the material point with some physically compatible loading paths. This is performed by solving the discrete balance of internal energy written in their respective configurations between times t_n and t_{n+1}.

In the Eulerian setting, the balance of internal energy reads

$$\rho\frac{de}{dt} = \boldsymbol{\sigma} : \mathbf{d}. \tag{226}$$

However, it is convenient to change $\mathbf{d}$ in order to avoid its direct numerical integration, and to drive the kinematics through the deformation gradient $\mathbf{F}$. From Eq. (10), one deduces the following relation

$$\mathbf{d} = -\frac{1}{2}\mathbf{F} \cdot \frac{d\mathbf{C}^{-1}}{dt} \cdot \mathbf{F}^T. \tag{227}$$

Introducing Eq. (227) into Eq. (226), then discretizing with a second order accurate mid-point time scheme, the discrete balance of internal energy in the Eulerian setting reads

$$\rho_{n+\frac{1}{2}}\Delta e = -\frac{\mathbf{T}_{n+\frac{1}{2}}}{2} : \Delta\mathbf{C}^{-1}; \quad \rho_{n+\frac{1}{2}} = \frac{\rho_n + \rho_{n+1}}{2}; \quad \mathbf{T}_{n+\frac{1}{2}} = \frac{\mathbf{T}_n + \mathbf{T}_{n+1}}{2}, \tag{228}$$

where $\mathbf{T} = \mathbf{F}^T \cdot \boldsymbol{\sigma} \cdot \mathbf{F}$ denotes some Lagrangian stress tensor. In the Lagrangian setting, an analog mid-point time discretization of the balance of internal energy yields its discrete expression

$$\rho_0\Delta E = \mathbf{P}_{n+\frac{1}{2}} : \Delta\mathbf{F}; \quad \mathbf{P}_{n+\frac{1}{2}} = \frac{\mathbf{P}_n + \mathbf{P}_{n+1}}{2}. \tag{229}$$

At each load step, Eulerian and Lagrangian constitutive updates are performed iteratively within a fixed point loop until the respective discrete internal energy balances (228) and (229) are satisfied. Then, the respective stresses are deduced as

$$\boldsymbol{\tau}_{n+1} = \rho_0 \left.\frac{\partial \mathscr{J}(\Delta e, \Delta\mathbf{C}^{-1})}{\partial \mathbf{d}}\right|_{n+1}; \quad \mathbf{S}_{n+1} = 2\rho_0 \left.\frac{\partial \mathcal{J}(\Delta E, \Delta\mathbf{F})}{\partial \mathbf{C}}\right|_{n+1}. \tag{230}$$

Table 1
Material parameters.

Elasticity parameters	$E = 200$ GPa	$\nu = 0.3$	$\rho_0 = 7800$ kg m^{-3}
Thermal parameters	$C = 452$ J kg^{-1} K^{-1}	$\alpha = 12 \times 10^{-6}$ K^{-1}	$T_0 = 293$ K
Plasticity	$\sigma_y = 400$ MPa	$c = 10$ GPa	$b = 5$

For numerical illustration purpose in this paper, and for all the following test cases, the volumetric part of Helmholtz's specific free energy is chosen as

$$w^H(J^e, T) = W^H(J^e, T) = \frac{\kappa}{2\rho_0}(J^e - 1)^2 - C_0\Gamma_0(T - T_0)\ln J^e, \tag{231}$$

where $\Gamma_0 = \frac{3\kappa\alpha}{\rho_0 C_0}$ denotes the Grüneisen coefficient, α is the thermal dilatation coefficient, and $\kappa = \frac{E}{3(1-2\nu)}$ is the elastic bulk modulus. A simple neo-Hookean isotropic hyperelastic model is considered for the isochoric component of the specific free energy. In the Lagrangian setting, it reads

$$\bar{W}^e\left(\bar{\mathbf{C}}^e\right) = \frac{\mu}{2\rho_0}\left(\bar{I}_1\left(\bar{\mathbf{C}}^e\right) - 3\right); \quad \bar{I}_1\left(\bar{\mathbf{C}}^e\right) = \mathrm{tr}\left[\bar{\mathbf{C}}^e\right], \tag{232}$$

where $\mu = \frac{E}{2(1+\nu)}$ refers to the shear elastic modulus. The interest of taking mathematical forms (231) and (232) for the elastic part of the specific free energy is that strong ellipticity condition of the acoustic tensor is enforced [74], hence hyperbolicity will be guaranteed in dynamics [75]. The analog Eulerian writing is obtained via the Cayley–Hamilton theorem, which gives

$$\bar{w}^e\left(\bar{\mathbf{C}}^{e^{-1}}\right) = \frac{\mu}{2\rho_0}\left(\bar{I}_2\left(\bar{\mathbf{C}}^{e^{-1}}\right) - 3\right); \quad \bar{I}_2\left(\bar{\mathbf{C}}^{e^{-1}}\right) = \frac{1}{2}\left(\mathrm{tr}\left[\bar{\mathbf{C}}^{e^{-1}}\right]^2 - \bar{\mathbf{C}}^{e^{-1}} : \bar{\mathbf{C}}^{e^{-1}}\right). \tag{233}$$

Besides, the Mises J_2−stress norm is used for both Eulerian and Lagrangian yield functions (26) and (72), with the equivalence (70). Table 1 gathers the values of the material parameters considered for test cases presented in this paper.

7.1.1. One-dimensional strain test

We start with a one-dimensional strain test, whose deformation gradient is of the form

$$\mathbf{F} = F_{11}\mathbf{e}_1 \otimes \mathbf{e}_1 + \mathbf{e}_2 \otimes \mathbf{e}_2 + \mathbf{e}_3 \otimes \mathbf{e}_3, \tag{234}$$

hence simulating the kinematics of a plane wave. Fig. 4 shows the evolution of various quantities plotted as a function of $F_{11} \in [0.8, 1.2]$ during one cycle of loading, and computed with 500 loading increments. Both Eulerian and Lagrangian variational constitutive updates give almost superposed results. The longitudinal component of the deviatoric part of Cauchy stresses shows a cycle, associated with these of kinematic variables V_{11} and χ_{11}, which are superposed in this particular 1D strain case. Next, both the cumulated plastic strain and the specific entropy follow a monotonic increasing evolution along the loading cycle, the latter being the signature of the satisfaction of the second principle of thermodynamics. The evolution of various specific energies (free, internal, incremental) are also plotted. Finally, the temperature evolution results from both the thermoelastic effects (thermal dilatation) computed through the equation of state, and from the plastic work.

Next, Fig. 5 shows convergence curves for various quantities of the solution extracted at the end of the cycle as a function of the number of load steps carried out during the cycle. Relative errors are computed with respect to a numerical solution obtained with a higher number of load steps. As expected from the first order accurate incremental variational updates (126) and (183), a convergence rate of about one is observed for all plotted quantities. Besides, convergence curves computed with both the Eulerian and Lagrangian variational constitutive updates are superposed on the same graphs, and show very close results.

Next, several loading cycles with an increasing trend are investigated, whose results are shown in Fig. 6 when computed with both the Eulerian and Lagrangian constitutive updates with 450 loading increments. The 'time' evolution of the driven deformation gradient F_{11} is shown in green, as a function of the load increment number: the loading magnitude of each load cycle is greater than the unloading one. As a result, the plastic strain component F^p_{11} continues increasing over loading cycles, while the peaks of kinematic variables V_{11}, χ_{11} tend to decrease over cycles, so does these of the deviatoric longitudinal stress. This results in a ratchetting at each loading cycle, as shown in Fig. 7, whose pitch depends on the ratio of loading/unloading magnitudes. Again, the specific entropy shows a monotonically increasing evolution, while the temperature peaks reached at the end of each unloading stage tend to rise over cycles.

7.1.2. Combined one-dimensional strain/shear test case

A combined non-proportional one-dimensional strain/shear loading is now considered, whose deformation gradient is of the form

$$\mathbf{F} = F_{11}\mathbf{e}_1 \otimes \mathbf{e}_1 + \mathbf{e}_2 \otimes \mathbf{e}_2 + \mathbf{e}_3 \otimes \mathbf{e}_3 + F_{12}\mathbf{e}_1 \otimes \mathbf{e}_2. \tag{235}$$

More precisely, and as shown in Fig. 8 (top right graph), a monotonic increasing 1D strain loading is first applied, then hold while applying two ratchetting loading cycles on the shear component F_{12}, whose loading magnitude is greater than the unloading one. The solution is here computed with the Eulerian constitutive update, with 350 loading increments. Basically, the evolutions observed in Fig. 8 follow these already shown for the cyclic and ratchetting 1D strain loadings in Section 7.1.1. However, interesting combined

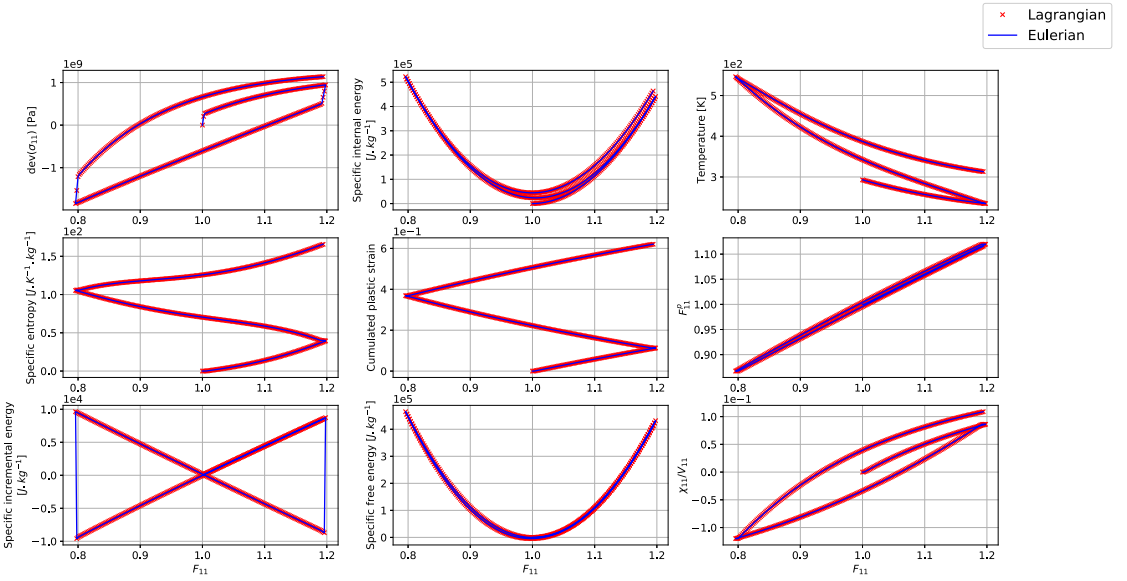

Fig. 4. Plots of the evolution of various quantities computed with both the Eulerian and Lagrangian constitutive updates, as a function of the deformation gradient component F_{11} over one loading cycle performed at one material point in the case of a one-dimensional strain test.

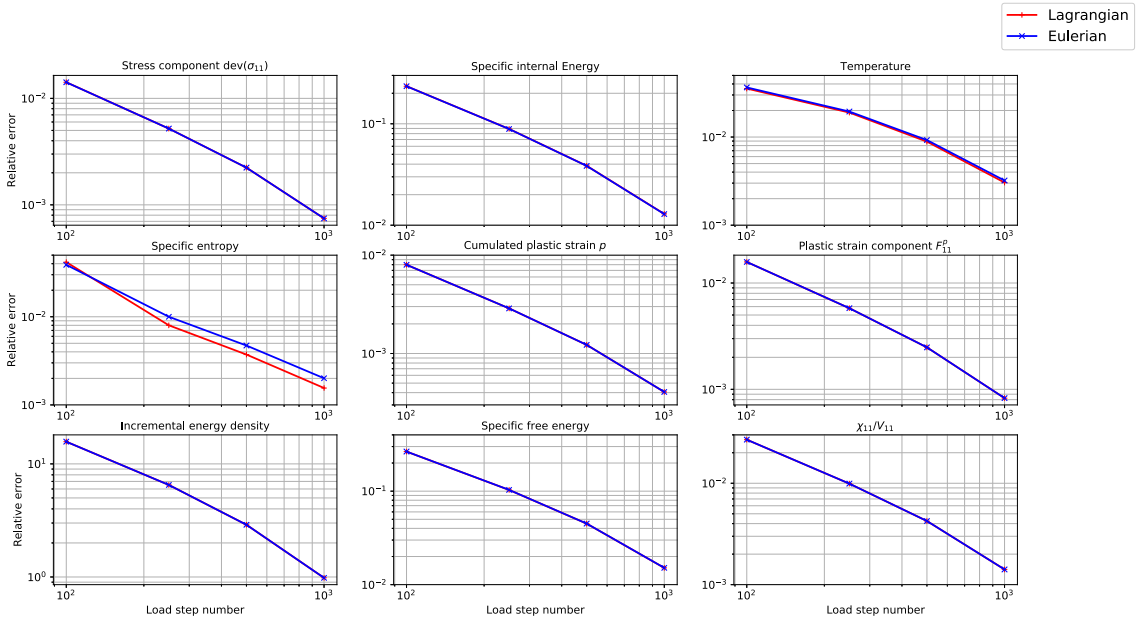

Fig. 5. Plots of convergence curves of the relative errors associated with various quantities computed with both the Eulerian and Lagrangian constitutive updates, in the case of a one-dimensional strain test, with the solution extracted at the end of the loading cycle performed at one material point.

effects can be observed. For instance, the stress component dev(σ_{11}) softens during the shearing stage. After a first drop during the 1D strain loading stage, the temperature rises monotonically during the shearing one. Besides, the components 11 and 12 of the Eulerian $\mathbf{V}$ and Lagrangian $\boldsymbol{\alpha}$ kinematic variables are also plotted. Their evolutions, in accordance with Eq. (104), are significantly different, especially for the longitudinal ones. Next, Fig. 9 shows the evolution of these various quantities in the phase spaces. For convenience of plots, components 11 are plotted as a function of $F_{11} - 1$, 12 ones as a function of F_{12}, and scalar quantities are plotted as a function of the norm of the deformation gradient $\|\mathbf{F}\|$.

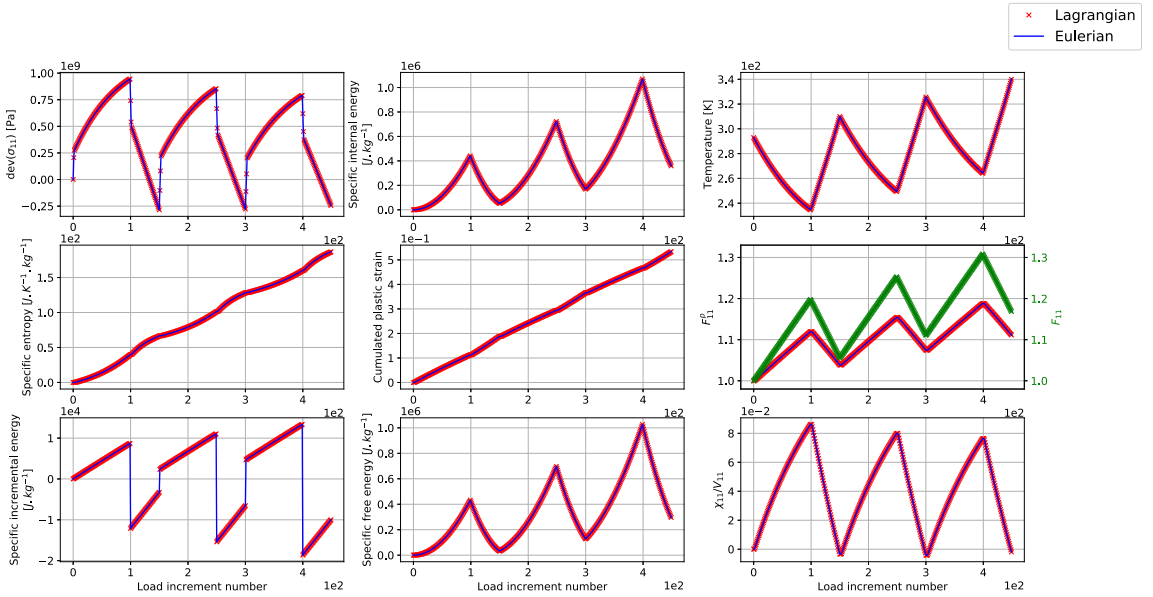

Fig. 6. Plots of the 'time' evolution of various quantities computed with both the Eulerian and Lagrangian constitutive updates, as a function of the load increment number over a set of ratchetting cycles performed at one material point in the case of a one-dimensional strain test. The driven deformation gradient component F_{11} is plotted in green. (For interpretation of the references to color in this figure legend, the reader is referred to the web version of this article.)

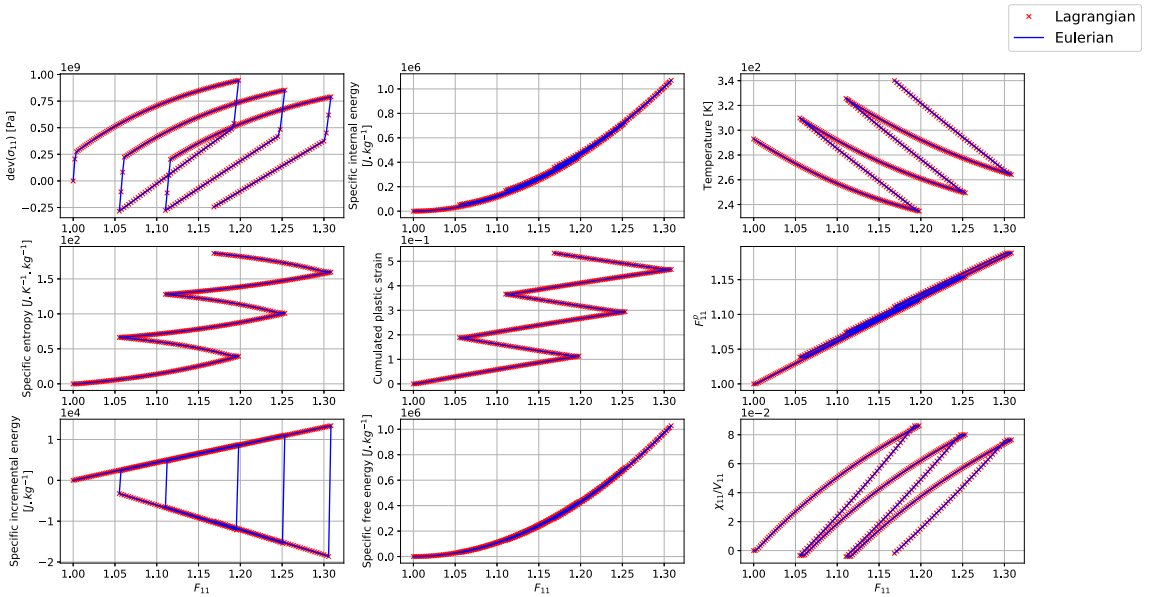

Fig. 7. Plots of the evolution of various quantities computed with both the Eulerian and Lagrangian constitutive updates, as a function of the deformation gradient component F_{11} over a set of ratchetting cycles performed at one material point in the case of a one-dimensional strain test.

7.2. Cyclic one-dimensional shear wave test

One considers a one-dimensional computational domain $x \in [0, L]$, with $L = 1$ m, through which the propagation of shear waves is studied. Dirichlet boundary conditions are prescribed at the two ends of this medium. A cyclic discontinuous velocity time evolution is prescribed at the left end (at $x = 0$):

$$v(x = 0, t) = \bar{v} \left[H(t) + \sum_{i=1}^{N} (-1)^i 2H \left(t - \frac{iT}{2} \right) \right], \tag{236}$$

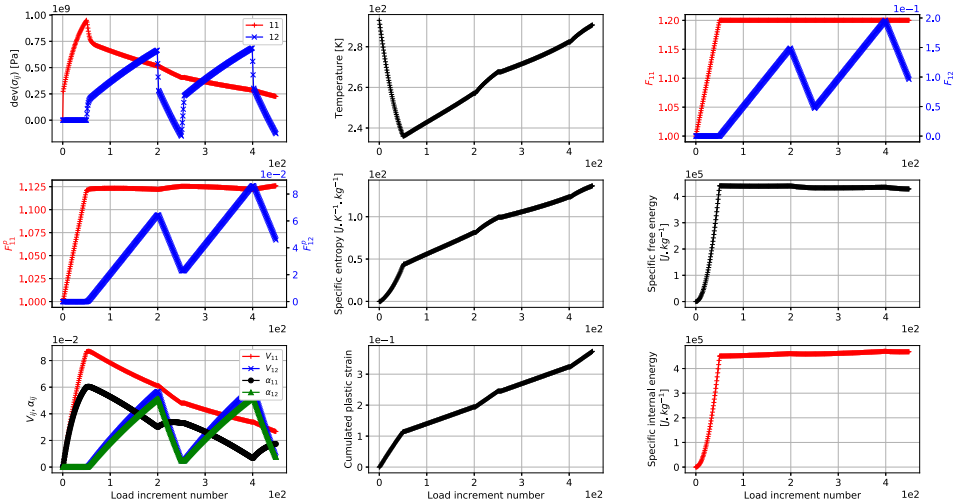

Fig. 8. Plots of the 'time' evolution of various quantities computed with the Eulerian constitutive update, as a function of the load increment number over a non-proportional 1D strain/shear loading performed at one material point.

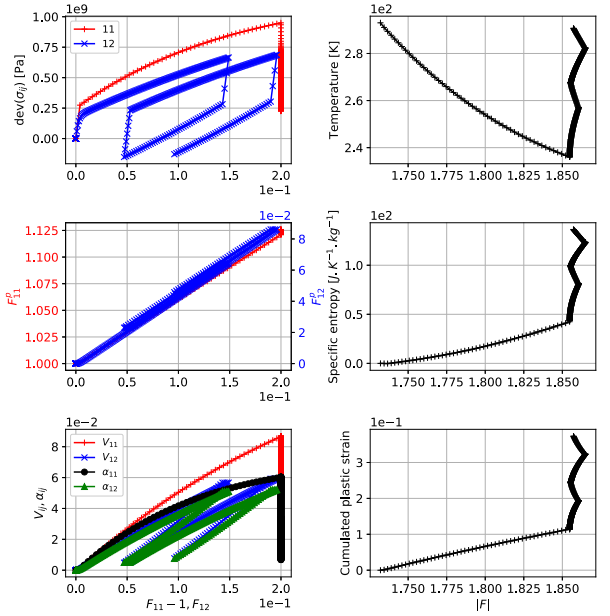

Fig. 9. Plots of the evolution of various quantities computed with the Eulerian constitutive update, as a function of the deformation gradient over a non-proportional 1D strain/shear loading performed at one material point.

where $H(t)$ denotes the Heaviside function, $\bar{v} = 50$ m s^{-1} is the velocity magnitude, and $T = \frac{2L}{c_s}$ the period of the signal, that is one round trip of shear wave of celerity $c_s = \sqrt{\frac{\mu}{\rho_0}}$ in the one-dimensional medium. The Eulerian (58) and Lagrangian (99) first order systems of equations are solved with the finite volume scheme (224), and coupled via a splitting scheme (102) with their respective variational constitutive updates (126) and (183), including an Armstrong–Frederick-type kinematic hardening. The HLLC approximate Riemann solver recalled in Section 6.2 is used to compute the Eulerian numerical solution, and an acoustic one for the Lagrangian solution. Both numerical solutions are here easy to compare because the prescribed shear loading allows to avoid to post-process updated positions of the matter for comparison purpose.

Figs. 10 and 11 show the profile at times $t \approx 5.5 \times 10^{-4}$ and $t \approx 8 \times 10^{-4}$ s of various quantities plotted along the longitudinal coordinate. Fig. 10 shows the solutions after the first reverse loading (Eq. (236) with $N = 1$), while Fig. 11 shows the solutions after the second forward loading (Eq. (236) with $N = 2$). The computational mesh consists of 200 grid cells in the longitudinal direction, and the time stepping follows from a CFL number set at 0.5. First of all, both Eulerian and Lagrangian numerical solutions computed with a kinematic hardening are very close to each other at these two computation times. The differences between both

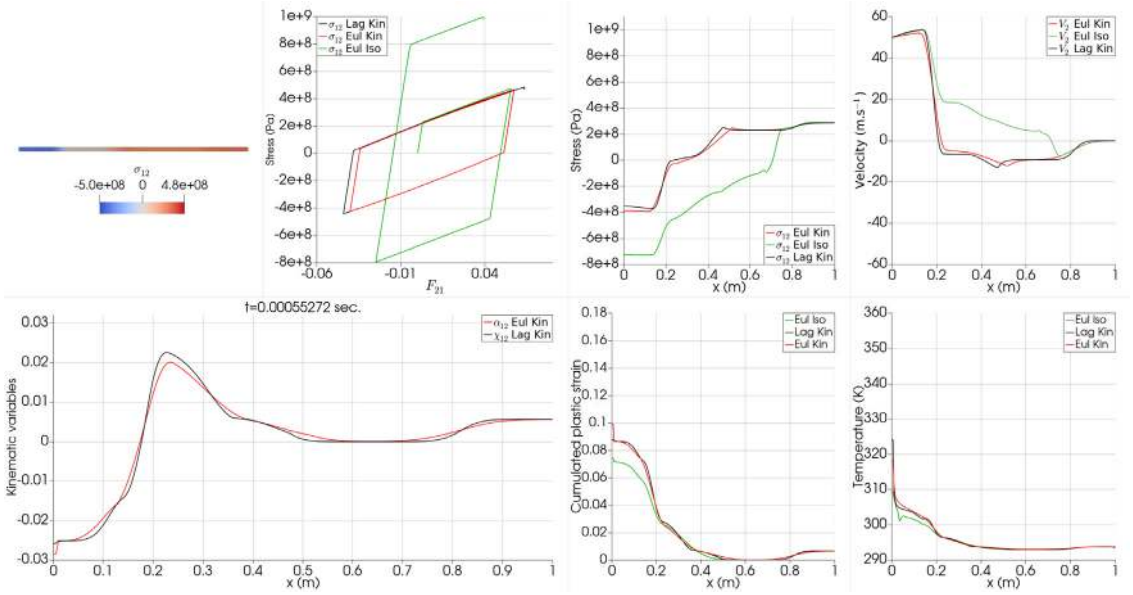

Fig. 10. Plots at time $t \approx 5.5 \times 10^{-4}$ s of the space profile of various quantities, computed with the Eulerian and Lagrangian formulations with a kinematic hardening, and the Eulerian one with an isotropic hardening on the one-dimensional shear wave test.

essentially result from the different numerical viscosities of the schemes and the different approximate Riemann solvers. Especially, it is interesting to observe that the two Lagrangian kinematic components α_{12} and χ_{12} respectively extracted from Lagrangian and Eulerian solutions almost perfectly match for this special loading case. For completeness, an Eulerian numerical solution is also computed with an isotropic hardening, and superposed with the two other solutions. Its hardening modulus is set as $Q = \frac{3}{2}c$, the numerical value of c being given in Table 1. The comparison between results obtained with kinematic and isotropic clearly show a net difference between the respective predicted solutions in case of a cyclic loading. Not only the stress and velocity profiles are radically different, but induced plastic flow and temperature rise also significantly depart. At last, the response of a material point located at coordinate $x = 0.1$ m is plotted in the phase space (F_{21}, σ_{12}). Solutions computed with a kinematic hardening clearly show a closed loading cycle, and are very close to each other, while as expected the isotropic one exhibits an open cycle, which triggers the different space profiles of the various plotted quantities with respect to these computed with a kinematic hardening.

Next, Fig. 12 shows the time evolutions of the total, kinetic, internal energies and of the entropy when computed with the three previous numerical solutions. First, it is clearly observed that the Eulerian and Lagrangian solutions are very close to each other when computed with a kinematic hardening. Second, the third solution computed with an isotropic hardening starts to depart from the two others at time $t \approx 3.18 \times 10^{-4}$ s, as soon as the first reverse loading occurs.

To complement the results obtained with the above mesh, Fig. 13 shows superposed results computed during the forward propagation of elastic and plastic waves with a finer mesh consisting of 2000 cells, still with the same CFL number. On the one hand, it can be observed that the capturing of discontinuous wave fronts is steepened upon refinement, and that differences between Lagrangian and Eulerian solutions reduces with refinement, especially on the plastic wave. On the other hand, the profile of the specific entropy shows that the numerical viscosity of the two solutions decreases upon refinement, and that the Eulerian one remains slightly more diffusive than the Lagrangian one, as already mentioned previously.

7.3. Wave reflexion from a wedge

One considers now a two-dimensional computational domain consisting a channel partially cut by a wedge. Its geometry is extracted from the associated well-known test case, and is for instance described in [64, Sec. 17.2]. This channel is here made of the aforementioned solid medium, with values of material parameters listed in Table 1, and treated in plane strain conditions. The input of the channel (i.e. the left face) is prescribed a velocity field whose longitudinal component (along the x direction) is given by Eq. (236), with a period of the signal now defined as $T = \frac{2L}{c_p}$, where L stands for the length of the channel and $c_p = \sqrt{\frac{\kappa + \frac{4\mu}{3}}{\rho_0}}$ is the pressure wave celerity. Besides, a symmetry condition is prescribed on the remaining part of the boundary.

Figs. 14 and 15 show the maps of the Cauchy stress component σ_{11} and the temperature at times $t \approx 3.8 \times 10^{-5}$ and $t \approx 1.1 \times 10^{-4}$ s respectively, extracted from both the Lagrangian and Eulerian numerical solutions. Fig. 14 shows the solutions during the first forward loading (Eq. (236) with $N = 0$), while Fig. 15 shows the solutions after the second forward loading (Eq. (236) with $N = 2$).

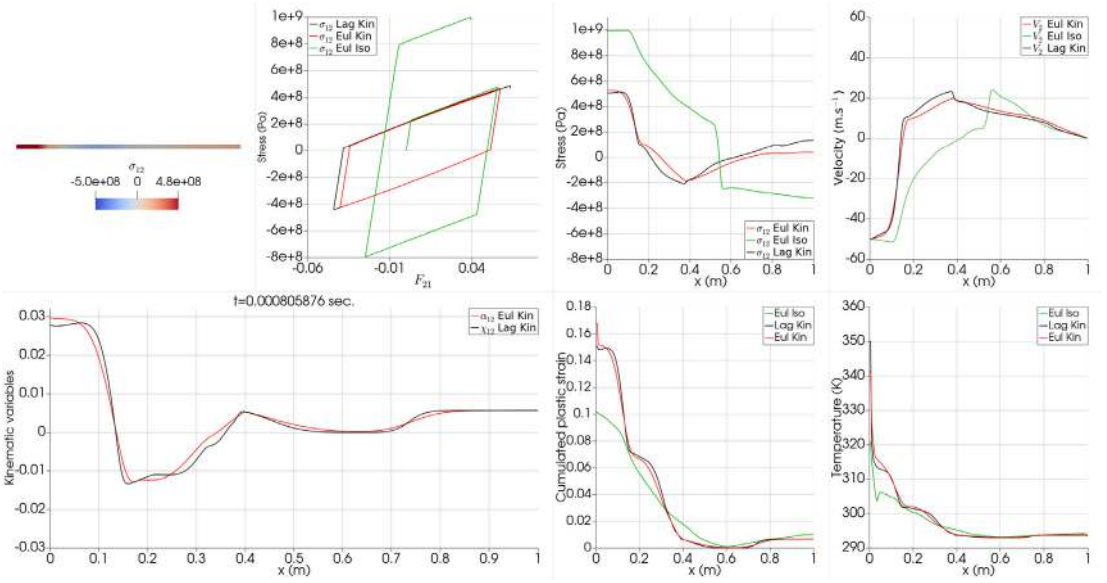

Fig. 11. Plots at time $t \approx 8 \times 10^{-4}$ s of the space profile of various quantities, computed with the Eulerian and Lagrangian formulations with a kinematic hardening, and the Eulerian one with an isotropic hardening on the one-dimensional shear wave test.

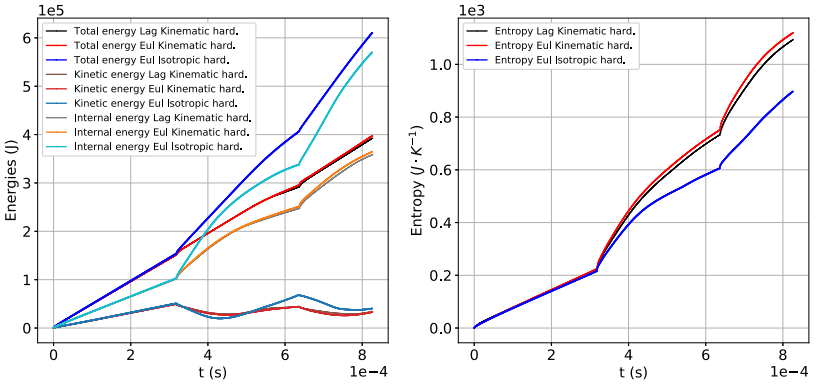

Fig. 12. Time evolutions of the total, kinetic and internal energies (left picture), and of the entropy (right picture), computed via the Eulerian and Lagrangian formulations with a kinematic hardening, and the Eulerian one with an isotropic hardening on the one-dimensional shear wave test.

Maps of the Lagrangian solution are plotted on the deformed configuration. Overall, a good agreement is shown between the two Eulerian and Lagrangian numerical solutions on these two snapshots. Temperature peaks at corners are higher in the Lagrangian solution since the Eulerian one tends to diffuse more due to the transport.

Figs. 16 and 17 show the space profile of various quantities plotted at times $t \approx 3.8 \times 10^{-5}$ and $t \approx 1.1 \times 10^{-4}$ s along the top line of the wedge computational domain, extracted from both the Lagrangian and Eulerian numerical solutions. Plots of the Lagrangian solution are still made on the deformed configuration. Fig. 16 clearly shows the discontinuous elastic precursor and pressure plastic waves. After one loading cycle, Fig. 17 shows more complex profiles of the plotted quantities. Overall, a good agreement is shown between the two Eulerian and Lagrangian numerical solutions, although some small discrepancies appear on the cumulated plastic strain in Fig. 17 after one loading cycle.

7.4. Extrusion die

A last illustration example consists of an extrusion die within which the solid medium flows, as shown in Fig. 18. Such example is typically one of those for which the Eulerian formulation is better suited to carry out the numerical simulation than the Lagrangian one, because large levels of strains may be involved. The extrusion die here consists of a double-bend pipe of opposite curvatures, hence generating forward then reverse loading to the matter flowing in it. The die width is $D = 0.05$ m, its height is $H = 0.1$ m, the bend junction angle with respect to the vertical direction is $\alpha = \pi/3$, and heights of input and output tubes are 0.02 m.

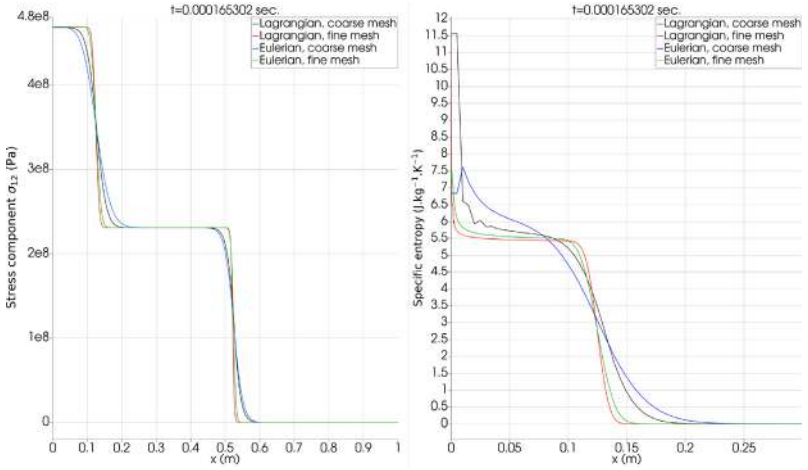

Fig. 13. Plots at time $t \approx 1.65 \times 10^{-4}$ s of the space profiles of the shear stress component σ_{12} and the specific entropy η when computed on coarse (200 cells) and fine (2000 cells) meshes, with the Eulerian and Lagrangian formulations embedding a kinematic hardening. The plot of the entropy profile is zoomed on the interval $x \in [0, 0.3]$ m.

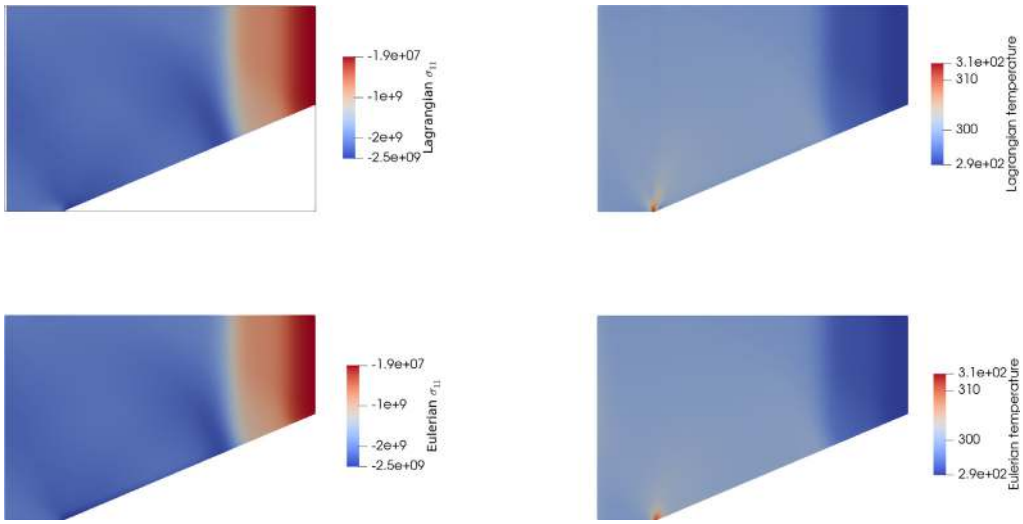

Fig. 14. Maps of the stress component σ_{11} and the temperature in the wedge computational domain, extracted from both the Lagrangian and Eulerian numerical solutions at time $t \approx 3.8 \times 10^{-5}$ s.

Input and output normal velocity component is prescribed at the two ends of the die, at constant and uniform magnitude equal to 50 m s^{-1}, and symmetry conditions are set at the die lateral boundaries for the sake of simplicity. A velocity field of homogeneous magnitude equal to that of prescribed boundary velocities, and parallel to the flow direction is set as initial conditions. After a computation time of $t \approx 1.8 \times 10^{-4}$ s, Fig. 18 shows the maps of the velocity field, the cumulated plastic strain and the temperature computed with the Eulerian numerical solver. Areas inside the two elbows are the locii of increased velocity magnitude, high cumulated plastic strain and temperature rise. At that computation time, the flow is still transient since the particles were transported over only a short distance, as shown on the map of cumulated plastic strain (top right picture) in Fig. 18.

8. Conclusion

Two Eulerian and Lagrangian hyperbolic modelings of thermo-hyperelastic–plastic solids with a non-linear kinematic hardening in finite strains have first been proposed in this work. The consistency between constitutive equations written with both kinematical descriptions is enforced by the choice of the definition of back stresses, here related with the mapping, which then naturally involve a convected or Lie objective time derivative for the Eulerian kinematic variable. It is also enforced by the writing of the plastic evolutions laws in the initial and current configurations rather than in the intermediate one, as usually followed in finite plasticity. Especially, the plastic flow rule defined in the initial setting involves the definition of a Lagrangian Mandel-like stress tensor. The

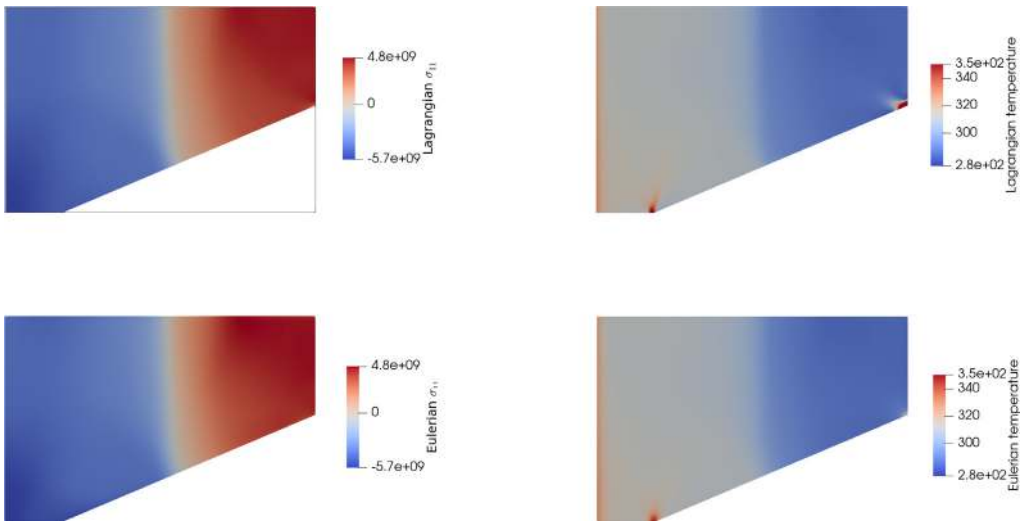

Fig. 15. Maps of the stress component σ_{11} and the temperature in the wedge computational domain, extracted from both the Lagrangian and Eulerian numerical solutions at time $t \approx 1.1 \times 10^{-4}$ s.

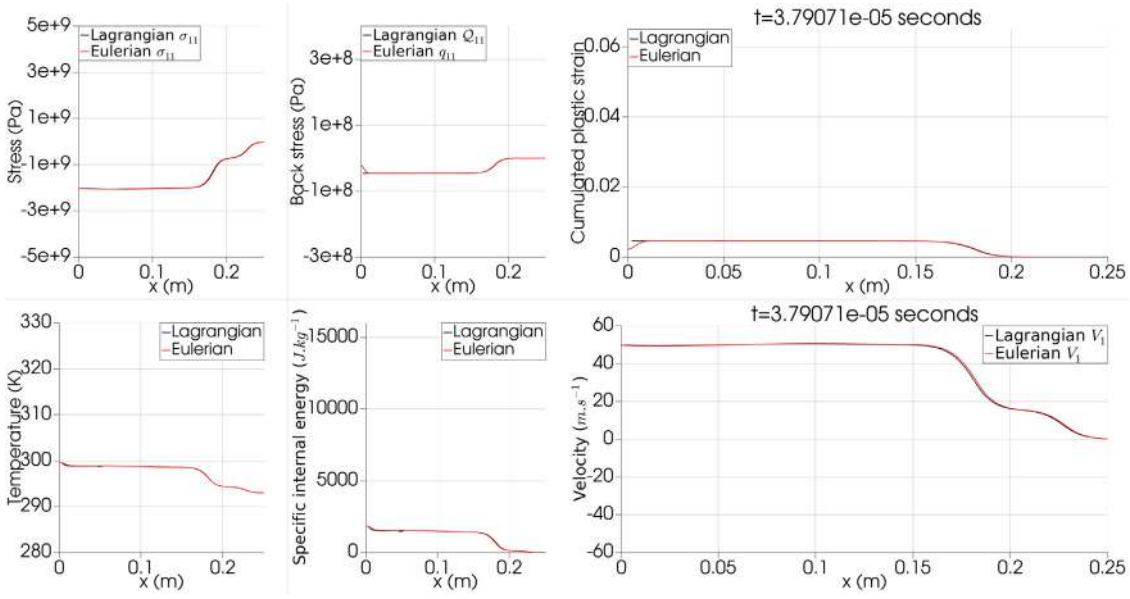

Fig. 16. Profile of various quantities plotted at time $t \approx 3.8 \times 10^{-5}$ s along the top line of the wedge computational domain, extracted from both the Lagrangian and Eulerian numerical solutions.

constitutive equations in the two settings are coupled with their respective multi-field first order systems of conservation (or balance) equations, so that the well-posedness of the Eulerian and Lagrangian hyperbolic modelings are ensured.

The structure of the constitutive modelings then naturally allows to build variational formulations of the dissipative thermo-mechanical local constitutive problem written in both Eulerian and Lagrangian descriptions. These variational principles are based on the parameterization of evolution equations via some pseudo-stresses, analog to that performed by Mosler and collaborators [5, 14,15], but here achieved with Kirchhoff pseudo-stresses. First order accurate variational constitutive updates are then derived from their continuous counterparts. A first particular point here is that the updated right elastic Cauchy–Green strain tensor is not coaxial to its trial value (or their respective inverse), as it was the case for an isotropic hardening [14,15]. This results from that kinematic hardening variables and associated plastic evolution rules have been defined in the initial or current settings for consistency purpose. However, the price to pay is an increased number of unknowns (only one for 2D problems) with respect to formulations written in the intermediate configuration with a sole isotropic hardening [14,15]. A second particular feature of these variational constitutive updates is that they admit updated values of specific internal energies as input data [36] in place of the traditional temperature, in

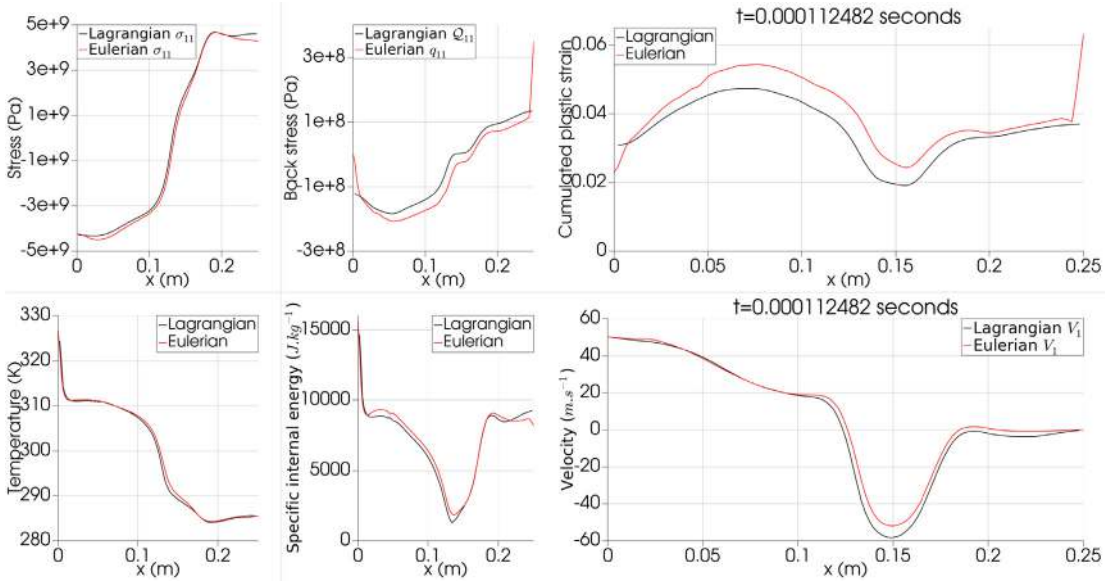

Fig. 17. Profile of various quantities plotted at time $t \approx 1.1 \times 10^{-4}$ s along the top line of the wedge computational domain, extracted from both the Lagrangian and Eulerian numerical solutions.

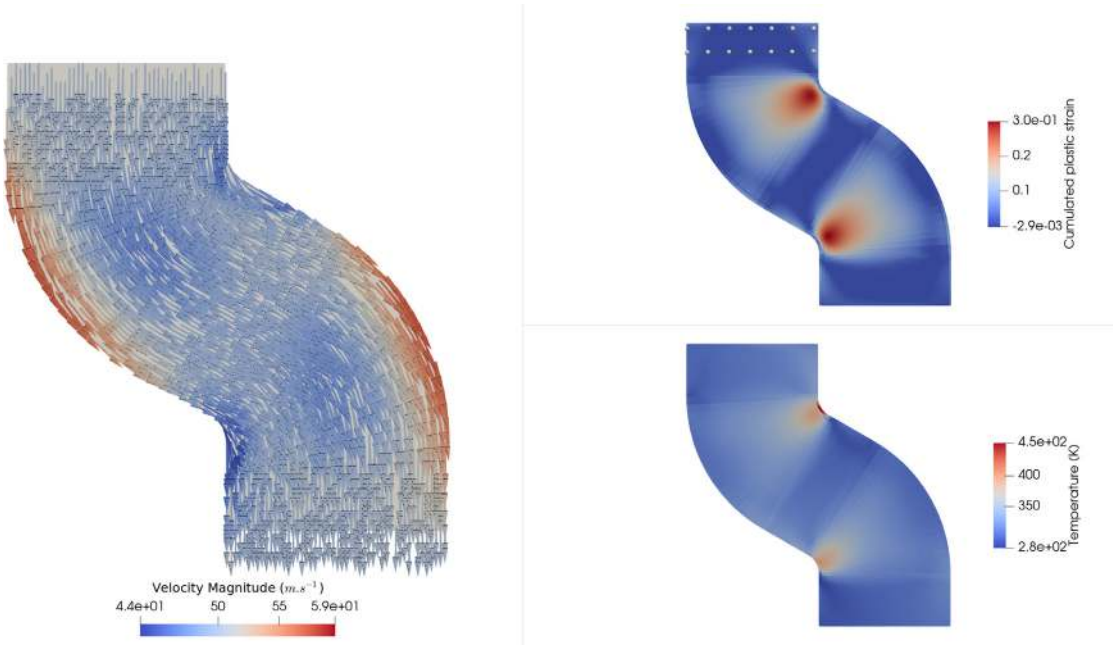

Fig. 18. Maps of the velocity field, the cumulated plastic strain and the temperature in the extrusion die computed with the Eulerian numerical solver, plotted at time $t \approx 1.8 \times 10^{-4}$ s.

addition to some updated strain value. This makes these integrators naturally couplable with any numerical scheme dedicated to the solution of a set of conservation laws, and allow to compute the right shock speeds since these conservation laws reduce to the well-known Rankine–Hugoniot jump conditions across discontinuities of the fields.

Space discretization of conservation (balance) laws is here performed via the second order accurate flux difference splitting finite volume, embedding non-conservative fluxes arising in the Eulerian formulation. A first set of test cases are performed at one material point, showing the consistent cyclic and eventually ratchetting response for one-dimensional and non-proportional biaxial loadings, computed with both Eulerian and Lagrangian constitutive updates. Then, numerical simulations of wave propagations

in one-dimensional then two-dimensional media allow to show the good agreement between solutions computed with the two descriptions. In particular, the shear wave test allows to show and particularly emphasize the truly different predicted solutions when accounting for kinematic or isotropic hardenings in case of a cyclic loading.

CRediT authorship contribution statement

Thomas Heuzé: Writing – review & editing, Writing – original draft, Visualization, Validation, Software, Resources, Project administration, Methodology, Investigation, Formal analysis, Data curation, Conceptualization. **Nicolas Favrie:** Writing – review & editing, Validation, Methodology, Investigation, Funding acquisition, Formal analysis, Conceptualization.

Declaration of competing interest

The authors declare that they have no known competing financial interests or personal relationships that could have appeared to influence the work reported in this paper.

Acknowledgments

N.F. acknowledges support from the ANR under grants ANR-ASTRID project SNIP ANR-19-ASTR-0016-01. N.F. and T.H. also acknowledge Clément Wozniak for his support to this work.

Data availability

Data will be made available on request.

References

[1] J. Lemaitre, J.L. Chaboche, Mechanics of Solid Materials, Cambridge University Press, 1994.
[2] C. Frederick, P. Armstrong, A Mathematical Representation of the Multiaxial Baushinger Effect, Technical Report, Central Electricity Generating Board, Berkeley, UK, 1966.
[3] C. Frederick, P. Armstrong, A mathematical representation of the multiaxial Bauschinger effect, Mater. High Temp. 24 (2007) 1–26.
[4] W. Dettmer, S. Reese, On the theoretical and numerical modelling of Armstrong–Frederick kinematic hardening in the finite strain regime, Comput. Methods Appl. Mech. Engrg. 193 (1–2) (2004) 87–116.
[5] J. Mosler, Variationally consistent modeling of finite strain plasticity theory with non-linear kinematic hardening, Comput. Methods Appl. Mech. Engrg. 199 (45–48) (2010) 2753–2764.
[6] A. Lion, Constitutive modelling in finite thermoviscoplasticity: a physical approach based on nonlinear rheological models, Int. J. Plast. 16 (5) (2000) 469–494.
[7] M. Wallin, M. Ristinmaa, N.S. Ottosen, Kinematic hardening in large strain plasticity, Eur. J. Mech. A Solids 22 (3) (2003) 341–356.
[8] I.N. Vladimirov, M.P. Pietryga, S. Reese, On the modelling of non-linear kinematic hardening at finite strains with application to springback—Comparison of time integration algorithms, Internat. J. Numer. Methods Engrg. 75 (1) (2008) 1–28.
[9] A. Shutov, R. Kreißig, Finite strain viscoplasticity with nonlinear kinematic hardening: Phenomenological modeling and time integration, Comput. Methods Appl. Mech. Engrg. 197 (21–24) (2008) 2015–2029.
[10] R. Pethe, T. Heuzé, L. Stainier, Remapping-free variational h-adaption for strongly coupled thermo-mechanical problems, Finite Elem. Anal. Des. 176 (2020) 103435.
[11] J. Mosler, M. Ortiz, Variational h-adaptation in finite deformation elasticity and plasticity, Internat. J. Numer. Methods Engrg. 72 (2007) 505–523.
[12] J. Mosler, M. Ortiz, An error-estimate-free and remapping-free variational mesh refinement and coarsening method for dissipative solids at finite strains, Internat. J. Numer. Methods Engrg. 77 (2009) 437–450.
[13] J. Mosler, O. Bruhns, Towards variational constitutive updates for non-associative plasticity models at finite strain: models based on a volumetric-deviatoric split, Int. J. Solids Struct. 46 (7–8) (2009) 1676–1684.
[14] J. Mosler, O. Bruhns, On the implementation of rate-independent standard dissipative solids at finite strain–Variational constitutive updates, Comput. Methods Appl. Mech. Engrg. 199 (9–12) (2010) 417–429.
[15] N. Bleier, J. Mosler, Efficient variational constitutive updates by means of a novel parameterization of the flow rule, Int. J. Numer. Methods Eng. 89 (9) (2012) 1120–1143.
[16] M. Canadija, J. Mosler, On the thermomechanical coupling in finite strain plasticity theory with non-linear kinematic hardening by means of incremental energy minimization, Int. J. Solids Struct. 48 (7–8) (2011) 1120–1129.
[17] M. Canadija, J. Mosler, A variational formulation for thermomechanically coupled low cycle fatigue at finite strains, Int. J. Solids Struct. 100 (2016) 388–398.
[18] A. Bartels, T. Bartel, M. Canadija, J. Mosler, On the thermomechanical coupling in dissipative materials: a variational approach for generalized standard materials, J. Mech. Phys. Solids 82 (2015) 218–234.
[19] Q. Yang, L. Stainier, M. Ortiz, A variational formulation of the coupled thermo-mechanical boundary-value problem for general dissipative solids, J. Mech. Phys. Solids 54 (2) (2006) 401–424.
[20] M. Wilkins, Methods in Computational Physics, vol. 3, Academic Press, 1964, pp. 211–263, (Chapter Calculation of elastic-plastic flow).
[21] J. Trangenstein, P. Collela, A higher-order Godunov method for modeling finite deformation in elastic-plastic solids, Commun. Pure Appl. Math. 47 (1991) 41–100.
[22] G. Camacho, M. Ortiz, Adaptive Lagrangian modelling of ballistic penetration of metallic targets, Comput. Methods Appl. Mech. Engrg. 142 (3–4) (1997) 269–301.
[23] G. Miller, P. Collela, A high-order Eulerian Godunov method for elastic-plastic flow in solids, J. Comput. Phys. 167 (2001) 131–176.
[24] N. Favrie, S. Gavrilyuk, Mathematical and numerical model for nonlinear viscoplasticity, Phil. Trans. R. Soc. A 369 (2011) 2864–2880.

[25] P. Maire, R. Abgrall, J. Breil, R. Loubère, B. Rebourcet, A nominally second-order cell-centered Lagrangian scheme for simulating elastic-plastic flows on two dimensional unstructured grids, J. Comput. Phys. 235 (2013) 626–665.
[26] P. Barton, D. Drikakis, E. Romenskii, A high-order Eulerian Godunov method for elastic-plastic flow in solids, Internat. J. Numer. Methods Engrg. 81 (2010) 453–484.
[27] I. Peshkov, W. Boscheri, R. Loubère, E. Romenski, M. Dumbser, Theoretical and numerical comparison of hyperelastic and hypoelastic formulations for Eulerian non-linear elastoplasticity, J. Comput. Phys. 387 (2019) 481–521.
[28] A. Renaud, T. Heuzé, L. Stainier, The discontinuous Galerkin material point method for variational hyperelastic–plastic solids, Comput. Methods Appl. Mech. Engrg. 365 (2020) 112987.
[29] S. Hank, S. Gavrilyuk, N. Favrie, J. Massoni, Impact simulation by an Eulerian model for interaction of multiple elastic-plastic solids and fluids, Int. J. Impact Eng. 109 (2017) 104–111.
[30] A. Thakur, S. Nemat-Nasser, K. Vecchio, Dynamic bauschinger effect, Acta Mater. 44 (7) (1996) 2797–2807.
[31] J. Peirs, P. Verleysen, J. Degrieck, Study of the dynamic bauschinger effect in Ti6Al4V by torsion experiments, in: EPJ Web of Conferences, Vol. 26, EDP Sciences, 2012, p. 01023.
[32] T. Heuzé, Lax–Wendroff schemes for elastic-plastic solids, J. Comput. Phys. 396 (2019) 89–105.
[33] V. Over, Y. Lawrence Yao, Laser shock peening induced back stress mitigation in rolled stainless steel, J. Manuf. Sci. Eng. 144 (6) (2022) 061010.
[34] G. Mie, Zur kinetischen theorie der einatomigen Körper, Ann. Phys., Lpz. 316 (8) (1903) 657–697.
[35] E. Grüneisen, Theorie des festen zustandes einatomiger elemente, Ann. Phys., Lpz. 344 (12) (1912) 257–306.
[36] T. Heuzé, L. Stainier, A variational formulation of thermomechanical constitutive update for hyperbolic conservation laws, Comput. Methods Appl. Mech. Engrg. 394 (2022) 114893.
[37] M. Aguirre, A. Gil, J. Bonet, C. Lee, An upwind vertex centred finite volume solver for Lagrangian solid dynamics, J. Comput. Phys. 300 (2015) 387–422.
[38] J. Bonet, C.H. Lee, A.J. Gil, A. Ghavamian, A first order hyperbolic framework for large strain computational solid dynamics. Part III: Thermo-elasticity, Comput. Methods Appl. Mech. Engrg. 373 (2021) 113505.
[39] B. Cockburn, C.-W. Shu, Runge–Kutta discontinuous Galerkin methods for convection-dominated problems, J. Sci. Comput. 16 (3) (2001) 173–261.
[40] S. Busto, S. Chiocchetti, M. Dumbser, E. Gaburro, I. Peshkov, High order ADER schemes for continuum mechanics, Front. Phys. 8 (2020) 32.
[41] A. Ghavamian, C.H. Lee, A.J. Gil, J. Bonet, T. Heuzé, L. Stainier, An entropy-stable smooth particle hydrodynamics algorithm for large strain thermo-elasticity, Comput. Methods Appl. Mech. Engrg. 379 (2021) 113736.
[42] A. Renaud, T. Heuzé, L. Stainier, A discontinuous Galerkin material point method for the solution of impact problems in solid dynamics, J. Comput. Phys. 369 (2018) 80–102.
[43] A. Renaud, T. Heuzé, L. Stainier, Stability properties of the discontinuous Galerkin material point method for hyperbolic problems in one and two space dimensions, Internat. J. Numer. Methods Engrg. 121 (4) (2020) 664–689.
[44] A. Lakiss, T. Heuzé, M. Tannous, L. Stainier, ADER discontinuous Galerkin material point method, Internat. J. Numer. Methods Engrg. 125 (1) (2024) e7365.
[45] M.E. Gurtin, E. Fried, L. Anand, The Mechanics and Thermodynamics of Continua, Cambridge University Press, 2010.
[46] S.L. Gavrilyuk, N. Favrie, R. Saurel, Modelling wave dynamics of compressible elastic materials, J. Comput. Phys. 227 (5) (2008) 2941–2969.
[47] R.J. Leveque, Wave propagation algorithms for multidimensional hyperbolic systems, J. Comput. Phys. 131 (1997) 327–353.
[48] R. Leveque, Finite Volume Methods for Hyperbolic Problems, Cambridge University Press, 2002.
[49] T. Heuzé, Simulation of impacts on elastic–viscoplastic solids with the flux-difference splitting finite volume method applied to non-uniform quadrilateral meshes, Adv. Model. Simul. Eng. Sci. 5 (1) (2018) 9.
[50] N. Favrie, S.L. Gavrilyuk, R. Saurel, Solid–fluid diffuse interface model in cases of extreme deformations, J. Comput. Phys. 228 (16) (2009) 6037–6077.
[51] D.L. Youngs, Time-dependent multi-material flow with large fluid distortion, Numer. Methods Fluid Dyn. (1982).
[52] M.B. Friess, J. Breil, P.-H. Maire, M. Shashkov, A multi-material CCALE-MOF approach in cylindrical geometry, Commun. Comput. Phys. 15 (2) (2014) 330–364.
[53] V. Dyadechko, M. Shashkov, Reconstruction of multi-material interfaces from moment data, J. Comput. Phys. 227 (11) (2008) 5361–5384.
[54] S. Hank, N. Favrie, J. Massoni, Modeling hyperelasticity in non-equilibrium multiphase flows, J. Comput. Phys. 330 (2017) 65–91.
[55] E. Lee, Elastic-plastic deformation at finite strains, J. Appl. Mech. 36 (1) (1964) 1–6.
[56] M. Ortiz, L. Stainier, The variational formulation of viscoplastic constitutive updates, Comput. Methods Appl. Mech. Engrg. 171 (3–4) (1999) 419–444.
[57] S. Ndanou, N. Favrie, S. Gavrilyuk, Multi-solid and multi-fluid diffuse interface model: Applications to dynamic fracture and fragmentation, J. Comput. Phys. 295 (2015) 523–555.
[58] B. Coleman, W. Noll, The thermodynamics of elastic materials with heat conduction and viscosity, Arch. Ration. Mech. Anal. 13 (1963) 167–178.
[59] B. Coleman, Thermodynamics of materials with memory, Arch. Ration. Mech. Anal. (1964).
[60] B. Coleman, M. Gurtin, Thermodynamics with internal state variables, J. Chem. Phys. 47 (1967) 597–613.
[61] B. Halphen, Q.S. Nguyen, Sur les matériaux standard généralisés, J. Méc. 14 (1975) 39–63.
[62] J. Simo, C. Miehe, Associative coupled thermoplasticity at finite strains: Formulation, numerical analysis and implementation, Comput. Methods Appl. Mech. Engrg. 98 (1) (1992) 41–104.
[63] J. Bonet, A.J. Gil, C.H. Lee, M. Aguirre, R. Ortigosa, A first order hyperbolic framework for large strain computational solid dynamics. Part I: Total Lagrangian isothermal elasticity, Comput. Methods Appl. Mech. Engrg. 283 (2015) 689–732.
[64] E. Toro, Riemann Solvers and Numerical Methods for Fluid Dynamics, Springer, 2013.
[65] C. Carstensen, K. Hackl, A. Mielke, Non–convex potentials and microstructures in finite–strain plasticity, Proc. R. Soc. Lond. Ser. A Math. Phys. Eng. Sci. 458 (2018) (2002) 299–317.
[66] M. Ortiz, R. Radovitzky, E. Repetto, The computation of the exponential and logarithmic mappings and their first and second linearizations, Internat. J. Numer. Methods Engrg. 52 (12) (2001) 1431–1441.
[67] D.E. Keyes, L.C. McInnes, C. Woodward, W. Gropp, E. Myra, M. Pernice, J. Bell, J. Brown, A. Clo, J. Connors, et al., Multiphysics simulations: Challenges and opportunities, Int. J. High Perform. Comput. Appl. 27 (1) (2013) 4–83.
[68] F. Armero, J. Simo, A new unconditionally stable fractional step method for non-linear coupled thermomechanical problems, Int. J. Numer. Methods Eng. 35 (4) (1992) 737–766.
[69] T. Belytschko, W. Liu, B. Moran, Nonlinear Finite Elements for Continua and Structures, Wiley, 2000.
[70] S.K. Godunov, Finite difference method for numerical computation of discontinuous solutions of the equations of fluid dynamics, Math. Sb. 47 (89) (1959) 271–306.
[71] S. Davis, Simplified second-order Godunov-type methods, SIAM J. Sci. Stat. Comput. 9 (3) (1988) 445–473.
[72] P. Sweby, High resolution schemes using flux limiters for hyperbolic conservation laws, SIAM J. Numer. Anal. 21 (1984) 995–1011.
[73] J.A. Trangenstein, Numerical Solution of Hyperbolic Partial Differential Equations, Cambridge University Press, 2009.
[74] J.M. Ball, Convexity conditions and existence theorems in nonlinear elasticity, Arch. Ration. Mech. Anal. 63 (4) (1976) 337–403.
[75] S. Ndanou, N. Favrie, S. Gavrilyuk, Criterion of hyperbolicity in hyperelasticity in the case of the stored energy in separable form, J. Elasticity 115 (1) (2014) 1–25.